1-1-2015

Systems Approach to Producing Electrospun Polyvinylidene Difluoride Fiber Webs with Controlled Fiber Structure and Functionality

Brian D. Bell
University of South Florida, bbell@stetson.edu

Systems Approach to Producing Electrospun Polyvinylidene Difluoride Fiber Webs with Controlled Fiber Structure and Functionality

by

Brian D. Bell

A dissertation submitted in partial fulfillment
of the requirements for the degree of
Doctor of Philosophy in Mechanical Engineering
Department of Mechanical Engineering
College of Engineering
University of South Florida

Co-Major Professor: Delcie Durham, Ph.D.
Co-Major Professor: Sylvia Thomas, Ph.D.
Nathan Crane, Ph.D.
Sarath Witanachchi, Ph.D.
Jing Wang, Ph.D.

Date of Approval:
March 17, 2015

Keywords: Nanomanufacturing, Porosity, Beads, Fiber Diameter, Defects

Dedication

A man named Charles Spurgeon once told a story, and it began like this. “Once upon a time, there was a king who ruled over everything in a land. One day there was a gardener who grew an enormous carrot. He took it to his king and said, ‘My lord, this is the greatest carrot I’ve ever grown or ever will grow; therefore, I want to present it to you as a token of my love and respect for you.’ Here is one rather large paper for the One that I love. I want to dedicate this paper to my wife, my parents, my friends, and my advisor who were the chief forms of grace and blessed support that He provided.

Acknowledgments

I would like to further acknowledge Dr. Delcie Durham. Without her vision and commitment to research, I would not have had the opportunity to pursue my PhD. Her support was outstanding, and working with her was a privilege. I want to acknowledge Dr. Sylvia Thomas and all the members of the AMBIR research group at USF for their insight into the electrospinning process and for allowing the author to share lab equipment. The author would like to thank Sam Perez for his thoughts and willingness to discuss the complexities of the electrospinning process. The author would also like to acknowledge the strong work ethic and contribution of Salman Abbasi for his help in the experimental work of this project. The author would like to thank the Nanotechnology Research and Education Center (NREC) at USF for providing training and access to characterization equipment, in particular Robert Tufts for his advice and help on characterization as he managed the NREC. Fei Gui did extensive work on the surface tension of polymer solutions for this research, and he deserves credit for these measurements. I am grateful to the University of South Florida for its academic and financial support throughout the process. The author would also like to thank the U.S. Department of Education for its support through the GAANN fellowship program and for providing funding support for this research.

Table of Contents

List of Tables

List of Figures

Abstract

Polyvinylidene difluoride (PVDF) is a functional polymeric material that can be used for a wide variety of applications. There are many new future applications that were recently suggested for electrospun PVDF fibers. Electrospinning is a process capable of producing nano to micro sized PVDF fibers in a web. It is important to control the structure of the web during electrospinning because by controlling the structure of the web it is possible for the PVDF fiber web to have increased performance in comparison to other common forms of PVDF.

While past scientific literature focused on applications of PVDF fibers, little was known on how to control structure of PVDF fiber webs during production. Even though defects can alter the structure and performance of the web only a few studies reported defect occurrence and how to reduce the occurrence of defects in fiber webs. This research investigated the defect free production space of electrospun PVDF and provided streamlined guidelines for manufacturers to use for electrospinning PVDF webs.

Many studies looked at influencing fiber diameter and beading with one factor at a time experimentation; this work was foundational and was able to identify many important electrospinning parameters. But this methodology neglected the possibility of parameter interactions and often did not look at the effects of parameters on the occurrence of defects and the structure of those defects. Therefore a systematic understanding that included all of the important electrospinning parameters in relation to fiber and defect structure was needed to present a clear picture of the possibilities for controlling the structure of electrospun PVDF webs. This research explored ways to control the structure of PVDF fiber webs. The production space

and control of web structure was explored by using a regression analysis to identify important parameters and interactions. Then the regression analysis was used to determine the effects of the important parameters that influenced the web structure.

This research showed that the web structure can be controlled using solution parameters and processing parameters and monitored by system parameters. In addition, this study showed that by controlling the web structure it was possible to influence the porosity and piezoelectric properties of PVDF fiber webs. In its entirety, this research presents a systematic approach to producing PVDF fibers for tailored web performance.

Chapter 1: Introduction

1.1 Scope of This Research

The motivation for this research was based on the increasing societal demand for high performance materials, specifically polyvinylidene difluoride (PVDF) fiber webs. Electrospinning was identified as a high rate production technique capable of producing nano to microscale functional polymeric fiber webs. The objective of this research was to tailor the web functionality by controlling the structure of electrospun PVDF fiber webs. The challenges for controlling electrospun fiber webs were the following: a limited knowledge on the effect of parameters on production defects; the unknown and currently debated influence of many parameters on fiber diameter and bead structure, there was limited understanding of the complex relationships between electrospinning parameters and the resulting web structure, it was not clear how defects and defect structure influence web performance, therefore methods for controlling the web functionality were limited by a lack of control and inadequate knowledge on how the structure of PVDF webs influences the overall web performance.

A systems approach, based on regression models relating web structure to electrospinning parameters, was hypothesized to advance the scientific communities' understanding to ultimately achieve a desired fiber web performance.

1.2 Materials and Society

There is a great deal of synergy between society and materials science. Throughout human history the growth of society and societal complexity was linked with the development of new materials and increased levels of processing complexity. Perhaps this was most evident in

the way historians have partitioned historical time periods based on the defining use of materials such as the Stone Age, Bronze Age, Iron Age, and Steel age. Therefore, the storyline of humanity may be likened to a polymer where individual lives are strung together, twisted around each other, and often bonded together to create a complex interconnected web of human history.

Materials influence everyday lives - whether it is the preference of cotton or polyester clothing, affinity for the latest and fastest smart phone, or the car that is driven to work. Yet, these developments would not be a reality without material science, which made possible durable synthetic clothing, fast and portable computer processors, or safe and reliable cars. Many of the largest technological changes in the last century were due to an increased understanding of how to process materials. If the old axiom is correct that history repeats itself, the future economic sustainability and technological advancement of society will again be tied together with the ability to use and process materials. Therefore, it is critically important that society continue to develop new materials and processing techniques.

1.3 Contemporary Materials Science and Engineering

Currently, materials science is focused on the development of new materials and the improvement of existing materials by understanding structure-processing-function relationships. Materials engineering utilizes fundamental knowledge in materials science to design and make functional structures and devices. In order to organize and categorize materials, scientists have developed a classification system that breaks down a material into one the following categories: metals, semiconductors, ceramics and glasses, polymers, or composites.

1.4 Polymers and Functional Materials

A polymer, also known as a plastic, is a long chain molecule composed of many repeating subunits. There are primarily two ways to make polymer, both result in a process

called polymerization. The first method occurs when long chains of molecules become entangled but not chemically connected to form a larger entangled structure. A polymer that is made using this method is called a thermoplastic. The second method occurs during a chemical reaction process where molecules combine to form cross linked chains. A polymer that is made using this method is called a thermoset.

Certain polymers behave in a way that classifies them in a subcategory of material called a functional material. Functional materials, also called smart materials, refer to a material or composite that can sense environmental, mechanical, and/or chemical changes. The push for increased functionality of materials drives the need for increased levels of control on the structure of materials. There is a need for smart materials that are lightweight, multifunctional, self-powered, chemically stable, and affordable for flexible electronic applications. Piezoelectric PVDF is one option for meeting the aforementioned criteria. It's ability to stretch, act as a pressure/force sensor, and harvest vibration energy makes PVDF a great candidate for flexible sensors in electronic devices. In the past investigation of smart materials focused on thin films of PVDF, but now the majority of research is focused on controlling new structures at the nanoscale.

1.5 Nanotechnology

The use of nanotechnology can be traced back well before the knowledge of nanoscale phenomena. Hundreds of years ago, gold nanoparticles were used to give a red color in stained glass windows [1], and nanotubes were found in 17th century blades made in Damascus [2]. These examples illustrate that nanotechnology is not new technology. Only recently have scientists had the tools to study nanomaterials, and this has resulted in a surge of nanotechonogy related research.

The growth in interest of modern nanotechnology is often attributed to Richard Feynman in his 1959 lecture, "There's Plenty of Room at the Bottom". In addition to Feynman's visionary talk, advances in characterization technology were instrumental in accelerating the study of nanotechnology. In the 1980's, IBM created the first Atomic Force Microscope (AFM) capable of atomic resolution. This invention would eventually lead to the first bottom-up approach of nanoscale fabrication. Modern nanotechnology is understood to be a cross disciplinary science that focuses on materials with at least one dimension in the range of 1 nm to 100 nm. Common nanostructures include rods, tubes, belts, wires, fibers, pillars, films, sheets, channels, spheres, pillars, pyramids, and chevrons. Many nanostructured materials were reported to have new or improved functionality over their bulk counterparts.

1.6 Nanomanufacturing

The rise in nanostructured products has lead to a field of study called nanomanufacturing. Manufacturing is a broadly used term referring to the making of a product. Manufacturing involves transforming raw materials into designed products. While manufacturing does not have to be high-tech, current industrial scale manufacturing is always steeped with engineering in order to produce a product at a certain price with a certain performance to meet a specific societal or individual demand. Nanomanufacturing is a term used when manufacturing products and materials with features under 100 nm, and sometimes under 1 µm. Manufacturing of nanofibers is a growing interest for researchers and engineers. Recent analyses suggest future economic growth in nanofiber production due to an increased demand for the applications that nanofibers can meet [3, 4].

Manufacturing is typically considered a wealth producing sector of the economy. Many developed nations that moved towards service based economies are now finding that economic

conditions would benefit from an increase in manufacturing, but manufacturing is often viewed as having a high environmental cost and health risks [5]. This tension is a reality, but using improved engineering to optimize manufacturing processes the engineers can maximize the benefits of producing materials and products while reducing negative impacts to the environment and human health. Therefore, it is important to have high production efficiencies for industrial scale processes.

The major challenges of nanomanufacturing are to produce nanomaterials at high efficiencies and high production rates. One nanoscale material that is poised for future economic growth is Polyvinylidene Difluoride (PVDF). New processing techniques have overcome many of these manufacturing challenges and allow nanoscale fiber webs to be produced at high production rates. However, there are many aspects of electrospun fiber web production that remains unknown and uncontrolled.

Chapter 2: Background

2.1 Polyvinylidene Difluoride

2.1.1 Discovery and Properties of Polyvinylidene Difluoride

Polyvinylidene Difluoride is a piezoelectric thermoplastic. It was not until the 1970's that the ferroelectric properties of PVDF were discovered. The material is widely used due to its inherent chemical inertness and high mechanical strength - particularly in orientated fibers and films. Bulk PVDF is known for exceptional resistance to fatigue and abrasion resistance, and is virtually unaffected by solar radiation [6]. These properties are due, in part, to the chemical structure of the molecule [6]. Because PVDF is a thermoplastic, it is possible to process the material using casting, drawing, blowing, rolling, molding, and spinning.

2.1.2 Polymorphic Transitions

The crystalline phase of PVDF is influenced by the processing used. PVDF is a semi-crystalline polymer. From a molecular level PVDF's basic units are carbon, hydrogen, and fluorine. $C_2H_2F_2$ is the molecular unit for PVDF and is shown in Figure 1.

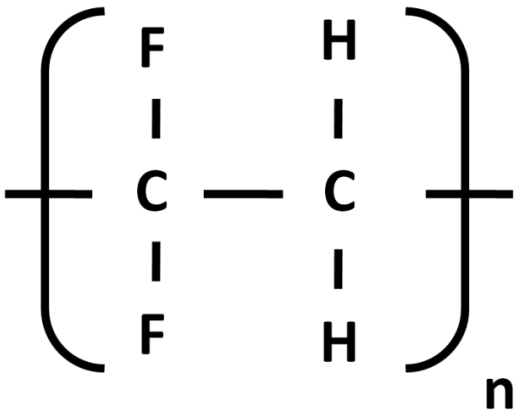

Figure 1. The molecular unit of PVDF.

This molecular unit has a dipole moment. The dipole moment is the result of a non uniform distribution of charge. The fluorine side of the molecule is more electronegative because the electron density is higher than the hydrogen end. The all-trans conformation has a bulk dipole moment when the crystal structure is aligned. The all-trans conformation is referred to as the β phase [7]. The effects of traditional processing on the cyrstalline structure of PVDF are well documented [6]. Often, manufacturing processes are used to create aligned beta phase PVDF which has piezoelectric properties. In its common phase, PVDF is typically 50% crystalline [6]. The long range order of the crystalline structure of PVDF can be characterized using X-ray diffraction (XRD) patterns.

2.1.3 Piezoelectricity

The word piezo means to squeeze or press in Greek. The word is meant to convey that when pressure is applied to a piezoelectric material there is an electric response. This process is reversible and when electric voltage is applied to a piezoelectric material that material experiences a corresponding strain. Traditional piezoelectric PVDF thin films must be processed by stretching to the beta phase and then poled to attain maximum piezoelectric properties [8, 9]. The ferroelectric properties result in an electric response that can be used for sensing strain, sensing temperature change, and charging electronics [10-13]. The electrical properties and piezoelectric properties of PVDF film and other piezoelectric materials are listed in Table 1.

Table 1. Properties of common piezoelectric materials [14].

Property	PVDF Film	PZT	$BaTiO_3$
Density ($10^3 kg/m^3$)	1.78	7.5	5.7
Relative Permittivity ($\varepsilon/\varepsilon_0$)	12	1200	1700
D_{31} (C/N)	23	110	78
G_{31} (V·m/N)	216	10	5
K_{31} (% at 1KHz)	12	30	21

It is observed from Table 1 that there are other materials with higher piezoelectric coefficients than PVDF. But these other materials are not polymers and are limited in their flexibility, chemical resistance, and how they can be processed. PVDF and its copolymers have the highest known piezoelectric response of any piezoelectric polymer.

2.2.4 Applications of Electrospun PVDF Fibers

Recently, new applications are suggested for PVDF due to new advances in nanoscale production by using electrospinning. Because of the size and structure of electrospun PVDF fibers, they were suggested for applications including antibacterial membranes [15], protein absorbers [16], bone growth stimulators [17], tissue scaffolds [18], actuators [19], glucose sensors [20], energy generators [21], force sensors [22-24], hydrophobic coatings [25], and ultra-filtration membranes [26, 27]. Different desired fiber web structures were required for different applications in order to control the desired function such as the mechanical properties, piezoelectric effect, hydrophobicity, and pore size [28]. The challenge to optimizing fiber web performance was a limited understanding of how to control the web structure. Many of these studies provide a starting point to know what structures need to be controlled for each specific application.

2.2.4.1 Mechanical and Electric Properties

Nanofibers showed increased mechanical properties: higher flexibility, larger critical strain, and longer operational lifetimes than microfibers [29]. Therefore, nanofiber webs would be a good choice for robust sensors and actuators. In addition to mechanical strength, it was observed that polarization, that is associated with the piezoelectric properties, occurred due to shear forces caused by the stretching of the fiber, the applied electric field, and rapid evaporation of the solvent in the jet [24, 30-32]. Electrospun PVDF fibers were reported with a piezoelectric

constant d_{33} of −57.6 pm/V which is almost twice the value reported for PVDF thin films [33]. Polymer chains were aligned along the axis of the fiber [34, 35] and also through the thickness of the web [13, 22]. In addition, it was observed that 70 nm diameter fibers have higher beta phase crystallinity than 170 nm and 400 nm diameter fibers, suggesting a higher piezoelectric constant for smaller diameter nanofibers [36]. Also, novel electrical properties of nanosized PVDF structures were reported [37]. Therefore it is desirable to produce nanoscale PVDF fibers, but this was challenging since it was difficult to know what processing conditions lead to nanoscale PVDF fibers.

2.2.4.2 Porosity and Permeability

The performance of desalination membranes was impacted by the PVDF fiber web thickness, interfiber spacing, and by the porosity [38]; this study reported that the fiber diameter did not have any direct effect on desalination performance. For desalination it, was desirable to have webs with high porosity and interfiber spacing. This study looked at porosities ranging from 0.85 to 0.93 and average fiber diameters in the range of 1 - 1.3 µm. Therefore it is desirable to produce PVDF webs with controlled pore size and porosity, but this was challenging since the only method reported to control pore size and porosity was by controlling the fiber diameter [39].

2.2.4.3 Surface Area and Biocompatibility

For applications to tissue engineering, the desired structure of the fiber webs was dependent on the tissue that was being repaired. Certain attributes were identified as desirable to control including, but not limited to, biocompatibility, porosity, surface to volume ratio, biodegradability, and the size of the web features [40]. Also, the wetting properties could alter the performance of fiber webs in certain applications. The influence of fiber structure on wetting properties was studied, and it was shown that the fiber structure, including beads, can modify the

contact angle [41]. Once again it is desirable to produce PVDF webs with controlled pore size and porosity. It is also desirable to produce PVDF webs with controlled bead structure, but this was challenging since there was limited understanding of how to control the structure of beads.

2.2 Electrospinning

In order to control the structure of fiber webs it is important to understand he electrospinning process. Electrospinning is a method for synthesizing a variety of polymer fibers that are used for a broad range of applications that include protective clothing, filters, drug delivery, catalysts for wound healing, and sensors [42]. The foundational work of electrospinning took place by Formhals in 1934. The patent issued to Formhals documents the formation of fibers using electrical charges [43]. Fundamentally an electrospinning setup consists of a dispenser or reservoir for a polymer solution, a high voltage power supply, and a collector, Figure 2 shows a schematic of a typical electrospinning setup.

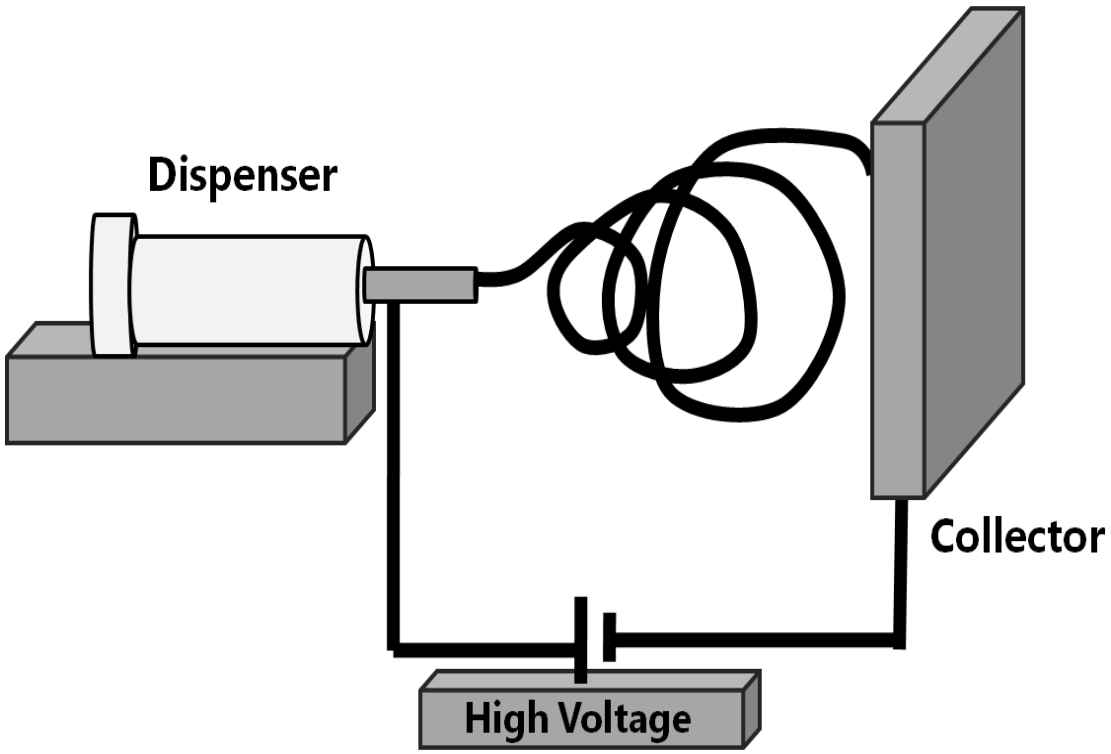

Figure 2. A schematic of a typical electrospinning setup.

The process of electrospinning occurs as electrostatic charges build up at the surface of a polymer solvent solution or polymer melt. A jet or multiple jets form and accelerate toward a collector due to an applied electric field. Under ideal conditions the fiber travels from the dispenser to the collector and the solvent evaporates leaving a polymer fiber. As the electrospinning jet is pulled towards the collector, the jet undergoes bending instabilities driven by the electrostatic forces. The instability is often visible in large diameter fibers and an example of the bending of the fiber is shown in Figure 3.

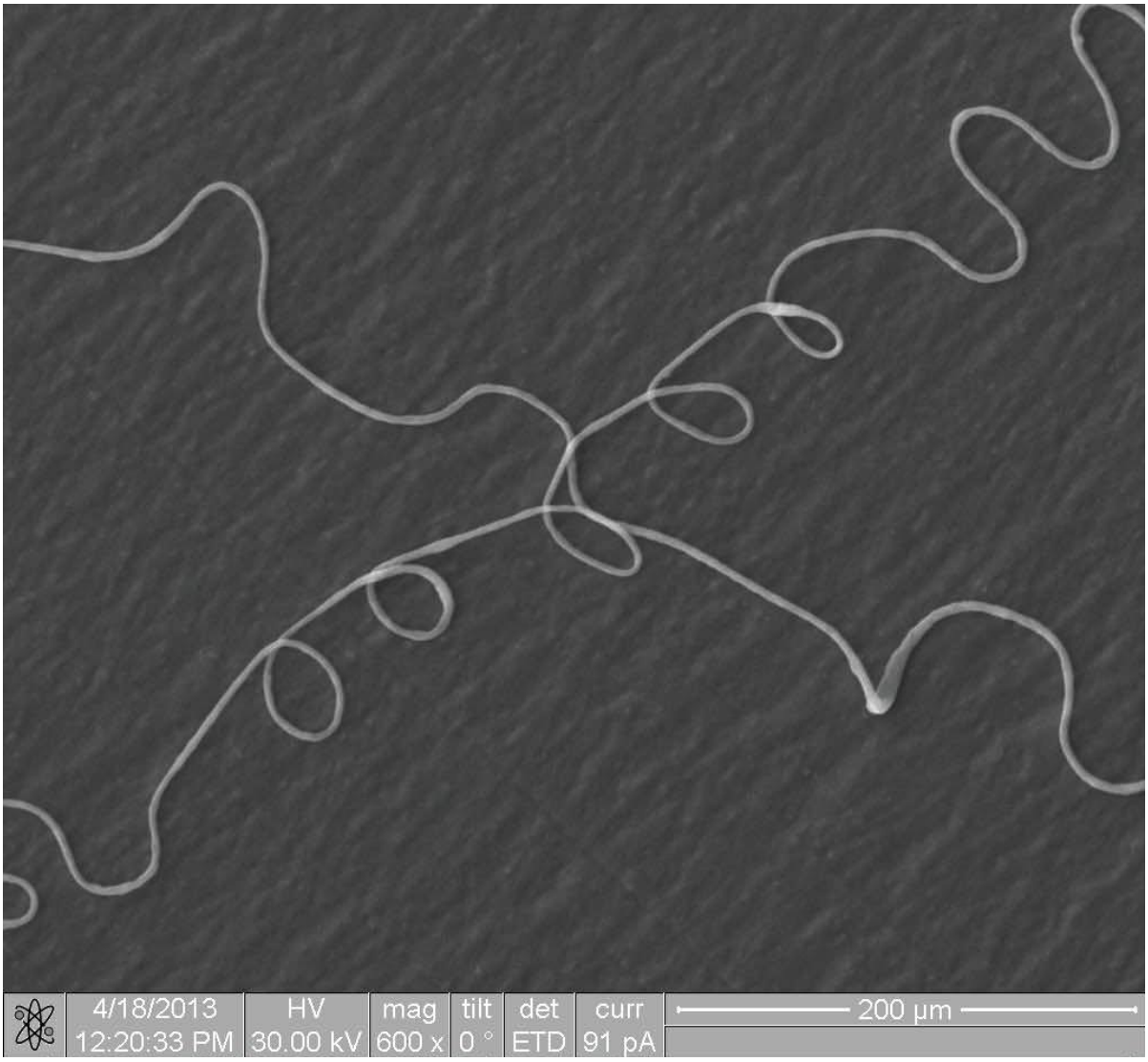

Figure 3. An SEM image that shows a PVDF fiber with looping and spiraling caused by the bending instability of the jet.

The bending instability gives rise to looping and spiraling motion and results in a nonwoven fiber web. Figure 4 shows a PVDF fiber web, and how the majority of fibers are deposited in a concentrated region.

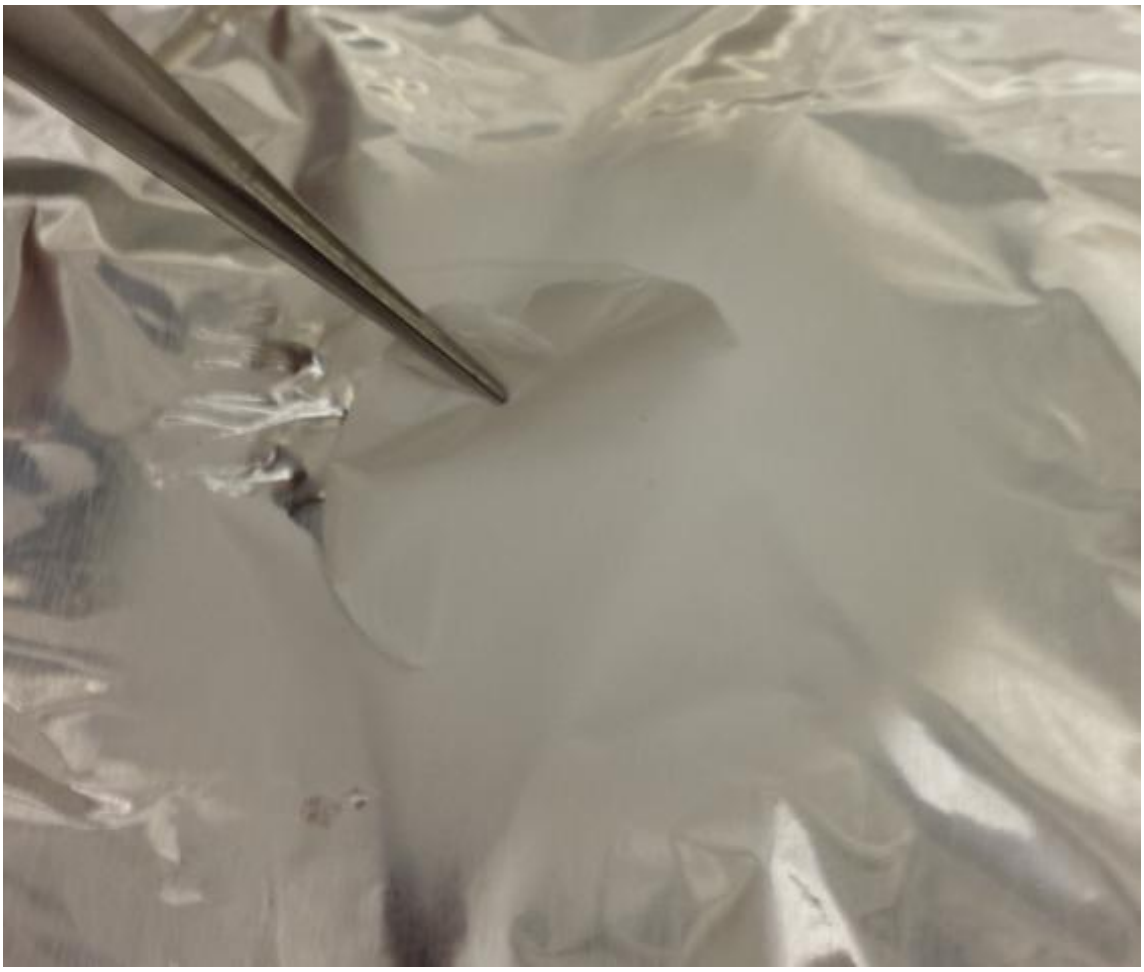

Figure 4. PVDF fiber web on an aluminum collector.

The primary advantage of electrospinning over other techniques is its ability to make nano and microsized fibers [44, 45]. Overall, there were many advantages of using the electrospinning process including:

1. It is capable of producing some of the smallest fibers and feature sizes.
2. It is a scalable production method [46].
3. A large range of possible feature sizes are possible.

4. It is suggested that because electrospinning is a continuous process fibers could be as long as several kilometer [34].
5. It does not require vacuum equipment.
6. There is minimal use of heat, reducing the production cost.
7. The process causes polarization of PVDF fibers [36, 47].

2.2.1 Electrospinning Setup

Different applications identified different electrospinning setups and parameters that could affect web structure. Typically researchers will use a dispenser driven by a syringe pump in order to control the material puming rate. Many industrial setups utilize different dispensers in order to increase production rates. For example, many systems work by transferring solution to a wire or a rotating drum instead of pumping it through a needle [48]. While these systems look different they still operate on the same principles. The high voltage power supply is used to create an electric field between the dispenser and the collector. Electrospun fibers can be collected in a number of ways to produce randomly orientated fiber webs [49], aligned fiber webs [50], spooled fibers, and controlled patterns [21, 51]. The collection of aligned electrospun fibers is achieved by using near field electrospinning, rotational collectors, or by controlling the electric field.

2.2.1.1 Far Field and Near Field Electrospinning

Traditional production of electrospun fibers used far field electrospinning (FFES) with a distance from the dispenser to the collector, referred to as the depth of field, greater than 1 cm. In FFES nanofibers will not be aligned unless there is control of the electric field or the collector [42]. During near field electrospinning (typically the depth of field is around 1 cm or less) it was possible to use direct write techniques by moving the spindle or collector to direct the deposition

of fibers similar to additive manufacturing techniques found in 3D printers [52]. This was possible because the jet instabilities are reduced at such small distances. There were examples that show that near field electrospinning allows highly controlled fiber deposition [53] and tailored three dimensional structures [52]. Direct write techniques for PVDF microfibers was explored by researchers at the UC Berkeley Microfabrication Laboratory. This work was replicated and in both cases the polarization direction was along the fiber length, and alignment was achieved with a combination of stretching and post electrospinning poling [33, 54]. This research showed the feasibility of PVDF as an energy generator and even an actuator [33]. Near field electrospinning has impressive control, but it was reported that polling was required for piezoelectric functionality due to the lack of fiber stretching and the large fiber diameters. Additionally, NFES is not suitable for producing large quantities of functional PVDF nanofibers due to low production rates [55].

2.2.1.2 Electrospinning Collectors

A variety of configurations of collectors can be used to control the fiber structure and orientation during the electrospinning process, including auxiliary electrodes, parallel electrodes, needle grids, rotating drums, moving belt collectors, spinning collectors, and water based collectors [56-58]. Typically the purpose of reconfiguring the collector is to create a preferential alignment, create a yarn, or to optimize nanofiber production rates. Rotational substrates provide a more scalable process, as a method capable of achieving a degree of fibers alignment. High rotational (1000 - 4000 rpm) drums have been used to get highly aligned PVDF fibers [59]. Figure 5 shows aligned PVDF fibers on an aluminum substrate using a rotating drum at approximately 4000 rpm's.

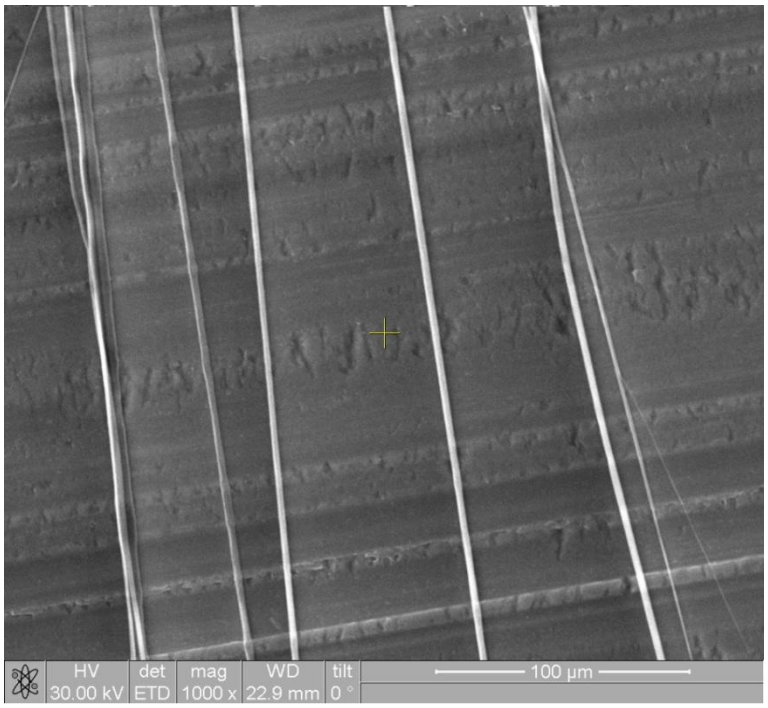

Figure 5. An SEM image showing PVDF fibers aligned using a rotating collector.

Collection is important because of the inherent directionality of piezoelectric materials [22]. Rotating collectors were used to fabricate aligned PVDF nanofibers and are reported to increase crystallinity of PVDF fibers [60]. Therefore, alignment is one of the ways to control the piezoelectric functionality, but as the thickness of the web increased the alignment of webs decreased for rotating collectors suggesting there are limits to using this approach. Therefore, due to this production challenge, additional methods for controlling piezoelectric functionality were desired.

2.2.2 Electrospinning Parameters

In addition to the collector there are processing parameters that can be used to influence the structure of the fiber web. As previously mentioned the main structural characteristics that were reported to affect the performance are the fiber diameter, bead structure, and web geometry [39]. Average fiber diameter of the web can affect properties associated with surface area, pore size, and web density. Defects can alter functionality by reducing uniformity, changing surface

area, altering permeability, and changing the mechanical properties of the fiber web. Due to the wide variety of applications it is critical that manufacturers and researchers are able to produce fiber webs that are tailored for a target application. Investigations into controlling the electrospinning process fell into three approaches:

1. studies investigated theoretical calculations involving fluid dynamics and electrostatics [61, 62],
2. studies investigated system parameters, typically rheological and electrical measurements, of the electrospinning system [35, 62, 63],
3. And studies investigated the influences of initial conditions including solution and processing parameters [64, 65].

Theoretical calculations provide key insights into which parameters were important and suggested mechanisms for modifying the electrospinning process. System parameters of the electrospinning system were difficult to control directly because they were dependant on multiple control variables and ambient parameters. The influence of initial conditions on the production of fiber webs was typically used to modify the structure of the fibers. By changing the solution and processing parameters it was possible to influence the structure of the fibers and overall web. Table 2 lists all of the electrospinning parameters identified by all three approaches.

Table 2. List of electrospinning parameters.

Solution Parameters	**Processing Parameters**	**System Parameters**	**Ambient Parameters**
Polymer M_w	Pumping Rate	Reynolds Number	Temperature
Solutions Concentration	Voltage	Surface Tension	Humidity
Additives	Needle Diameter	Electrospinning Current	Pressure
Solvent Ratio	Depth of Field	Electric Field	

A wide range of electrospinning parameters allowed for a wide variety of possible structures. Figure 6 gives a few examples of structures that are typically not reported for electrospun PVDF.

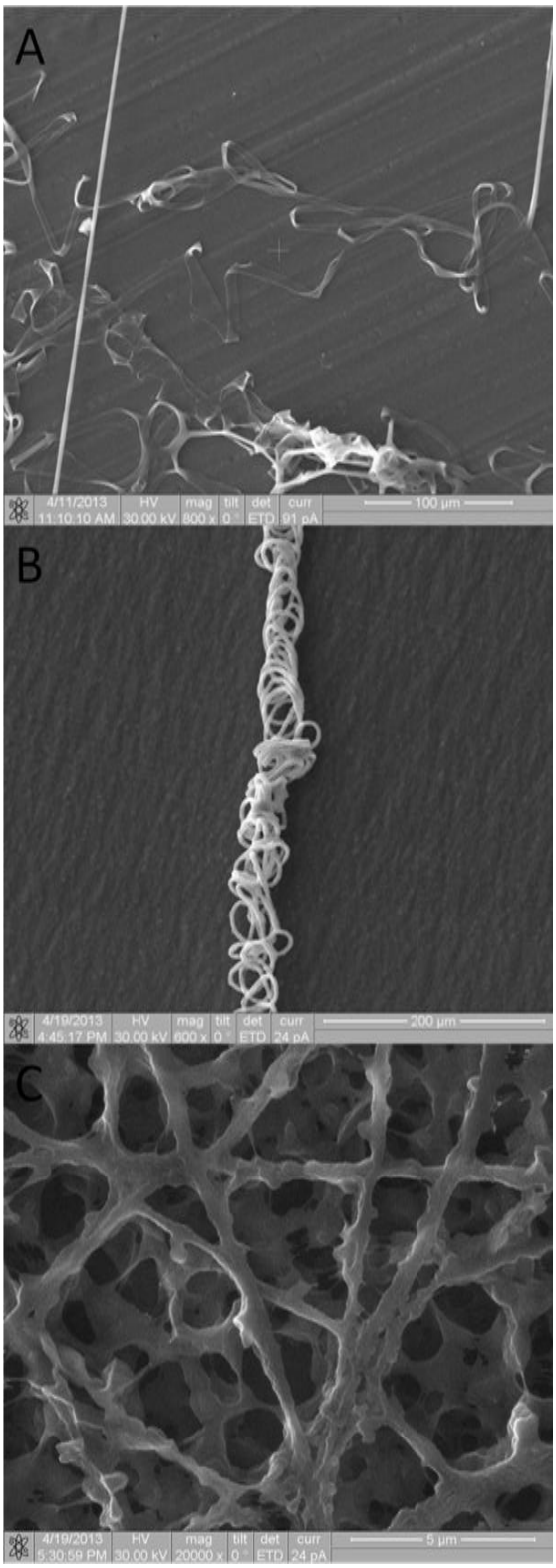

Figure 6. Shows three SEM images of different electrospun PVDF structures. Image A shows PVDF ribbons. Image B shows coiled PVDF fibers. Image C shows fibers rough fibers.

Solution parameters and processing parameters were directly controlled. It was reported that as the polymer molecular weight [45, 65, 66] and solution concentration [44, 65, 67-69] increased the diameter of the fibers increased. Furthermore, increasing depth of field [68, 70] and amounts of low vapor pressure solvents to the solution [71, 72] reduced the diameter of the fibers. The reported impacts of voltage [17, 44, 64, 67, 68, 73], needle diameter [64, 74, 75], conductive additives [67, 74], and pumping rate [44, 64, 67, 73] on fiber metrics varied. Additionally, it was reported that increased molecular weight [66], conductivity [76], and levels of low vapor pressure solvents [64] reduced fiber beading. While increased voltage [64] increased fiber beading and the impacts of increased needle diameter [64, 76] on fiber beading varied.

Many studies reported different influences for the same parameters. This may be due to a difference in the ranges each experiment explored or may be due to the interaction of electrospinning parameters altering the overall effect of the parameters. A survey of current literature on electrospinning of polymer solutions showed that research groups use a variety of processing parameters and their research yields a variety of results, which were often contradictory and rarely looked at statistical significance of the data [17, 32, 50, 71, 76, 77]. Since the influence of many parameters on the structure of fiber webs was unknown it was difficult to control the structure and influence the web performance. The findings of different studies are summarized in Figure 7. The numbers above the arrows correspond to literature that discussed the effect of the electrospinning parameters. A solid line indicates a positive correlation and a dashed line indicates a negative correlation. A grey line indicates that different studies reported different effects. The influence of parameters on fiber beading indicates an

increase, or decrease, in the number of beads, but does not indicate anything about the structure of the bead itself.

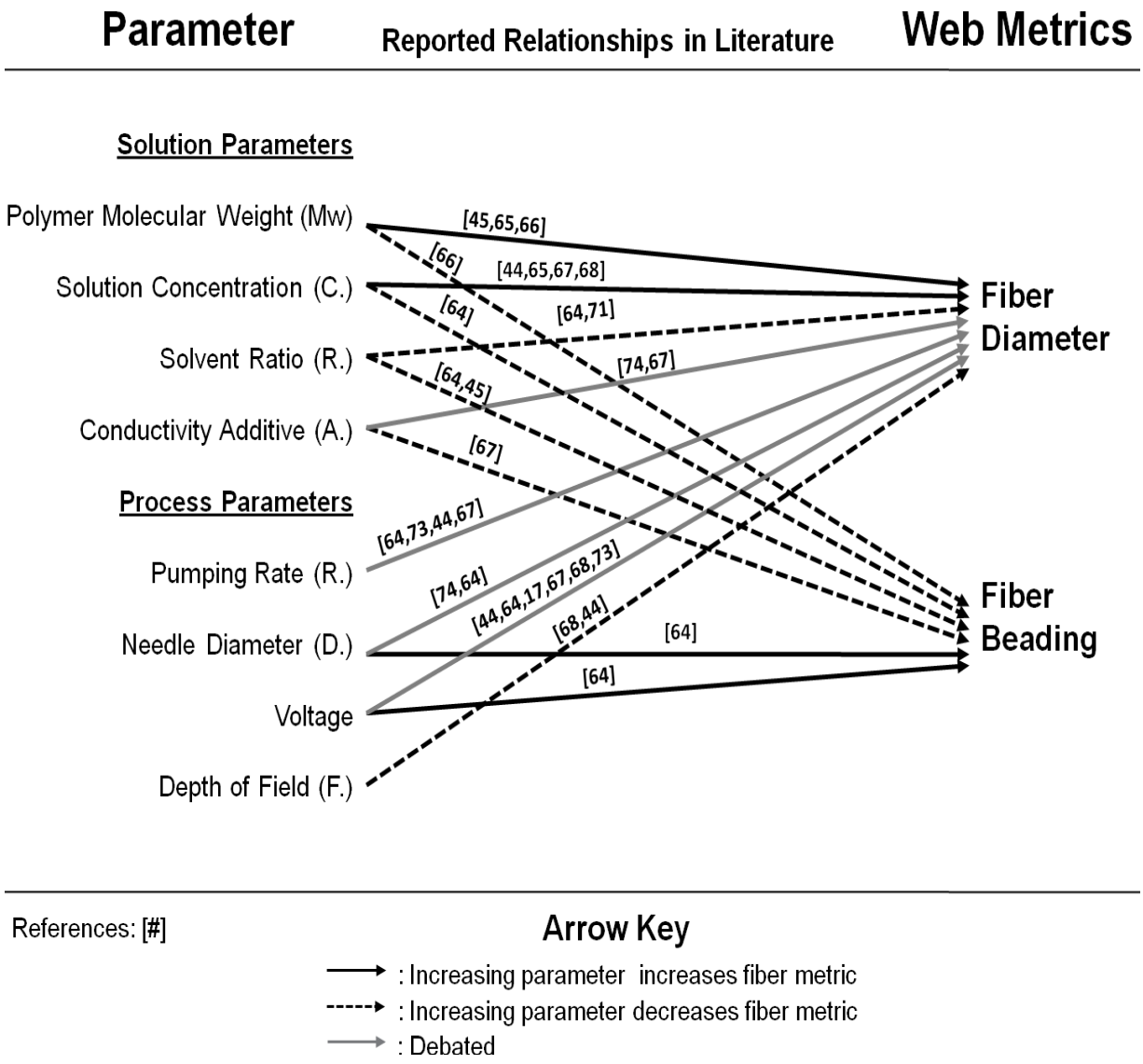

Figure 7. A figure showing the influence of solution and processing parameters on electrospinning reported in the literature.

In addition to solution parameters and processing parameters other studies reported that system parameters such as the Reynolds number, viscosity, surface tension, charge density, electric field, and electrospinning current can influenced the electrospinning process [35, 63, 65, 78-80].

2.2.3 System Parameters

2.2.3.1 Influence of System Parameters on Fiber Diameter

Reneker, Yarin, and Thompson modeled the diameter of electrospinning jets based on the continuity equation, momentum equation, and charge phenomena [35, 63, 65]. Using this approach, they identified important system parameters including the viscosity, electric field, and surface tension. They indicated that further experimental work was needed since the effect of parameters can vary due to the polymer and solvent, the electrospinning setup, and ambient conditions. Another analytical model was proposed by Fridrikh et. al. noted that the surface tension and electrical current influence the terminal jet diameter [81]. The terminal jet diameter refers to the diameter of the jet when it reaches the collector. This model was good at predicting the average fiber diameter of polyethylene oxide fiber webs based on select parameters, but showed difficulty in predicting fibers of other polymers and solvent combinations. This was attributed to differences in charge carriers and solvent properties. Therefore, regression models specific to electrospinning PVDF fibers were desired.

2.2.3.2 Influence of System Parameters on Fiber Beading

In addition to controlling the average fiber diameter these studies often reported the occurrence of fiber beading. Lord Rayleigh first reported the understanding of fluid dynamics of a jet [86]. His analysis identified the surface energy as a defining parameter to determine the preferential shape of a fluid. He noted that a cylindrical jet had a higher surface energy than a series of spherical droplets with a similar volume, and those jets would break up into drops in order to reduce the total surface area. Fong documents the impact of electrical charge on beaded fibers [82]. The work presented suggested that certain processing parameters influenced the number of beads in the web, which suggested that it is possible, in some cases, to control the

number of beads in the web. Fong's research reported that when the ionization of the system was small the fibers tended to be smoother and that as charges on the surface of the jet increased the number of bead nodes per length increased. The charge on the jet can be controlled by altering the electric field. Figure 8 shows an SEM image of beads in a fiber web.

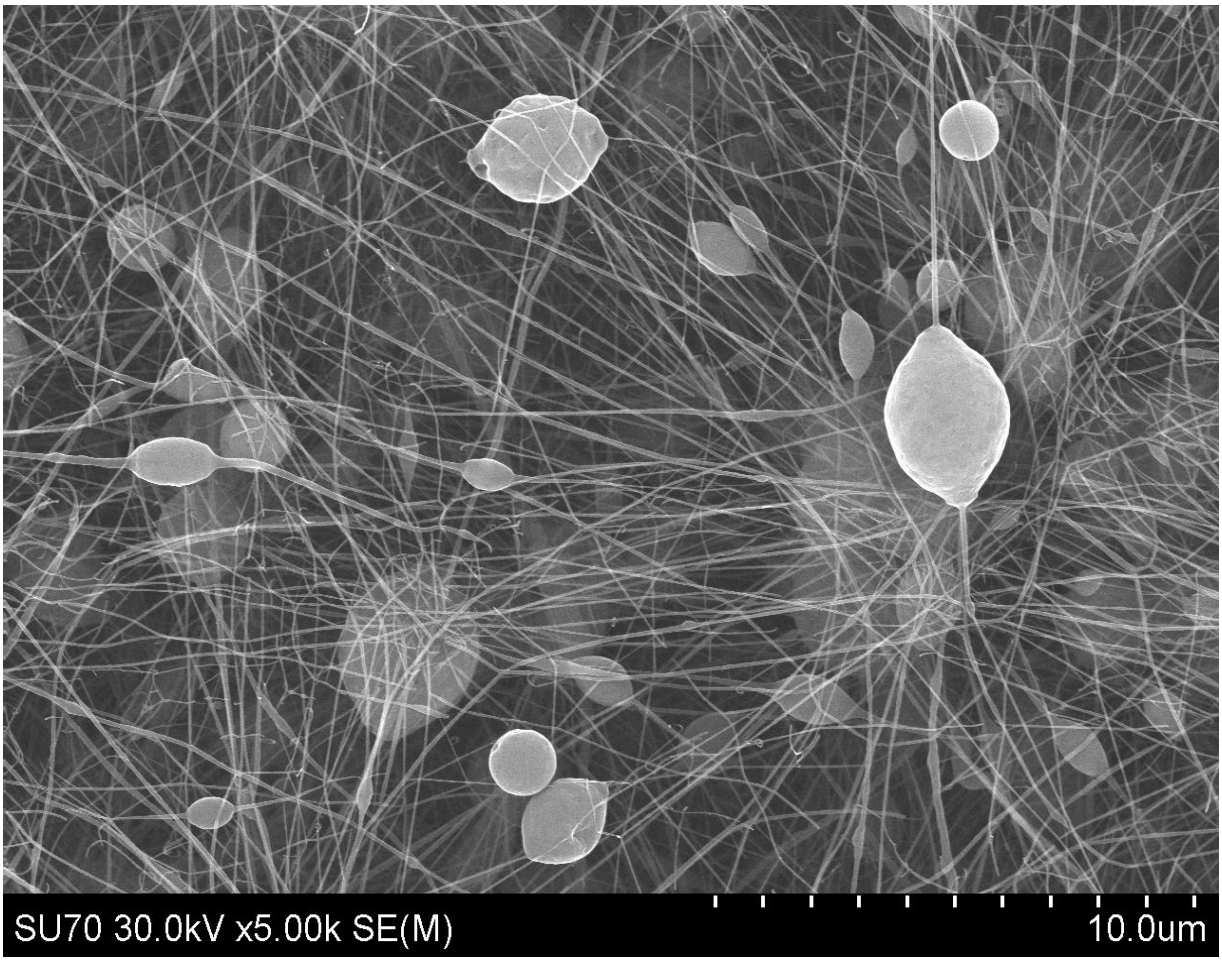

Figure 8. An SEM image of PVDF fibers and beads.

In other research, Liu presented data that suggested increasing solution concentration reduced beading, increasing surface tension increased beading, and changing solvents affected beading [83]. In other studies the viscosity and conductivity were found to impact bead length and bead width [82, 84].

2.2.3.3 Viscosity

Many studies that investigated the electrospinning process explored the influences of rheological properties. Viscosity is a measure of the resistance to shear stress. A fluid that is moving through a tube requires a pressure difference between the two ends in order to overcome the resistance of the fluid due to frictional forces between the fluid and the walls of the tube. The defining equation for viscosity is Equation 1.

$$F = \mu \frac{du}{dt} \quad (1)$$

The two dimension laminar shear flow of a fluid between two plates is shown in Figure 9.

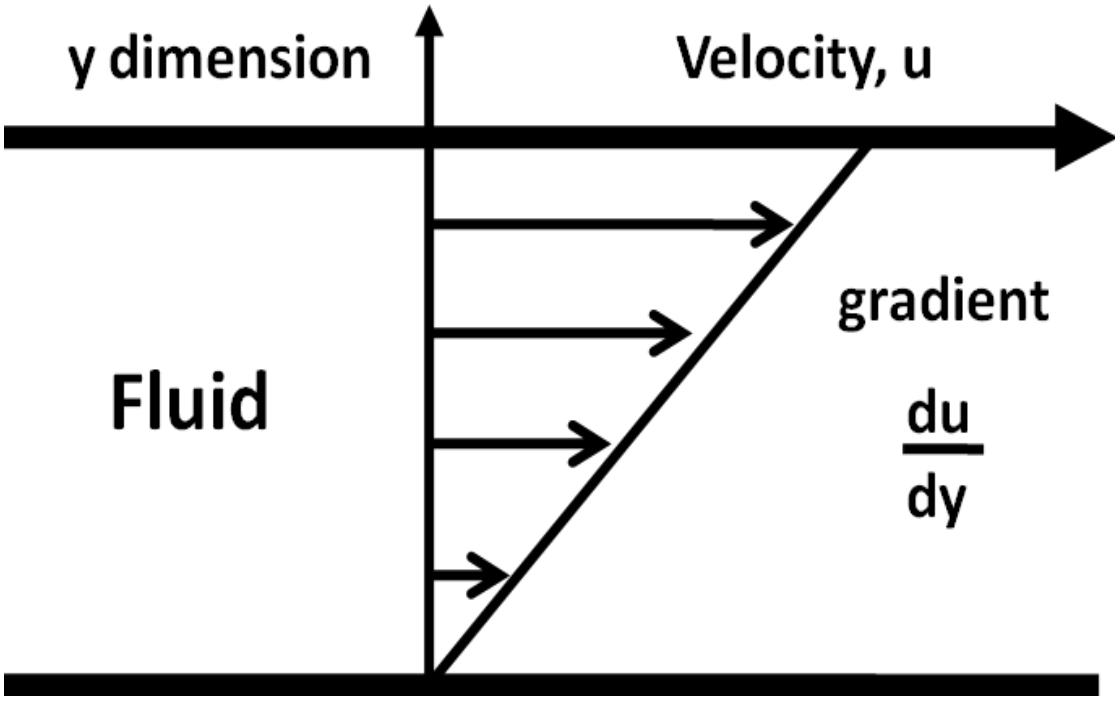

Figure 9. A schematic of laminar shear flow between two plates.

One of the first comprehensive works on the viscosity of solutions was by Arrhenius [85]. Arrhenius discussed the effects of temperature, dissociation of molecules, and the solute concentration on viscosity.

There are many different ways to analyze fluid properties. Viscometers use the principle of laminar shear flow between two plates to measure viscosity. Figure 10 shows one common type of viscometer that uses a motor to drive a measuring bob with a cup that is fixed.

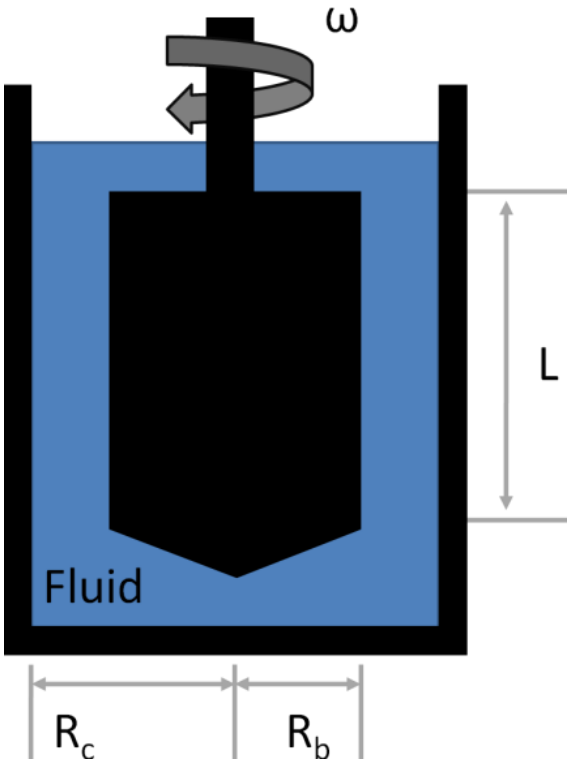

Figure 10. A schematic of a rotation viscometer.

The viscosity is measured by measuring the motor torque. Generally speaking, a higher viscosity sample will take more force to drive the motor; this is called the Searle principle. The motor is run at low rotational speeds in the laminar regime to avoid turbulent flow. The equation for the shear rate of the surface of the bob is

$$\dot{\gamma} = \frac{2\omega R_c^2}{(R_c^2 - R_b^2)} \tag{2}$$

R_c^2 = Radius of container (m)
R_b^2 = Radius of bob (m)
$\dot{\gamma}$ = Shear rate (s^{-1})
ω = Angular velocity (radians/s)

The shear stress in relationship to the measured torque is

$$\tau = \frac{M}{2\pi R_b^2 L} \quad (3)$$

M = Measured torque (Nm)
L = Length of bob

And finally, using Equation 2 and Equation 3, the dynamic viscosity can be calculated

$$\eta = \frac{\tau}{\dot{\gamma}} \quad (4)$$

τ = shear stress (N/m^2)
η = dynamic viscosity (Pa·s)
$\dot{\gamma}$ = Shear rate (s^{-1})

The dynamic viscosity is commonly reported in centipoise (1 cP = mPa·s) [86]. The dynamic viscosities for solvents used in this study were previously reported [71] and the values are recorded in recorded in Table 3.

Table 3. Viscosity of solvents.

Material	Acetone	DMF
Viscosity (cP) at 20°C	0.3	0.82

The impact of viscosity on fiber formation was investigated, and it was noted that increasing viscosity reduced beading and increased fiber diameter [80, 82, 87]. PVDF solution viscosity was studied for a variety of solvent ratios and it was reported that by changing the solvent ratio the viscosity was changed and influenced the average fiber diameter [88, 89]. In one case it was reported that the viscosity of the solution increased steadily with time, approximately 5 times more viscous after 10 minutes, showing that it may be a difficult parameter to control due to solvent evaporation [87]. Therefore, it was important to keep the solutions sealed to reduce evaporation of the solvent. It was reported that the viscosity was related to the concentration and the molecular weight by a power law relationship [66, 90]. Therefore, the viscosity is dependent on multiple solution parameters.

There were attempts to use single parameters models to predict the web structure by looking at the chain entanglement of the polymer solutions. The chain entanglement is related to the type of polymer, the molecular weight, and solution concentration [66]. The degree of chain entanglement is important as it relates to the state of the solution being either dilute, semidilute-un-entangled, or semidilute entangled. The state of the solution was shown to impact the electrospinning of polymer solutions by Pankaj Gupta [80]. Their work showed that solution parameters were important for fiber formation and controlling the average fiber diameter. This method traces back to the Huggins equation for solution viscosity and an understanding of the critical chain overlap. The results for this work suggested that viscosity of dilute solutions was linearly dependant on concentration. Therefore it is expected that relationships between the solutions parameters will linearly influence the system parameters, this supports the approach of using regression modeling.

2.2.3.4 Reynolds Number

The dependence of flow characteristics on fluid properties and flow volume was first documented by Osborne Reynolds in 1883 [91]. Reynolds was able to develop a dimensionless parameter based on the fluids velocity, dynamic viscosity, density, and a characteristic length.

$$\mathrm{Re} = \frac{\rho\, v\, L}{\mu} \tag{5}$$

v is the mean velocity (m/s)
L is a characteristic linear dimension (m)
μ is the dynamic viscosity of the fluid (Pa·s)
ρ is the density of the fluid (kg/m³)

From Equation 5, it is observed that the Reynolds number is a ratio of the inertial forces to the viscous forces. Therefore, the Reynolds number is influenced by both solution and processing parameters. The Reynolds number was used in analytical models [61, 62] and numerical

simulations [92] and is expected to influence the electrospinning process. These studies look at the Reynolds number of the jet during the process after the jet leaves the dispenser. These studies did not report the influence of the Reynolds number of the solution on the web structure before the solution left the dispenser.

2.2.3.5 Surface Tension

The surface tension is due to the cohesive forces between liquid molecules. Figure 11 is a force diagram showing the attractive forces that liquid molecules exert on one another due to Van der Waals forces.

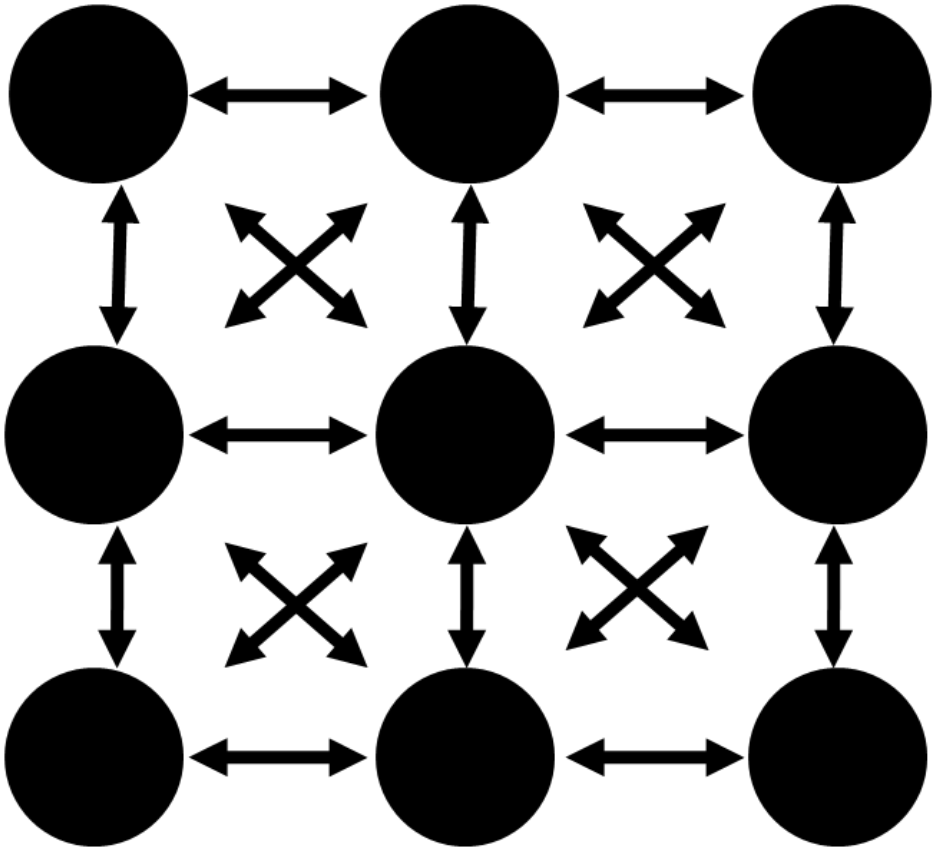

Figure 11. A force diagram that shows the cohesive forces between liquid molecules.

From the figure it is clear that the molecules on the outside surface do not have the same number of neighboring molecules that exert a force on them as the central molecule. This means that there is net force acting toward the center of the liquid on the outside surface molecules. This net

force is what results in surface tension. The surface tension can be measured for different liquids using a tensiometer. The theory behind a tensiometer can be explained using the model for a plate suspended in a liquid. The model is illustrated in Figure 12.

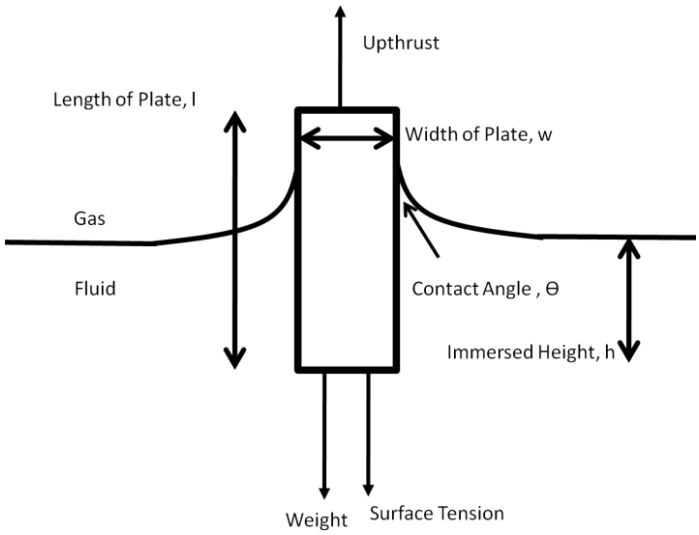

Figure 12. A schematic showing the force diagram of a plate in a liquid.

Figure 11 shows the forces on the plate and is the basis for Equation 6.

$$F_{plate} = \text{Weight} + \text{Surface Tension} + \text{Upthrust} \quad (6)$$

If thickness of the plate is defined as t then the force on the plate is

$$F_{plate} = \rho_P lwt + 2(w + t) \cdot \cos(\theta) \cdot \text{SurfaceTension} + \rho_L hwtg \quad (7)$$

ρ_P = Density of the plate
ρ_L = Density of the liquid
l = Length of the plate
w = Width of the plate
t = Thickness of the plate
Θ = Contact angle
g =Acceleration due to gravity
F = Total force

The equation is further simplified by eliminating the weight term. This can be done by zeroing the scale of the system; in effect the weight term is absorbed into the total force term. The upthrust can be eliminated by raising the plate out of the liquid until the lower edge is level with

the surface thereby making the immersed height zero. Another simplification can be made by assuming the contact angle to be zero. While this assumption is not valid for all cases, it can be forced to be approximately zero through a method discussed later. Therefore the remaining equation is

$$\text{Surface Tension} = \frac{\text{F}}{2(\text{w} + \text{t})} = \frac{\text{Force}}{\text{Perimeter}} \tag{8}$$

In the case of a plate, an absorbent material is used to reduce the contact angle to zero. In the case of a ring, the contact angle reduces to zero because the ring acts as a plate without ends. Further detail on theory and correction factors for tensiometers can be found in the Nima technology manual [93]. The surface tension can be affected by temperature, so it is recommended to always take measurements at the same temperature. The tensiometer used in this work is pictured in Figure 13.

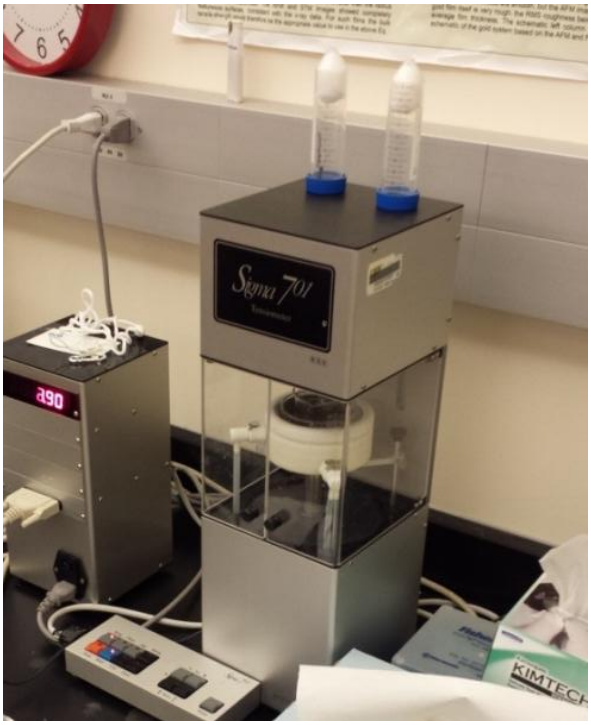

Figure 13. The Sigma 701 Tensionmeter that was used for measuring the surface tension of solutions in this research.

The surface tension was reported to influence the electrospinning process. Increasing surface tension was expected to increase beading, but was also expected to increase the jet diameter which was shown to reduce beading [80, 82, 83]. Also, it was identified that increasing the surface tension increased the critical electrospinning voltage, where the critical voltage is the minimum voltage at which a jet forms [94]. One research group suggested that solvent mixtures with lower surface tensions allow the fiber to stretch longer before complete solvent evaporation takes place producing a smaller fiber [65]. In addition to influencing the fiber diameter the surface tension of solutions was shown to influence the crystallinity of electrospun PVDF fibers [95].

2.3 Design of Experiments and Regression Modeling

So far in section two of chapter two it is clear from the reported literature that solution and processing parameters influence the system parameters and that these parameters are important for the electrospinning process. It is also apparent that not a single study investigated all of the electrospinning parameters simultaneously. Therefore the complexities that arise from the interaction of parameters were unknown. In addition many of the studies shown in Figure 7 looked at electrospinning polymers other than PVDF. Therefore the validity of applying these relationships was uncertain. These challenges can be overcome by utilizing an appropriate experimental design.

Previous studies on electrospinning PVDF investigated electrospinning using one factor at a time (OFAT) experimental designs. Yet, the large number of parameters and the complexity of the relationships suggested the need of an efficient experimental design. Design of experiments (DOE) can be used to investigate the relationships between parameters and a defined outcome. DOE is often used to optimize or minimize a desired outcome of a process.

Two level factorial designs are considered one of the most efficient and versatile experimental designs. The advantages are that the experiments have relatively small sizes when compared to other higher level approaches that are able to detect the interaction of parameters. Therefore, large production spaces can be studied.

Two level designs are best used for linear relationships, or nearly linear. In this study, a fractional factorial experiment was used due to the large number of parameters investigated. Often a fractional factorial experiment can be carried out in such a way as to lose little or no information about the model. This is true if high level interactions are not important for the model. The analysis of a two level factorial design assumes that the residuals are normally distributed and that the residuals are independent with constant variance. These assumptions can be investigated by plotting the normal of the residuals and plotting the residuals versus the predicted values. There were a few researchers who used orthogonal design and central composite design to investigate electrospinning, but the maximum number of parameters investigated was four which limited the production space and number of parameter interactions investigated [64, 68, 96, 97]. A two level factorial design by itself is not able to detect any curvature that may be associated with the effect of the parameters. This limitation is overcome with the addition of center points and axial points to the experimental design. This type of design is called a central composite design (CCD).

2.3.1 Central Composite Design

CCD is a response surface methodology that is built upon a foundation of a two level factorial design. By including axial points and center points to a factorial experimental design it is possible to account for curvature that a two level factorial design cannot detect. A comparison

of investigated production space between OFAT and CCD is shown in Figure 14 for a three parameter process. Each data point represents a different set of parameters.

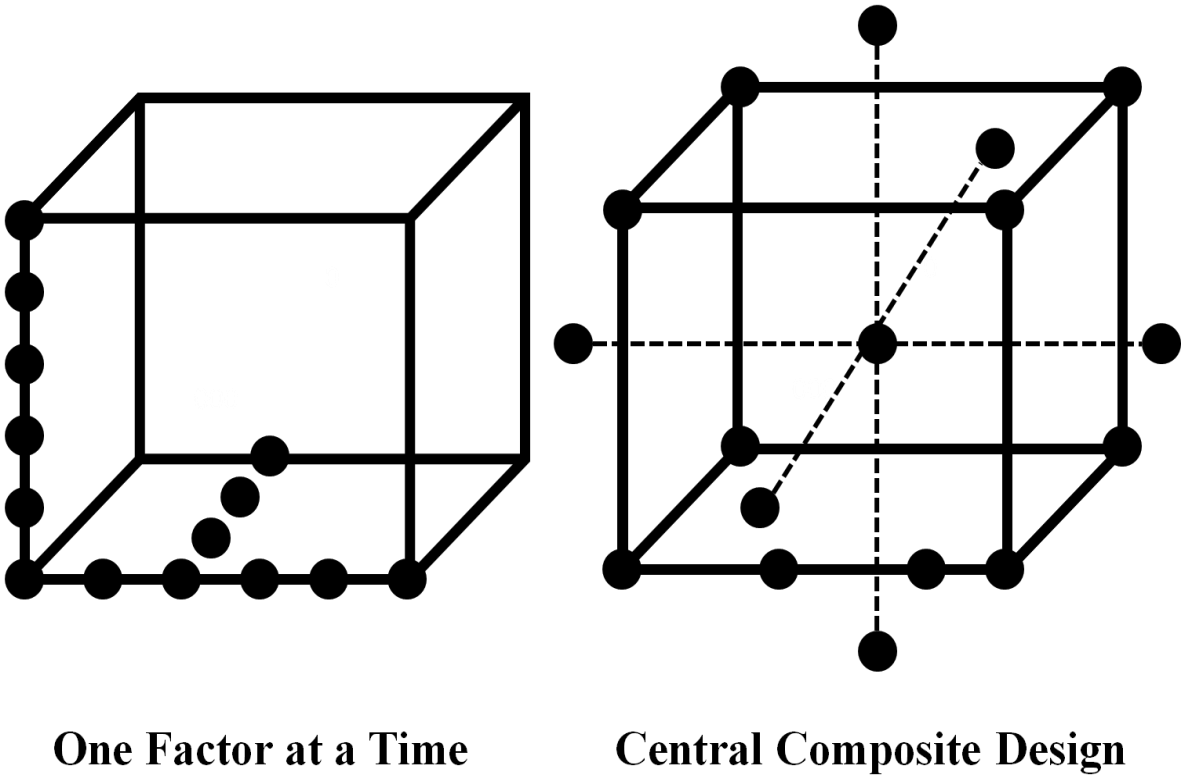

Figure 14. A schematic showing the investigated production space using one factor at a time and central composite design for an experiment with three control variables.

The figure illustrates how the CCD design is able to investigate a larger production space and still include curvature by including additional measurements in between and outside the investigated space of a two level factorial design. Once the experiment is performed, statistical methods are needed to evaluate which parameters are important and what their influence is.

2.3.2 AIC Method

The Akaike information criterion is a measure of the quality of a statistical model and was first proposed by Akaike in a 1971 symposium and later published in 1974 [98]. The AIC method works by comparing different models relative to one another. This approach is advantageous because it looks at the tradeoffs between the goodness of fit and the number of

model parameters. But the AIC method alone provides no indication of the goodness of fit. The AIC is defined as

$$\mathrm{AIC} = 2\mathrm{K} - 2\ln(\mathrm{L}) \tag{9}$$

K = Number of degrees
L = Maximized likelihood function

The AIC is reported to perform better then the Bayesian information criterion (BIC) and is, therefore, used in the presented work [99, 100].

2.3.3 Regression Models

The AIC method can be used to select the best fitting model. The terms in the model are based on the model parameters. The coefficients of each term are related to the influence of each parameter and the interaction. When a regression model is used to predict a continuous outcome, such as the average fiber diameter, a regression fit is used. When a regression model is used to predict a nominal value, such as the occurrence of beading, a nominal logistic regression equation is used. In both cases an R^2 value can be used to measure the goodness of fit.

For large models involving many parameters there is a danger in over fitting the data. One benefit of the AIC method is that the number of parameters is taken into account and the method attempts to reduce the number of parameters needed without reducing the goodness of fit. Another way to avoid over fitting the data was to examine the adjusted R^2 value for linear regression or the entropied R^2 value for nominal logistic regression. If the adjusted R^2 value is much lower than the R^2 value there may be over fitting occurring in the regression model. Once the regression model is established, using the AIC method, it is necessary to interpret the meaning of the equation. The interpretation of the model is based on the value of the model coefficients.

2.3.4 Systems Model

A systems model is a conceptual framework describing a system comprised of multiple subsystems. A systems model can be supported by regression models but these are different. A systems model helps plan and anticipate complex behavior in a comprehensive way. Systems models are often interdisciplinary in nature. For this research, a systems approach was investigated as a way to understand the electrospinning process. In this research the subsystems that comprised the systems model included the: processing system, solution system, web structure system, and the functional properties system. Therefore the systems approach encompassed aspects of materials science, fluid dynamics, electrostatics, and manufacturing.

Chapter 3: Producing Defect Free Fibers

3.1 Introduction to Producing Defect Free Fibers

The first step towards influencing the functional properties of electrospun PVDF webs was to identify what production defects commonly occur. The second step was to investigate at which settings these defects occurred within an experimental design. Completing these steps allowed for the possibility of developing regression equations and finally gaining an understanding of which parameters influenced the occurrence of production defects from the coefficients of the regression equation.

This had to be done because there was not any comprehensive method reported in the literature to anticipate the occurrence of production defects during the electrospinning process. Most electrospinning research focused on new materials, new setups, or new applications for fiber webs. Therefore many of the difficulties in producing defect free fiber webs were not reported in the literature. There were reports on the influence of parameters on beading [82, 83, 101]. There was also one study that documented the transition from electrospinning to electrospraying [71]. These two defects were documented and OFAT experiments were used to estimate the influence of a select set of parameters on the occurrence of these defects in the web.

Therefore the understanding of why beading and electrospraying occurred was confined to a small set of production parameters. Consequently, the possibility of applying the reported parameter relationships was limited to a small production range for different parameters in relationship to one another were unknown, and this reduced the range. This limitation was overcome in this study by exploring all solution and processing parameters.

Four production defects were observed during the production of PVDF fiber webs. These production defects included beading, electrospraying instead of electrospinning, incomplete solvent evaporation of the jet, and the fiber bridging from the dispenser to the collector. In all four of these cases fibers were produced along with the defect creating a web with fibers and defects.

The following research explores the possible production space for defect free fiber webs by utilizing experimental design. The parameters that were already reported to influence the electrospinning process were used as a starting point to investigate if these parameters could adequately control the occurrence of production defects in the explored production space. This was done by documenting the occurrence of defects and then fitting the data using logistic regression. Then the relationships of important parameters are reported by interpreting the terms of the regression models of different defects. Figure 15 shows four different samples with the production defects observed in this study.

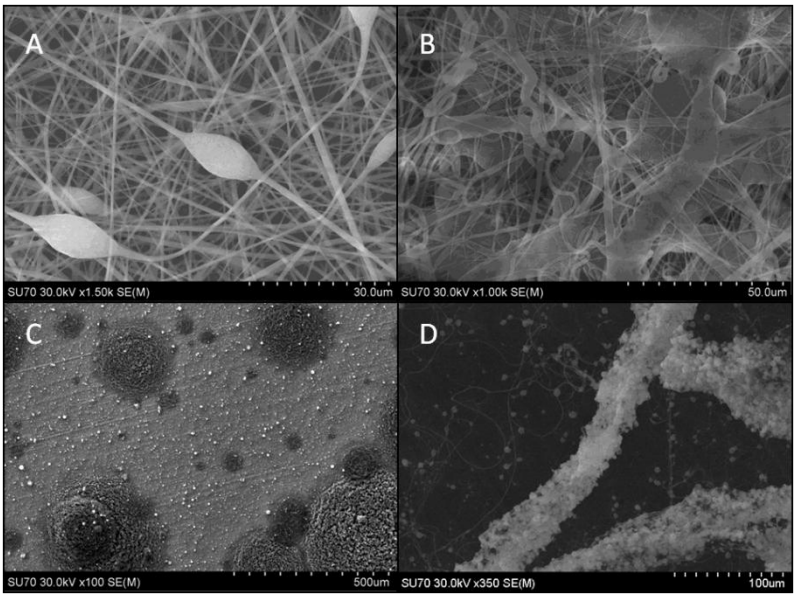

Figure 15. SEM image of four different fiber webs with production defects. Sample A shows a fiber web with beading. Sample B shows a fiber web with incomplete evaporation. Sample C shows a sample with electrospraying. Sample D shows a sample where bridging occurred.

Sample A shows fiber beading, sample B shows a web with incomplete solvent evpaoration, sample C shows a web with electrospraying, and sample D shows the results of a web that was produced when the fiber created a bridge betweeen the dispenser and collector. Fiber bridging could be visually observed during the electrospinning process and is shown in Figure 16.

Figure 16. Image showing a fiber that formed a bridge from the dispenser to the collector.

These production defects altered the structure of PVDF fiber webs. Beading resulted in the concentration of PVDF in the shape of an ellipsoid and was usually connected to the fibers in the web. Incomplete solvent evaporation created distorted fiber symmetry. Fiber bridging and electrospraying created production conditions that were constantly changing making it difficult to control the processing parameters. Therefore it was critical that any further analysis on the production of PVDF fibers must first deal with these defects. In order to understand why these

production defects occurred, a systematic study of how the processing parameters, solution parameters, and system parameters influence the occurrence of production defects was needed.

3.2 Experimental Setup

3.2.1 Electrospinning Equipment

Figure 17 is a schematic of the laboratory setup that was used in this research and shows the processing parameters that were controlled throughout the experiment.

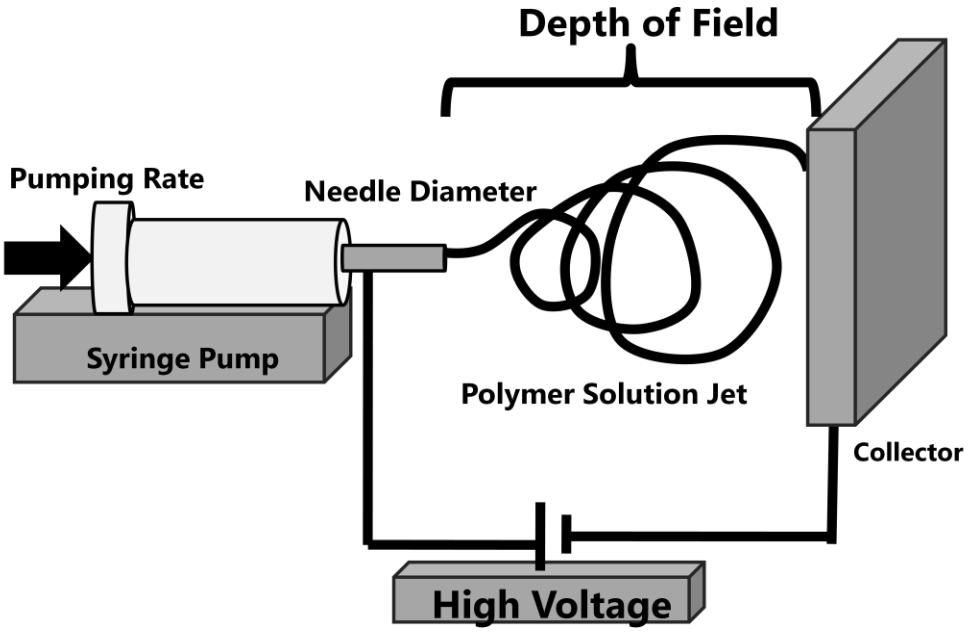

Figure 17. A schematic of the electrospinning setup with processing parameters.

The pumping system used was a PHD 2000 syringe pump. A 3 cc syringe was filled with solution; then a needle was attached using a luer lock. The high voltage power supply, produced voltages up to 30 kV, was connected to the dispenser and collector with alligator clips. The depth of field was changed manually by moving the collector. Pictured in Figure 18, the entire setup was enclosed in two separate acrylic containers for safety reasons and to reduce any nuisance variables from the environmental.

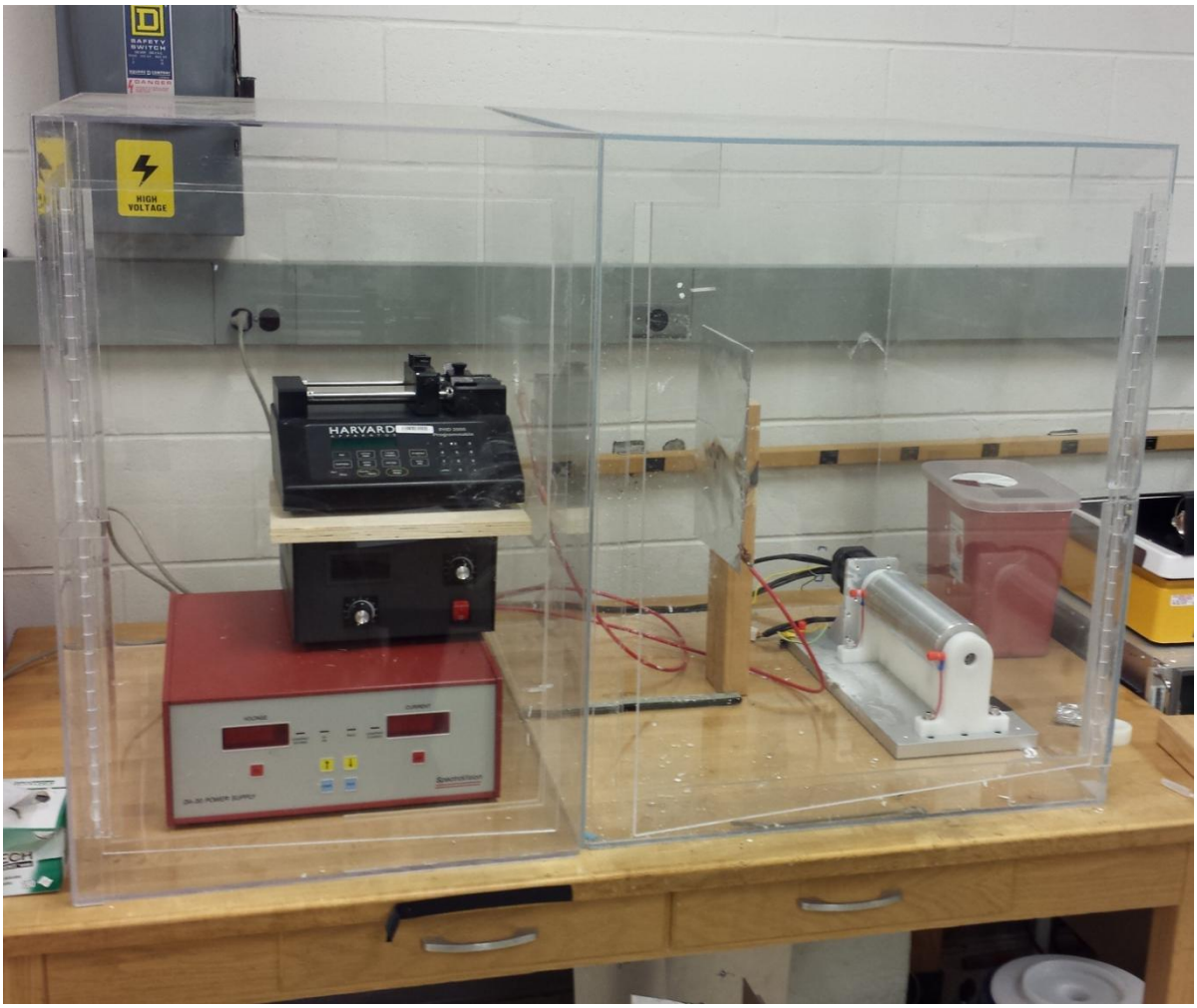

Figure 18. An image of the laboratory setup.

The electrospinning setup was used to control the processing parameters and measure the electrospinning current.

3.2.2 Materials used for Electrospinning PVDF

In addition to the processing parameters, the solution parameters were also controlled. The materials used in this work were PVDF with dimethylformamide (DMF) and acetone as solvents, and tetrabutylammonium chloride (TBAC) was added to modify the conductivity of the solution. The electrospinning solutions were prepared by mixing PVDF with the solvents and, in some cases, TBAC then stirring on a hotplate for 2 hours at 100°C. The solution was then set

aside for 22 hours and loaded into a syringe for spinning. Then the viscosity and surface tension was tested for each solutions mixture.

The system parameters were measured but not included in the orthogonal experimental design. One reason for this was that adding four additional parameters into the experimental design would exponentially increase the number of measurements needed in order to resolve the effects of the parameters and interactions. However, the system parameters were observed to see if there were any noticeable trends in the data. The viscosity was used to calculate the Reynolds number of the flow through the needle. The Reynolds number was calculated using the formula associated with pipe flow [91]. The electric field was calculated from the voltage and depth of field settings. And the electrospinning current was measured across the power supply. The surface tension was measured using a tensiometer.

3.2.3 Experimental Design

Setting up the CCD was the next step in understanding if any of these aforementioned parameters influenced the occurrence of production defects. A 2^{8-2} fractional factorial design with axial points and center points was used to identify the effects of the four solution parameters and the four processing parameters and their 2^{nd} level interactions on defect occurrence. Because this design included center points and axial points it was possible to know if there was any curvature, or non-linear correlations, associated with the parameters. Therefore, a minimum of 80 runs was needed. In addition to the minimum number of run, replicates were included to test repeatability resulting in a total of 155 runs, which were made from 16 different solution mixtures. The occurrence of production defects was documented for each sample. The degree of the defect was not measured since there was currently no standard way to measure the degree of electrospray, fiber bridging, or incomplete evaporation. Therefore, Nominal logistic regression

was used due to the type of data. The AIC method was used to select a model and the significance of individual parameters was judged based on their chi squared values.

The parameters included in the analysis were chosen due to relevance noted in the literature about electrospinning PVDF fibers and general electrospinning [64, 66, 67, 102, 103]. The ranges for each parameter investigated in this experiment are listed in Table 4; the range of system parameters measured is also listed. Ambient parameters, such as temperature and pressure, were monitored but not intentionally varied.

Table 4. Parameters and ranges used for the study of defects.

Solution Parameters	**Lowest Setting**	**Highest Setting**
Polymer M_w	180,000 g/mol	530,000 g/mol
Solution Concentration	15 wt%	17 wt%
Conductive Additive	None	3 wt% TBAC
Solvent Ratio	2 to 8 Acetone to DMF	1 to 1 Acetone to DMF
Processing Parameters	**Lowest Setting**	**Highest Setting**
Pumping Rate	5 µl/min	50 µl/min
Voltage	15 kV	20 kV
Needle Diameter	0.413 mm	0.838 mm
Depth of Field	10 cm	20 cm
System parameters	**Lowest Measured**	**Highest Measured**
Surface Tension	31.0 mN/m	41.3 mN/m
Electric Field	2 kV/m	0.75 kV/m
Reynolds Number	0.0002	2.2
Electrospinning Current	0 µA	35 µA

The significance of each parameter and the effect of each parameter were accomplished with JMP SAS©. The AIC method was used to determine the best fit model.

3.2.4 Characterization of Defects in Electrospun Webs

Scanning electron microscope (SEM) images were taken using a Hitachi SU-70 microscope. Fibers were coated with a thin layer of gold palladium, approximately 5 nm, to increase conductivity and consequently improve image quality. In addition to documenting the occurrence of defects, the average fiber diameters were also measured using QuartzPCI software. Typically over one hundred and fifty different fibers were measured per experimental run to get

an accurate average. The presence of fiber beading, incomplete solvent evaporation, and occurrence of electrospraying were documented for each sample. Examples of fiber beading are shown in Figure 19.

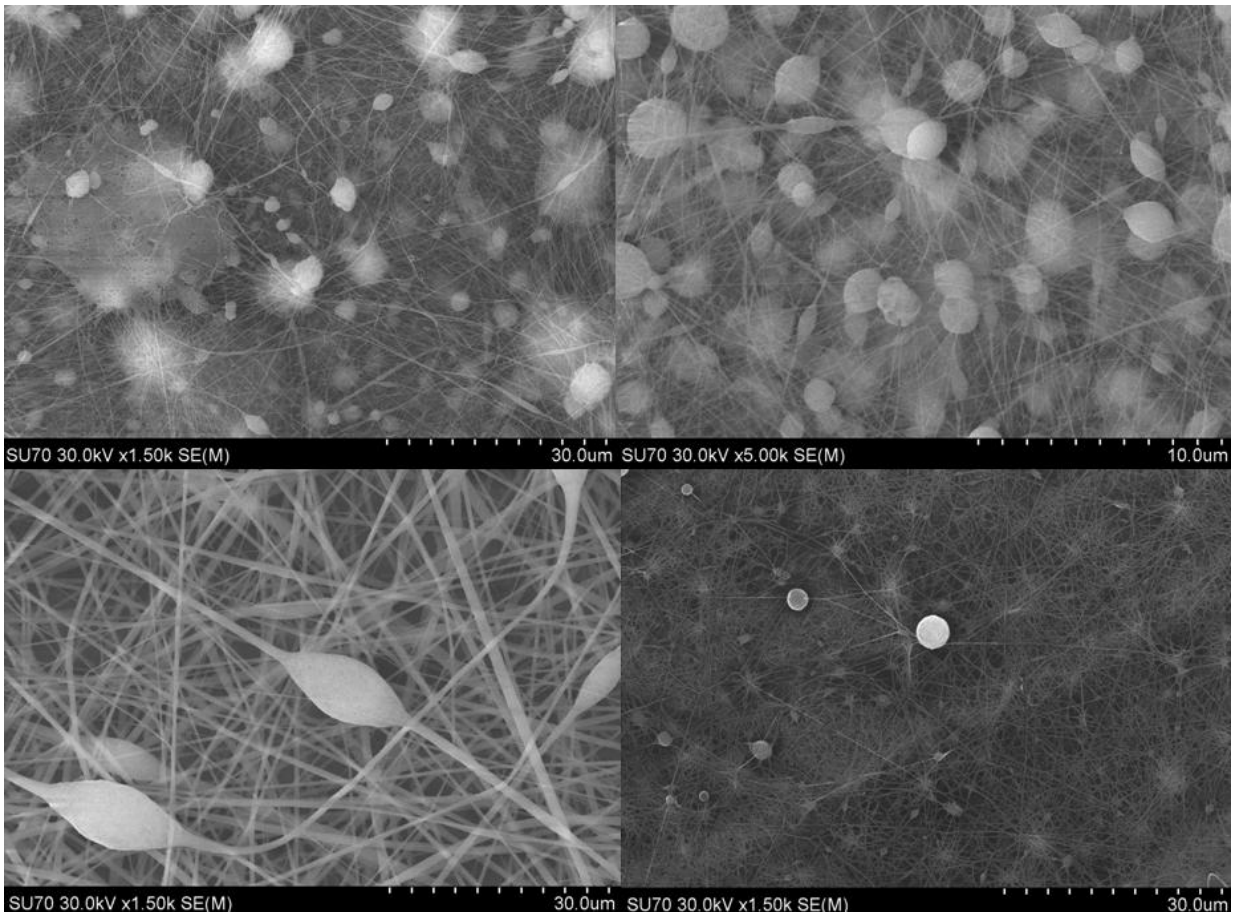

Figure 19. Shows SEM images of different samples with fiber beading.

Beading occurred for many of the samples. Beading is a result of the Rayleigh instability. As the solution jet was pulled, the jet desired to reduce surface area and therefore the surface energy. The level of beading varied significantly from one sample to the next indicating that there was not a single parameter that controlled the beading. In general, samples with a larger average fiber diameter had a lower number of beads. Another observation was that the beads tended to be more spherical in nanofiber webs than in microfiber webs. Another defect referred to as electrospraying is shown in Figure 20.

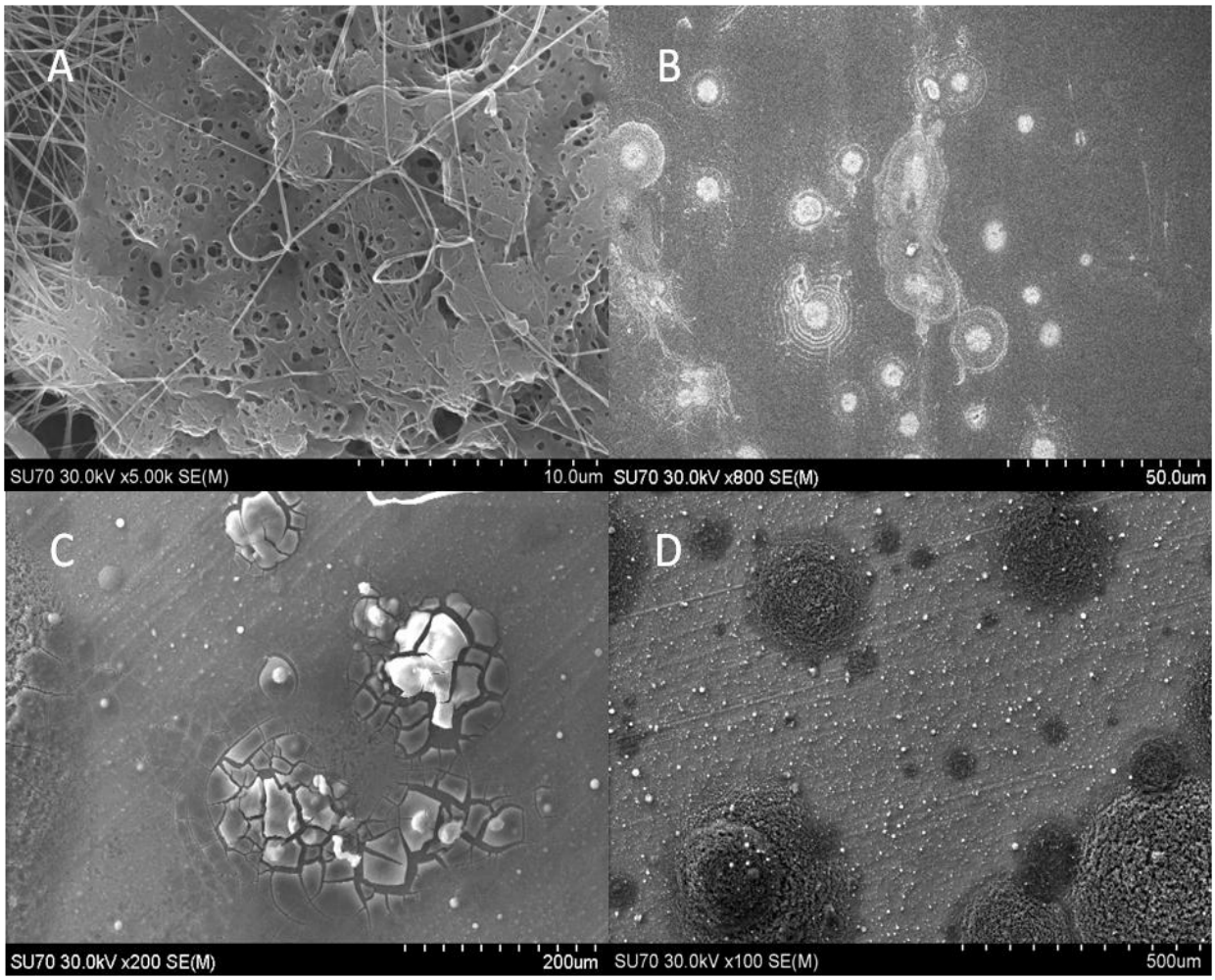

Figure 20. Shows SEM images of different samples with the electrospraying defect.

Electrospraying occurred as the force due to the electric field exceeded the surface tension of the droplet on itself or the forces between the droplet and the needle. The result was a large charged droplet of solution being pulled toward the collector; often this drop would not make it to the fiber web. This resulted in a large amount of solution being wasted. Alternatively, the solution droplet would be pulled toward the collector leaving a pool of solution that would evaporate over a longer period of time leaving a portion of the web with various structural defects. Figure 20 shows the different effects of electrospraying on the web. Sample A shows how pore size is reduced by electrospraying; sample B shows how islands of solution formed on the web; sample C shows how the islands can had an appearance of cracks after drying; sample

D shows another sample with islands of solution with a different morphology. Figures 21 shows PVDF webs produced under processing conditions that resulted in incomplete solvent evaporation.

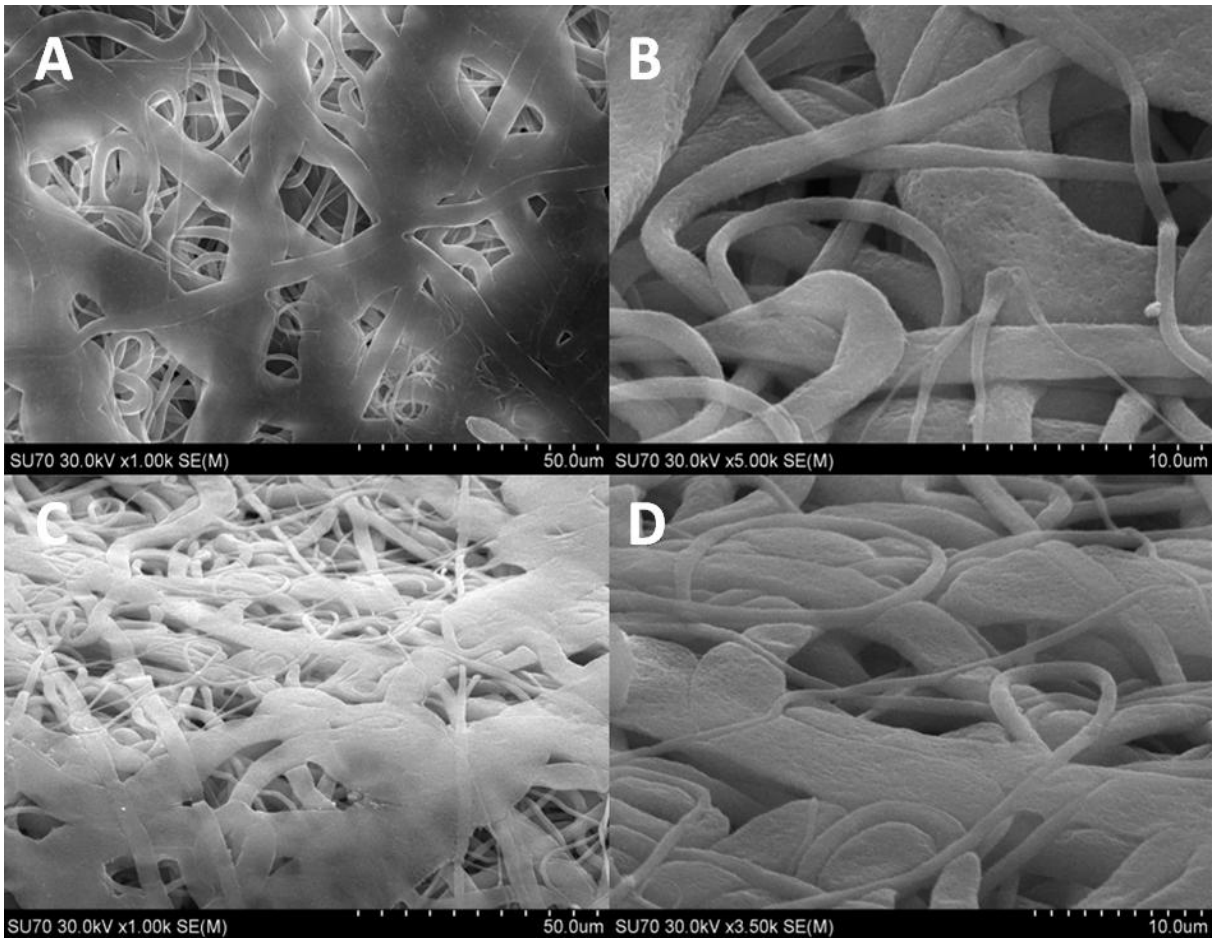

Figure 21. Shows SEM images of different samples with incomplete evaporation. The SEM image of sample A is a top view. SEM images of samples B, C, and D were taken at an angle.

The most notable characteristic of this production defect were asymmetric fibers. Image A shows a top view where images B, C, and D are tilted at an angle to give a different view of the asymmetric geometry. The side view reveals that these fibers appear pressed down. The forces due to the impact of the fiber on the collector as well as the electric force applied to the

polymer solution due to excess charge result in the diameter of the fibers being elongated in the same plan as the collector.

Figure 22 shows four different samples that were produced with procesing paramters that resulted in the fiber bridging from the dispensor to the collector. This created highly unstable conditions that resulted in high levels of beading, high fiber diameter standard deviation, and incomplete evaporation.

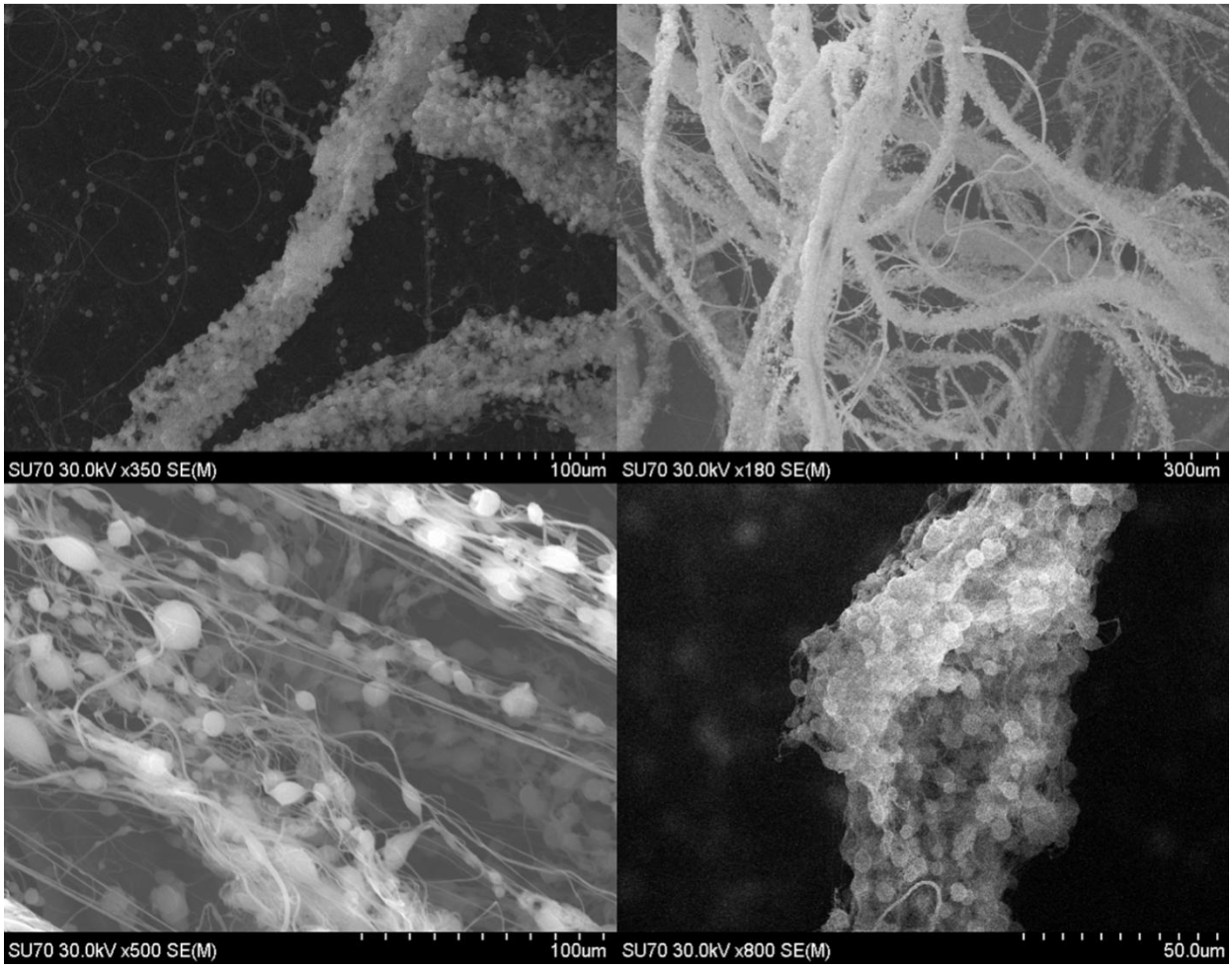

Figure 22. Shows SEM images of PVDF samples where fiber bridging occurred.

When fiber bridging occurred there was not a distinct characteristic of the webs, but rather fiber bridging resulted in a combination of high beading, incomplete solvent evaporation, and electrospraying. There were times when the solution jet came into contact with the bridged fiber

and resulted in a reduced depth of field. When this happened, it did not allow sufficient time for the solvent to evaporate before depositing onto the surface of the bridged fiber. Additional instabilities occurred as there were modifications to the electric field as charges built up on the fiber and current was able to travel along the bridged fiber. Excess charge was reported to influence beading, and this may be the cause of the high levels of beading that were observed in Figure 22.

3.2.5 Defect Free Production Space for Electrospun PVDF Fibers

Over 150 samples were produced within the experimental range and the occurrence of defects was documented. The occurrence of beading, electrospraying, and incomplete evaporation in relation to fiber diameter is shown in Figure 23.

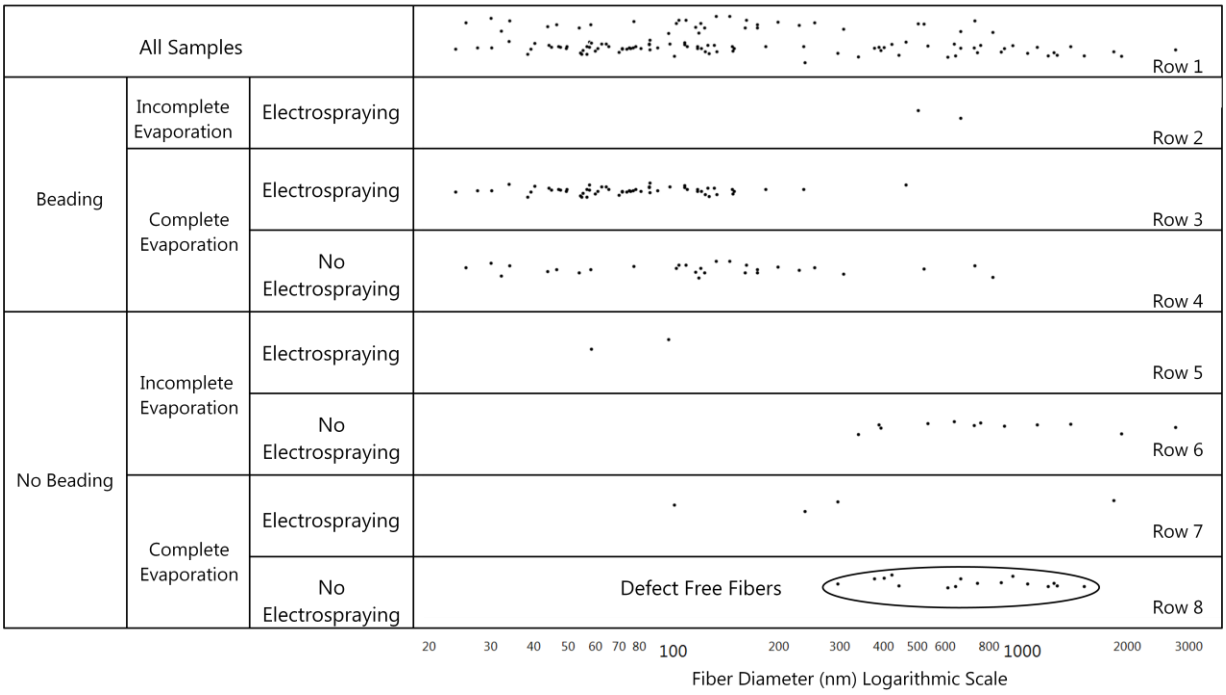

Figure 23. The figure shows the occurrence of defects and defect free fibers in relation to average fiber diameter, where each data point represents one sample. The data points are randomly jittered along the horizontal direction.

Fiber bridging was not included as a separate category since the fiber diameter distribution was bimodal and would not accurately describe the average fiber diameter of the web. In all there were eight samples that fell into the fiber bridging category. In Figure 23 each row represents a separate category. Each data point represents one sample; points are jittered about the horizontal axis in order to avoid overlap of data points. The first row shows all of the samples for this study plotted against the fiber diameter. The low sample count in the second row shows that it was rare for all defects to occur simultaneously. The third row shows that beading and electrospraying were associated with producing fibers below 200nm. The fourth row shows that it was possible to produce fibers that contained beading but no other defects from 25 nm - 800 nm. The fifth row had a couple of samples with no beading but did have the other two defects present. And the sixth row shows that as the average fiber diameter increased there was a higher likelihood of incomplete evaporation.

This trend was expected since the solvent in a thicker solution jet would not evaporate as quickly as the solvent in a smaller diameter jet, because the surface area to solvent volume ratio was much lower for a thicker jet. The seventh row contains a few samples that were free of beading and incomplete solvent evaporation but still had electrospraying.

The eighth row shows that it was possible to produce defect free fibers in a range between approximately 300 nm - 1400 nm. This does not mean it is impossible to produce defect free fibers outside this range, but this research showed that it was possible to produce defect free PVDF fiber in this range. It may be possible to expand this range by understanding how the electrospinning parameters impact the different production defects. In order to do this, the influence of each electrospinning parameter on defect occurrence must be understood.

3.3 Building Predictive Regression Models for Defect Occurrence

The next step was to build regression models from the data collected. The models were built from the orthogonal effects and were based on a coded experimental design. This is standard practice for design of experiments work because it is easier to compare one effect to another. But in order to make the regression equations user friendly, the equations are shown with respect to the actual values and not the coded values. This is why the normalized estimates are not the same as the coefficients for the regression model. The issue with using the inputs as opposed to the coded variables is that it was not as intuitive to compare coefficients. For instance, in the following model for fiber beading the coefficient for X_1 is smaller than the rest of the coefficients and could be mistakenly interpreted to mean that this is the least important term. But the main reason the coefficient is so small is because the input for the molecular weight term is a high numerical value. Therefore, for the equations, it is critical to look at both the coefficient and the input value of the parameter when comparing coefficients in these equations.

3.3.1 Logistic Regression Model for Fiber Beading

The logistic regression equation found for fiber beading is

$$\text{Likelihood Beading} = \frac{1}{(1 + e^{-\text{Lin}[\ \text{No Beading}\ ]})} \tag{10}$$

$$\begin{aligned}\text{Lin[No Beading]} &= -356 - 39.9\,(X_2 + 15.9) + 0.000702\,(X_1 + 32000) \\ &\quad - 58.8\,(X_4 + 1.1) + 221\,(X_4 + 0.592) - 10.7\,X_6 + 1.89\,X_6X_7\end{aligned} \tag{11}$$

$X_1 = \text{Polymer } M_w - 320000 \text{ g/mol}$
$X_2 = \text{Solution Concentration (wt\%)} - 15.9 \text{ wt\%}$
$X_3 = \text{Conductive Additive (wt\%)} - 1.1 \text{ wt\%}$
$X_4 = \text{Solvent Volume Ratio } (V_{Acetone}\ /V_{DMF}) - 0.592$
$X_5 = \text{Pumping Rate (µl/min)} - 25.8 \text{ µl/min}$
$X_6 = \text{Voltage (kV)} - 17.3 \text{ kV}$
$X_7 = \text{Needle Diameter (mm)} - 0.62 \text{ mm}$
$X_8 = \text{Depth of Field (cm)} - 14.5 \text{ cm}$

If the likelihood value was close to 0 then most likely there was not beading; if it was close to one then the formula is predicting beading will occur for that particular set of parameters. The high influence of molecular weight could be due to the visible change in the viscosity of the solution. The viscosity was noticeably higher in solutions with the higher molecular weight of 530,000. Decreasing viscosity increased beading possibly due to the reduced diameter of the electrospinning jet size. For a smaller jet size, it was more energetically beneficial for the jet to break up into beads and eventually drops. If the solvent evaporated quick enough the jet would not have time to break up into drops and instead resulted in beaded fibers. This observation supported the theory that beading was a result of the Rayleigh instability occurring in the jet and as the jet is in the transition stages of breaking into separate droplets it solidified before the bead breaks away from the fiber and forms a droplet. In light of this, the depth of field and the solvent interaction term may be important because as the depth of field changes the time the jet has to break up into beads increases, and the solvent ratio affects the evaporation time of the jet. The voltage influenced the amount of charge in the jet and influenced beading, which is in agreement with what is said in the literature. The interaction between the needle diameter and the voltage may be due to the influence of these parameters on charge concentration at the dispensing tip. The electrospinning current, as measured by the power supply, went above approximately six microamperes, as seen in Figure 24, the fibers were all beaded. This suggests that the charge in the jet does have some influence on the beading of fibers and may provide a route for monitoring beading in some cases. Figure 24 suggests that in order to reduce the likelihood of beading the amount of charge in the electrospinning jet should be minimized. This could be done by changing the conductivity of the solution or by changing the electric field.

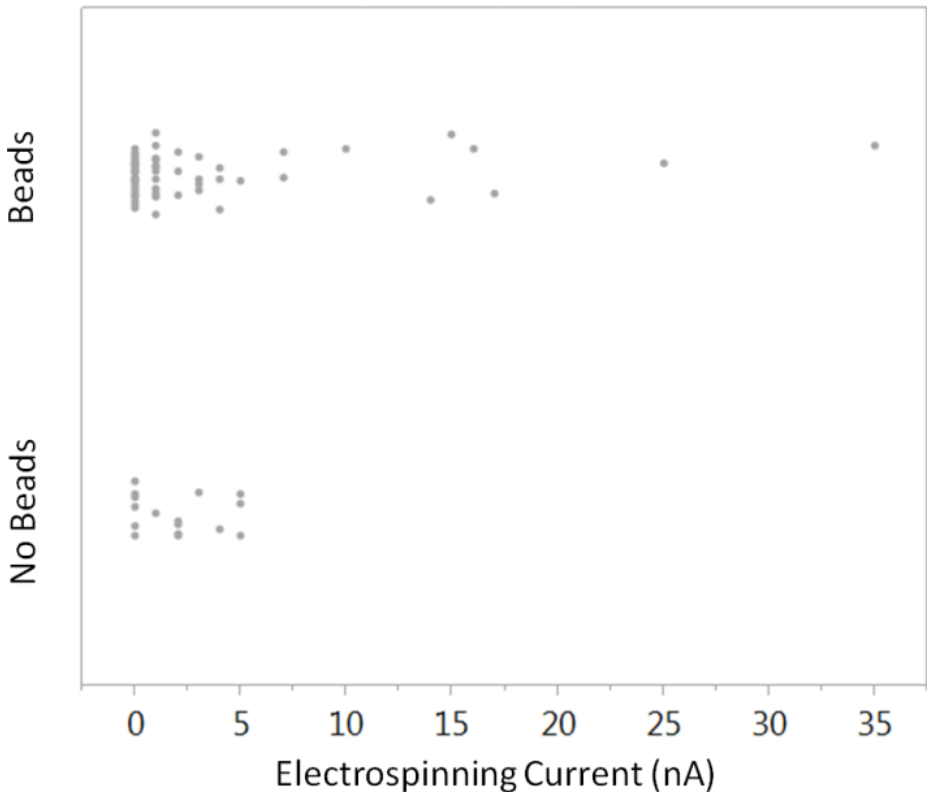

Figure 24. The occurrence of beading with respect to the electrospinning current, each data point represents one sample.

3.3.2 Logistic Regression Model for Electrospraying

The logistic regression equation found for the occurrence of electrospraying is

$$\text{No Electrospraying Likelihood} = \frac{1}{(1 + e^{-\text{Lin}[\quad \text{No Electrospray} \quad]})} \tag{12}$$

$$\begin{aligned}\text{Lin[No Electrosrpay]} &= -3.68 + 4.46\,(X_4 + 0.592) - 3.23\,(X_3 + 1.1) \\ &- 0.30\,(X_5 + 25.8) + 2.6\,X_2X_3 + 1.8 * 10^{-5}\,X_2X_1 \\ &+ 3.2 * 10^{-10}\,(X_1)^2 + 0.00593\,(X_5)^2\end{aligned} \tag{13}$$

$X_1 = \text{Polymer } M_w - 320000 \text{ g/mol}$
$X_2 = \text{Solution Concentration (wt\%)} - 15.9 \text{ wt\%}$
$X_3 = \text{Conductive Additive (wt\%)} - 1.1 \text{ wt\%}$
$X_4 = \text{Solvent Volume Ratio } (V_{Acetone} / V_{DMF}) - 0.592$
$X_5 = \text{Pumping Rate (µl/min)} - 25.8 \text{ µl/min}$
$X_6 = \text{Voltage (kV)} - 17.3 \text{ kV}$
$X_7 = \text{Needle Diameter (mm)} - 0.62 \text{ mm}$
$X_8 = \text{Depth of Field (cm)} - 14.5 \text{ cm}$

If the likelihood value is close to 0 then most likely there will not be electrospraying; if it is close to one then the formula is predicting electrospraying will occur for that particular set of parameters.

Once again the molecular weight played an important role in influencing the occurrence of this defect. As mentioned in the previous section on beading the same phenomenon applied for the molecular weight, only this time there was enough time for the electrospinning jet to break up into droplets. The conductivity of the solution played a significant role in the occurrence of electrospraying. As the conductivity of the solution increased the number of charge carriers increased. It may be that electric force per unit volume of solution was increased. When the electrostatic force in the droplet increased it allowed a jet to form. If the force was not high enough to form a jet the alternative was that the electrostatic force caused the solution from the dispenser to pull away, causing electrospraying. The pumping rate affects the mass transfer rate. As the mass transfer rate was increased electrospraying occurred more frequently. The mass transfer rate increased the size of the droplet at the tip of the syringe. Often this resulted in initial conditions that were in constant flux as the droplet increased to a point where the electric charge was large enough to pull the droplet away from the needle and to the collector, and then repeat the process. This would increase the vibrational perturbation of the droplet. Vibrational perturbation can cause the jets to break up and bead and explains why in the majority of cases where electrospraying was present so were beaded fibers.

This study reinforced earlier findings that the solution concentration plays a key role in the transition from electrospray to electrospinning due to the change in viscosity [104]. Although the finding were not as pronounced because the investigated range of solution concentration was not as large in our case. The molecular weight, solutions concentration, pumping rate suggest the

flow characteristic were important, therefore, the influence of Reynolds number on electrospraying was investigated. Electrospraying occurred at many different Reynolds numbers, but as the Reynolds number went above 0.005 all of the samples showed electrospraying as seen in Figure 25. Figure 25 suggests that at high mass transfer rates solutions with low viscosities should be avoided in order to reduce the occurrence of electrospraying. It was possible for electrospraying to occur at low Reynolds numbers suggesting there were other factors that contributed to the occurrence of electrospraying.

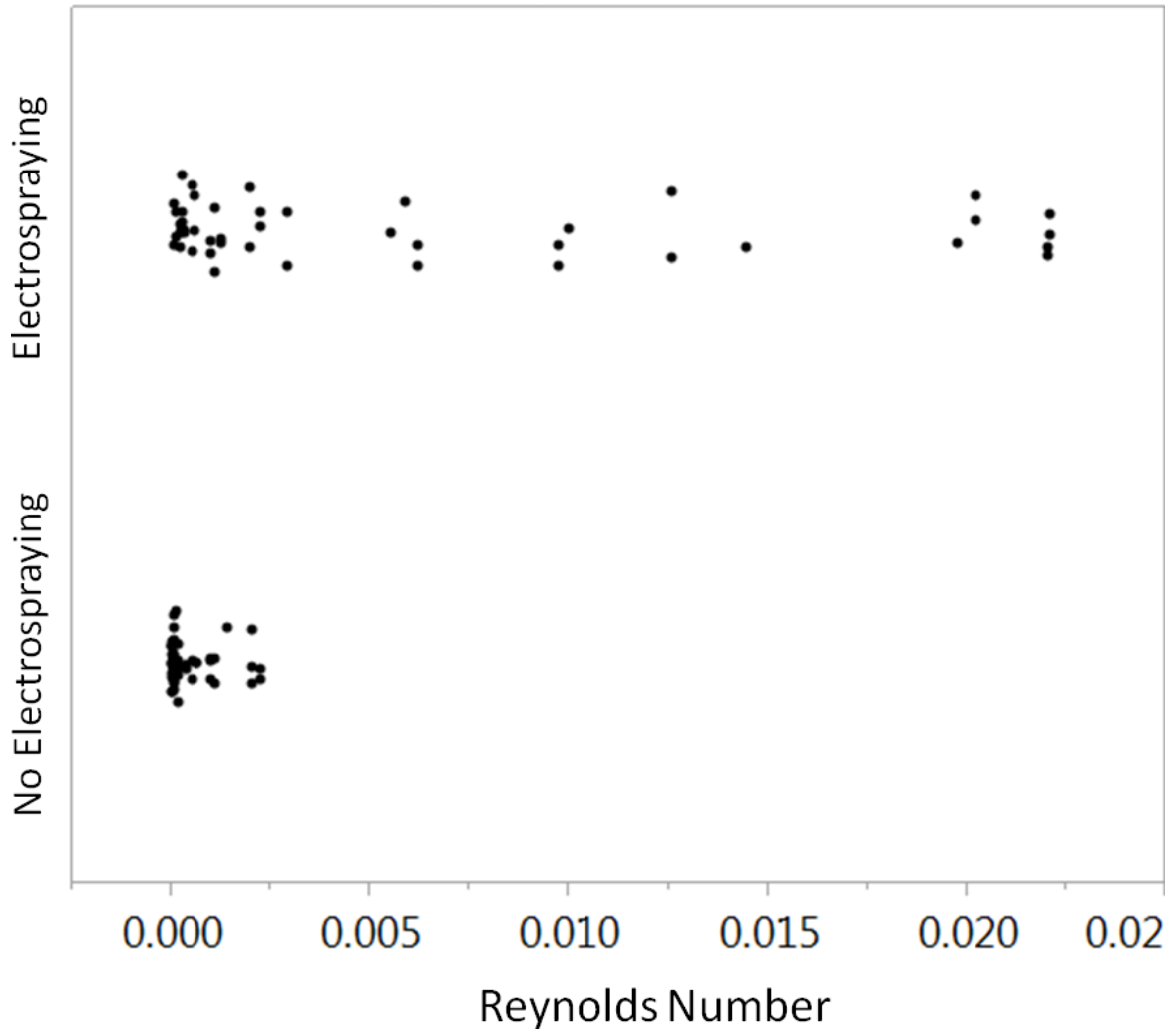

Figure 25. The occurrence of electrospraying with respect to the Reynolds number, each data point represents one sample.

3.3.3 Logistic Regression Model for Complete Solvent Evaporation

The logistic regression equation found for complete solvent evaporation is shown below

$$\text{Complete Evaporation Likelihood} = \frac{1}{(1 + e^{-\text{Lin}[\ \text{No Complete Evaporation}\ ]})} \tag{14}$$

$$\begin{aligned}\text{Lin[No Complete Evaporation]} &= -14.04 + 9.96\,(X_7 + 0.62) + 2.04 * 10^{-5}\,(X_1 \\ &+ 32000) - 0.417\,(X_8 + 14.5) + 1.16\,X_2X_6 - 2.15\,X_4X_6 \\ &- 0.98\,X_2X_8 - 2.33 * 10^{-6}\,X_1X_8\end{aligned} \tag{15}$$

$X_1 = \text{Polymer } M_w - 320000\ \text{g/mol}$
$X_2 = \text{Solution Concentration (wt\%)} - 15.9\ \text{wt\%}$
$X_3 = \text{Conductive Additive (wt\%)} - 1.1\ \text{wt\%}$
$X_4 = \text{Solvent Volume Ratio } (V_{Acetone}\ /V_{DMF}) - 0.592$
$X_5 = \text{Pumping Rate (µl/min)} - 25.8\ \text{µl/min}$
$X_6 = \text{Voltage (kV)} - 17.3\ \text{kV}$
$X_7 = \text{Needle Diameter (mm)} - 0.62\ \text{mm}$
$X_8 = \text{Depth of Field (cm)} - 14.5\ \text{cm}$

If the likelihood value is close to 0 then most likely there will be complete evaporation; if it is close to one then the formula was predicting incomplete evaporation for that particular set of parameters. The following were proposed reasons why the terms in the model influenced the occurrence of complete evaporation: The solution parameters, needle diameter, and pumping rate all influenced the flow characteristics. Therefore instead of discussing each parameter individually the Reynolds number was investigated. Figure 26 shows the occurrence of complete evaporation with respect to the Reynolds number. As the Reynolds number increased the occurrence of incomplete evaporation decreased. Incomplete evaporation tended to occur at lower Reynolds number most likely due to the increased viscous forces. As the viscosity was larger the jet diameter was larger and took longer to evaporate. In addition to the flow characteristics as the voltage was increased the electric force applied to the droplet was increased and may influence how much material was being pulled towards the collector. This may have

occurred by increasing the size of the jet or by increasing the number of jets being pulled from the droplet. The molecular weight term may be significant because of this jet size dependence.

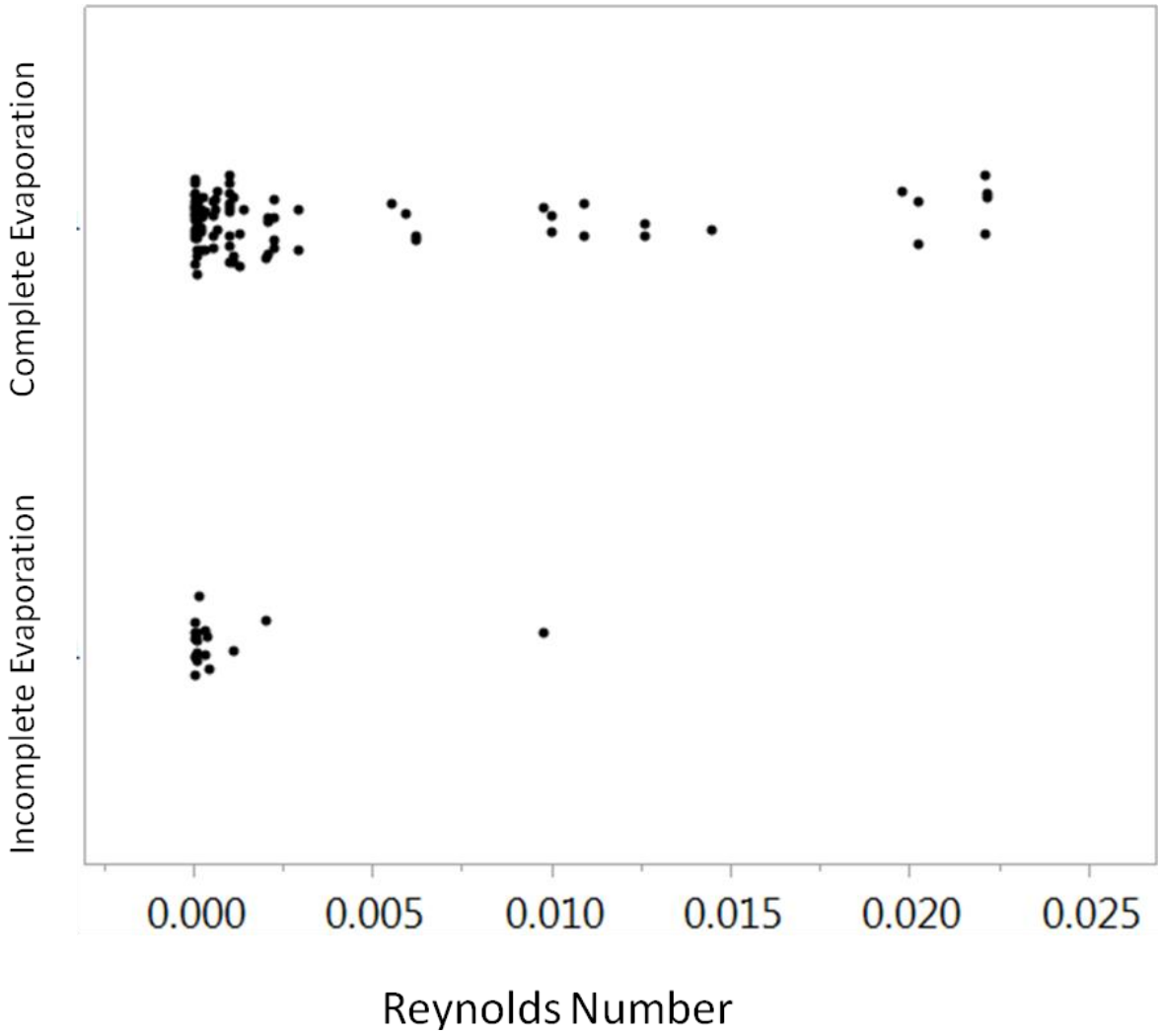

Figure 26. The occurrence of complete evaporation with respect to the Reynolds number, each data point represents one sample.

Also, the solution being pulled towards the collector would be dependent on the surface tension which was influenced by the solvent ratio which was another significant term. As the surface tension increased, incomplete evaporation tended to occur more frequently as shown in Figure 27.

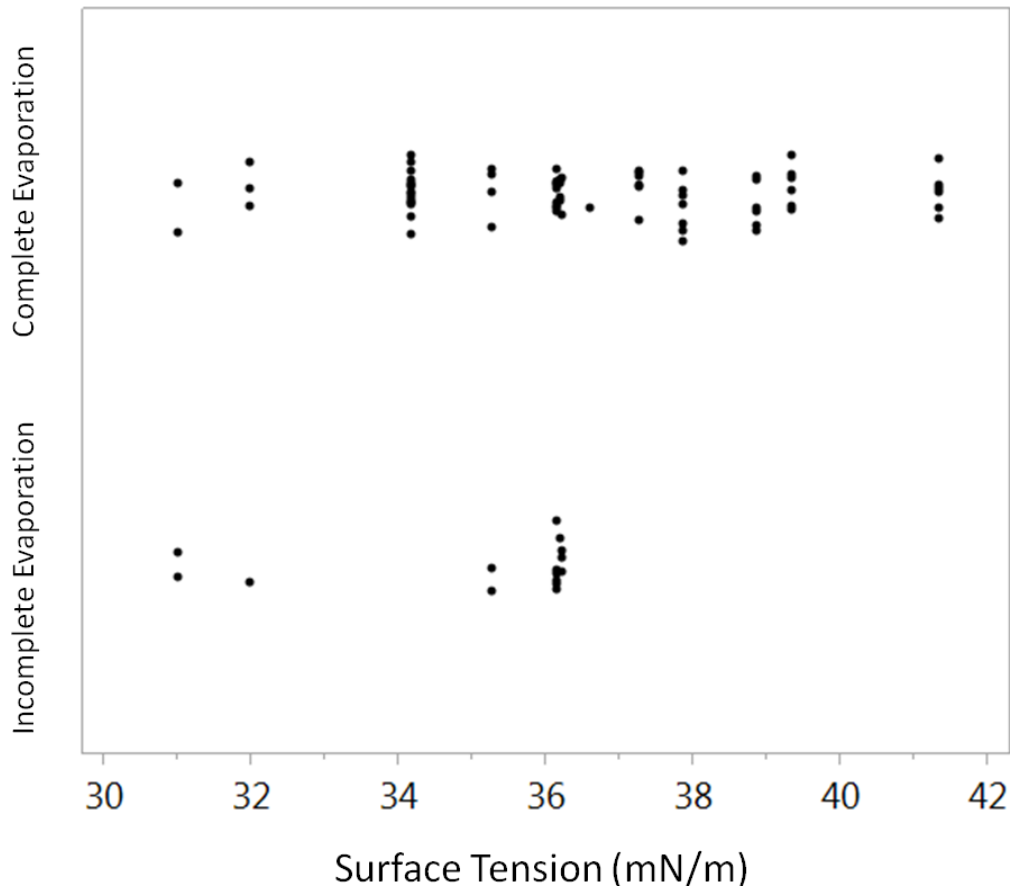

Figure 27. The occurrence of complete evaporation with respect to the surface tension, each data point represents one sample.

Figure 27 supports the theory that at lower surface tensions more solution is pulled toward the collector. The jets with more solution require longer times to evaporate. In addition to the solution properties, the voltage interacted with the depth of field. Increasing the voltage increased the jet size in some cases, but this affect was mitigated by increasing the depth of field which allowed more time for the jet to travel through the system. It should be noted that incomplete solvent evaporation may reduce the degree of molecular chain alignment. It was reported that chain alignment was dependant on the evaporation time and the chain relaxation time; therefore, it is desirable to have high evaporation rates in order to maximize chain orientation [80]. Consequently, incomplete solvent evaporation could reduce the piezoelectric properties of the webs.

3.3.4 Logistic Regression Model for Bridging Dispenser to the Collector

The logistic regression equation found for bridging likelihood is

$$\text{Bridging Likelihood} = \frac{1}{(1 + e^{-\text{Lin}[\ \text{No Fiber Bridge}\ ]})} \tag{16}$$

$$\begin{aligned}\text{Lin[No Fiber Bridge]} &= 27 + 2.7\,(X_3 + 1.1) + 3.1 * 10^{-5}\,(X_1 + 32000) - 2.83\,(X_2 \\ &+ 15.9) + 0.30\,(X_2 + 1.1) + 2.95 * 10^{-5}\,X_1X_2 + 0.67\,X_2X_6\end{aligned} \tag{17}$$

$X_1 = \text{Polymer } M_w - 320000\ \text{g/mol}$
$X_2 = \text{Solution Concentration (wt\%)} - 15.9\ \text{wt\%}$
$X_3 = \text{Conductive Additive (wt\%)} - 1.1\ \text{wt\%}$
$X_4 = \text{Solvent Volume Ratio } (V_{Acetone}\ /V_{DMF}) - 0.592$
$X_5 = \text{Pumping Rate } (\mu l/min) - 25.8\ \mu l/min$
$X_6 = \text{Voltage (kV)} - 17.3\ \text{kV}$
$X_7 = \text{Needle Diameter (mm)} - 0.62\ \text{mm}$
$X_8 = \text{Depth of Field (cm)} - 14.5\ \text{cm}$

If the likelihood value is close to 0 there will most likely not be bridging; if the probability is closer to 1 then most likely there will be bridging. Because the conductivity term is in Equation 17, it is suggested that the conductivity of the solution influenced the occurrence of fiber bridging. This is most likely because as the conductivity increased the force on the jet increased. The increased number of charge carriers allowed the fiber to be pulled toward the dispenser.

Once again the important terms in the model suggest that the viscosity and evporation rate were important as well. Increasing the solution concentration decreased the liklihood of bridging, this is due to a decrease in the amont of solvent that needed to evaporated from the jet. The voltage which impacted the electric field provided and influenced the forces on the fiber. As soon as a fiber formed that did not deposit to the collector but was only fixed at one end. It became energetically favorable for the subsequent jet to deposoit on the protruding fiber.

3.4 Validating the Defect Free Range for Electrospinning

The next step was to verify regression models were accurately predicting the occurrence of beading for the data collected. The R^2 values were used to determine the goodness of fit. The R^2 values for the models of the fiber beading, incomplete evaporation, electrospraying, and bridging were 0.93, 0.87, 0.79, and 0.71 respectively. One should note that this method was limited by the low occurrence of defects in some cases. For instance, there were eight cases of fiber bridging; therefore, only a few terms could be in the model without over fitting the available data. This may be one reason the goodness of fit was lower for fiber bridging.

This method was able to identify parameters that were significant in this experiment and should be accounted for when producing PVDF fiber webs. Additional experiments could reveal that other parameters are significant, even ones investigated in this study; but, there was not enough evidence in this study to suggest they were influencing the occurrence of defects. The high R^2 value means that the variation was accounted for by the model parameters.

Table 5 shows the number of correctly predicted values and incorrectly predicted values when the equations were applied to the defect occurrence data that was collected in this study.

Table 5. Validation of defects models.

Defect Type	Number of Correctly Predicted Values	Number of Incorrectly Predicted Values	Number Not Observed
Beading	134	3	12
Incomplete Evaporation	131	10	16
Electrospraying	131	5	14
Bridging	148	3	4

By creating a new model that is dependent on the findings from the four individual models, it is possible to create a comprehensive way to predict the occurrence of defects.

This new model can be built by using logistical operators and the four logistic regression models. The new model works by inputting a single set of parameters or a matrix of parameters.

Then, each logistic regression equation is checked one by one for the occurrence of a defect. If no equation predicts a defect then the likelihood of a defect occurring during production is low. Using this approach, generated thousands of data points and identified new areas to explore for defect free fiber web production. But further experimentation is needed to explore the production space outside of what was investigated in this research.

3.5 Production Guidelines

While the regression equations are, a streamlined understanding would also be beneficial for understanding how each individual parameter influences all four defects. This was done by establishing guidelines based on the orthogonal regression coefficients. Each normalized coefficient was put into the following scale based on the following value of that ratio: 0 - 0.1 very small, 0.10 - 0.35 small, 0.35 - 0.65 medium, 0.65 - 0.90 large, and 0.90 - 1.0 very large. A positive sign indicates a direct correlation, and a negative sign indicates an indirect correlation. The methodology is outlined in Table 6 for fiber beading.

Table 6. Development of guidelines for fiber beading using the regression coefficients.

Term	Orthogonal Regression Coefficient	Interpretation	Normalized by Regression Coefficient	Guideline Based on Normalized Value
Solution Concentration	24.1	Increasing solution concentration increased the likelihood of beading.	0.323	+Small (0.1-0.35)
Solvent Ratio	-50.0	Increasing solvent ratio decreased the likelihood of beading.	-0.669	-Large (0.65-0.9)
Conductive Additive	53.4	Adding the conductive additive increased the likelihood of beading.	0.716	+Large (0.65-0.9)
Molecular Weight	-74.5	Increasing the molecular weight decreased the likelihood of beading.	-1	-Very Large (0.9-1)
Voltage	15.6	Increasing voltage increased the likelihood of beading.	0.21	+Small (0.1-0.35)
Voltage · Needle Diameter	15.7	Increasing voltage and needle diameter at the same time increased the likelihood of beading.	0.210	Small (0.1-0.35)

Table 7 shows the guidelines developed for all significant parameters for all four defects. Parameter interactions that were not significant, such as the interaction between the pumping rate

and voltage, are not listed in the table. A dashed entry signifies that the parameter did not have a statistically significant impact in that category.

Table 7. Guidelines for reducing defects for electrospun PVDF webs.

Electrospinning Parameters	Influence on Defect Likelihood			
	Beading	**Electrospraying**	**Incomplete Evaporation**	**Bridging**
Solution Parameters				
Solution Concentration	+Small	-	-	-Medium
Solvent Ratio	-Large[6]	-Small	-	-
Molecular Weight	-Very Large[4]	-Very Large	+Very Large	+Very Large
Conductive Additive	+Large	+Medium	-	+Large
Processing Parameters				
Voltage	-Small	-	-	-
Depth of Field	-	-	-Medium	-Small
Pumping Rate	-	+Medium*	-	-
Needle Diameter	-	-	-Medium	-
Parameter Interactions				
Solution Concentration and Molecular Weight	-	-Small [11]	-	+Large
Solution Concentration and Conductive Additive	-	-Medium [11]	-	-
Solution Concentration and Depth of Field	-	-	-Very Large	-
Solution Concentration and Voltage	-	-	+Medium	-Small
Solvent Ratio and Voltage	-	-	-Small	-
Molecular Weight and Depth of Field	-	-	-Medium	-
Voltage and Needle Diameter	-Small [10]	-	-	-

*Parameter includes the coefficient from the quadratic term.

The guidelines with references next to them indicate that the finding was previously reported and supports the finding of this study. By using these guidelines, the influence of parameters on the likelihood of occurrence for multiple defects can be anticipated.

Chapter 4: Controlling the Structure of Fiber Webs

4.1 Introduction to Controlling the Structure of Fiber Webs

The control of defect occurrence was documented in Chapter 3, and, therefore, defects can be used to change the structure of fiber webs. In addition to defects, the structure of electrospun fibers was reported to influence the functionally of the PVDF fiber webs [40, 41, 101, 105]. Therefore, the functional properties of electrospun PVDF webs can be controlled if the structure of the webs can be controlled. In addition to defects, there was also the structure of the fibers and beads in the web. These were also important to control, Pham stated that the, "precise control of fiber morphology will be necessary for improved scaffold designs and better recreate the functions of native extracellular matrix" [40]. Also, the level of beading and the fiber diameter influenced the contact angle for fiber webs [41]. Likewise, the frequency of beading nodes was reported to affect the water collecting ability of biologically inspired fibers [105]. Beaded fibers were also suggested for photonic applications by utilizing nanoscale features [101]. But, because the majority of studies focused on the influence of web structure on the desired application, little is known on how to produce fiber webs with precise fiber and bead structures.

Until now, the structure of PVDF fibers was investigated using trial and error methods or by using what was reported in the literature as a starting point. Then, if possible, a desired structure would be controlled by utilizing single parameter relationships. For instance, if a larger fiber diameter was needed, the solution concentration was increased over a couple settings. This was successfully only in cases where there were no defects which limited the production space.

This required a large amount of time spent finding a viable set of production parameters for each desired application. Only a few reports looked at controlling the structure of beads [82, 94] and they did not present any method for controlling the structure of fibers and beads at the same time. Also they did not consider any interactions between control parameters which limited the ability of the trends to a small production space. By understanding the influence of parameters on the average fiber diameter, average bead diameter, and the number of beads per area the systems understanding of the electrospinning process would be greatly enhanced.

4.2 Experimental Setup

A similar experimental setup and design was used to develop regression models in order to identify and quantify which electrospinning parameters would influence the web structure. There were not any changes made to the original electrospinning setup used previously and shown in Figure 17. The ranges of the solution parameters and processing parameters were expanded from the previous investigation, shown in Table 4, and the system parameters were added parameters and were listed in Table 8.

Table 8. Electrospinning parameters and ranges explored for controlled web structure.

Solution Parameters	**Lowest Setting**	**Highest Setting**
Polymer Mw	180,000 g/mol	530,000 g/mol
Solution Concentration	14 wt%	18 wt%
Conductive Additive	None	4.5 wt% TBAC
Solvent Ratio	0.5 to 9.5 Acetone to DMF	6.5 to 3.5 Acetone to DMF
Processing Parameters	**Lowest Setting**	**Highest Setting**
Pumping Rate	0.5 µl/min	72.5 µl/min
Voltage	12 kV	23 kV
Needle Diameter	22 gauge	18 gauge
Depth of Field	6 cm	32 cm
System parameters	**Lowest Measured**	**Highest Measured**
Surface Tension	31.0 mN/m	41.3 mN/m
Electric Field	2 kV/m	0.75 kV/m
Reynolds Number	0.0002	2.2
Electrospinning Current	0 µA	35 µA

The electrospinning solutions were prepared the same way as in Chapter 2. The solutions were tested to determine their viscosity and surface tension. Viscosity of the solutions was measured using a Fungilab Alpha R rotational viscometer. Surface tension measurements were made using a KSV Sigma 701 Tensiometer. For both the viscosity and the surface tension multiple measurements were taken to ensure a repeatable value. The viscosity and surface tension measurements can be found in Table 9.

Table 9. Measurements of viscosity and surface tension for different solutions.

Solution Concentration (wt%)	Acetone to DMF Ratio	TBAC (wt%)	Molecular Weight (g/mol)	Viscosity (cP)	Surface Tension (mN/m)
15	2 to 8	3	180,000	128	36.18
15	1 to 1	3	180,000	461	41.32
15	2 to 8	0	180,000	136	34.16
15	1 to 1	0	180,000	118	38.84
17	2 to 8	3	180,000	193	35.26
17	1 to 1	3	180,000	15,066	37.25
17	2 to 8	0	180,000	234	37.85
17	1 to 1	0	180,000	5,324	39.32
15	2 to 8	3	530,000	Out of Range	36.58
15	1 to 1	3	530,000	13,127	31.98
15	2 to 8	0	530,000	5,163	36.15
15	1 to 1	0	530,000	7,341	31.60
17	2 to 8	3	530,000	18,511	36.21
17	1 to 1	3	530,000	140,821	31.01
17	2 to 8	0	530,000	15,839	Out of Range
17	1 to 1	0	530,000	44,359	Out of Range

The viscosity was used to calculate the Reynolds number of the flow through the needle. It should be noted that this was different than the flow during travel from the dispenser to the collector that others have reported. The electric field was calculated from the voltage and depth of field settings. And the electrospinning current was measured across the power supply.

Before the data collection, it was important to establish repeatability and time independence of the web structures. Figure 28 shows different samples made under identical electrospinning solution parameters and processing parameters. The only controlled parameter

that differed was the electrospinning time. Sample A had an electrospinning time of 20 min with an average fiber diameter of 661 nm; sample B had an electrospinning time of 30 min with an average fiber diameter of 642 nm; and, sample C had an electrospinning time of 120 min and an average fiber diameter of 658 min. The average fiber diameter for each sample was close for each case, with standard deviation around 10nm, and therefore time was not considered to be an important variable. The low variance in fiber diameter over the 120 minutes suggested that time did not play a significant role in the electrospinning process. For this work, the majority of samples were spun between 10 min and 30 min.

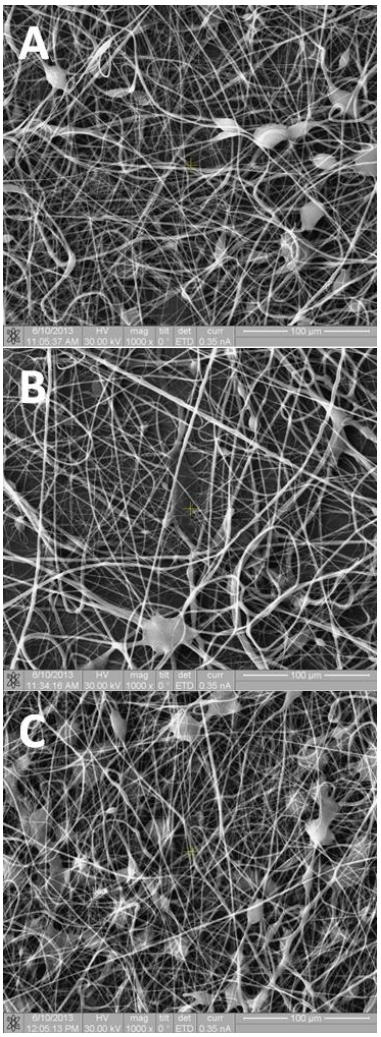

Figure 28. These SEM images show PVDF webs produced using the same electrospinning parameters for different deposition times.

4.3 Experimental Results

The experimental setup and design produced over 184 PVDF fiber webs; 64 of these were replicates. Over 2000 SEM images were taken and used to measure over 18,000 fiber diameters and over 2,800 bead diameters. Figure 29 shows SEM images of two different samples and the distribution for fiber diameter and bead diameter of each sample.

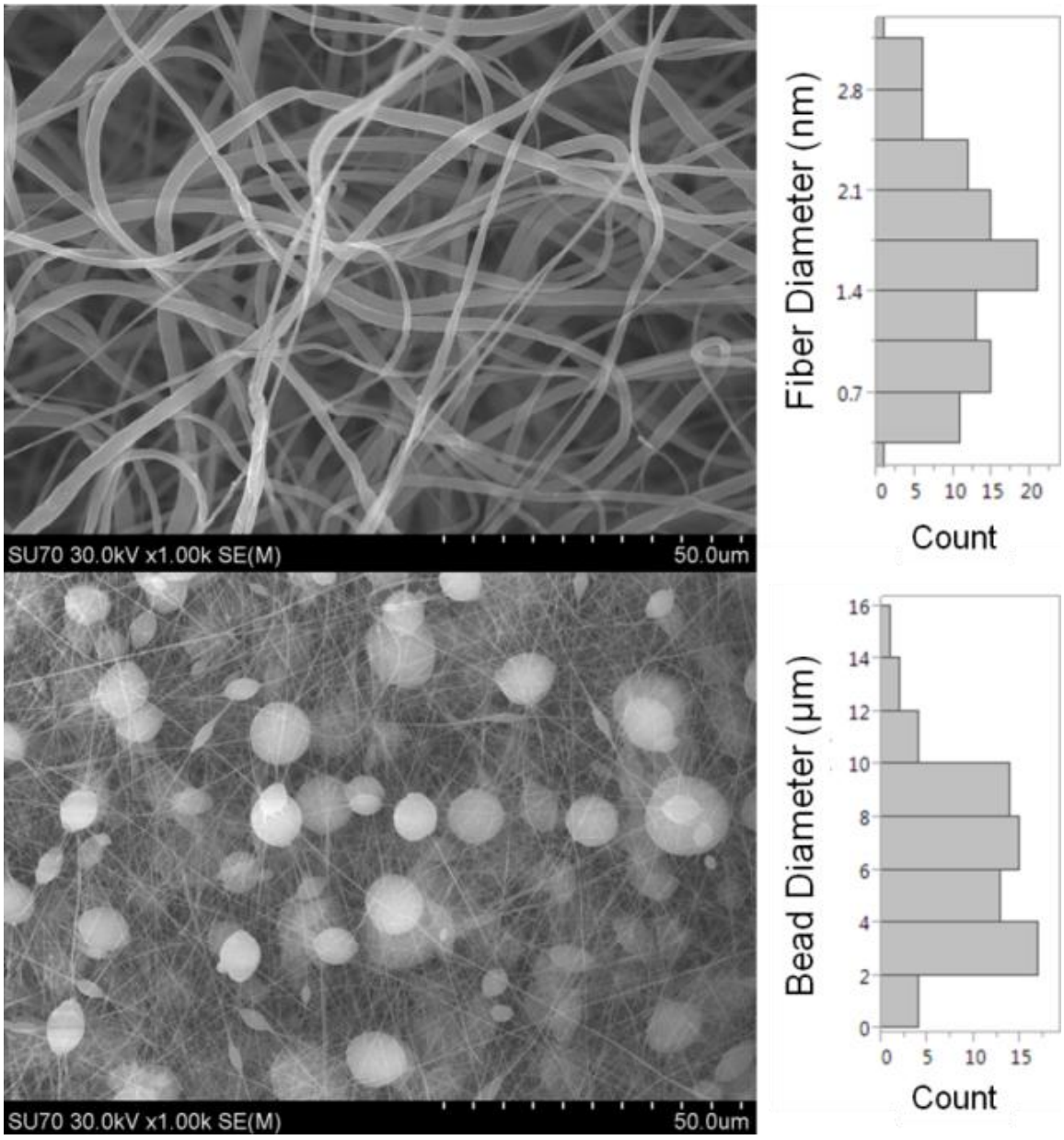

Figure 29. These SEM images show representative PVDF webs and show the average fiber diameter and average bead diameter distribution of the respective sample.

Figure 30 includes different samples produced using the experimental design with different fiber diameter, bead nodes per area, and bead diameters.

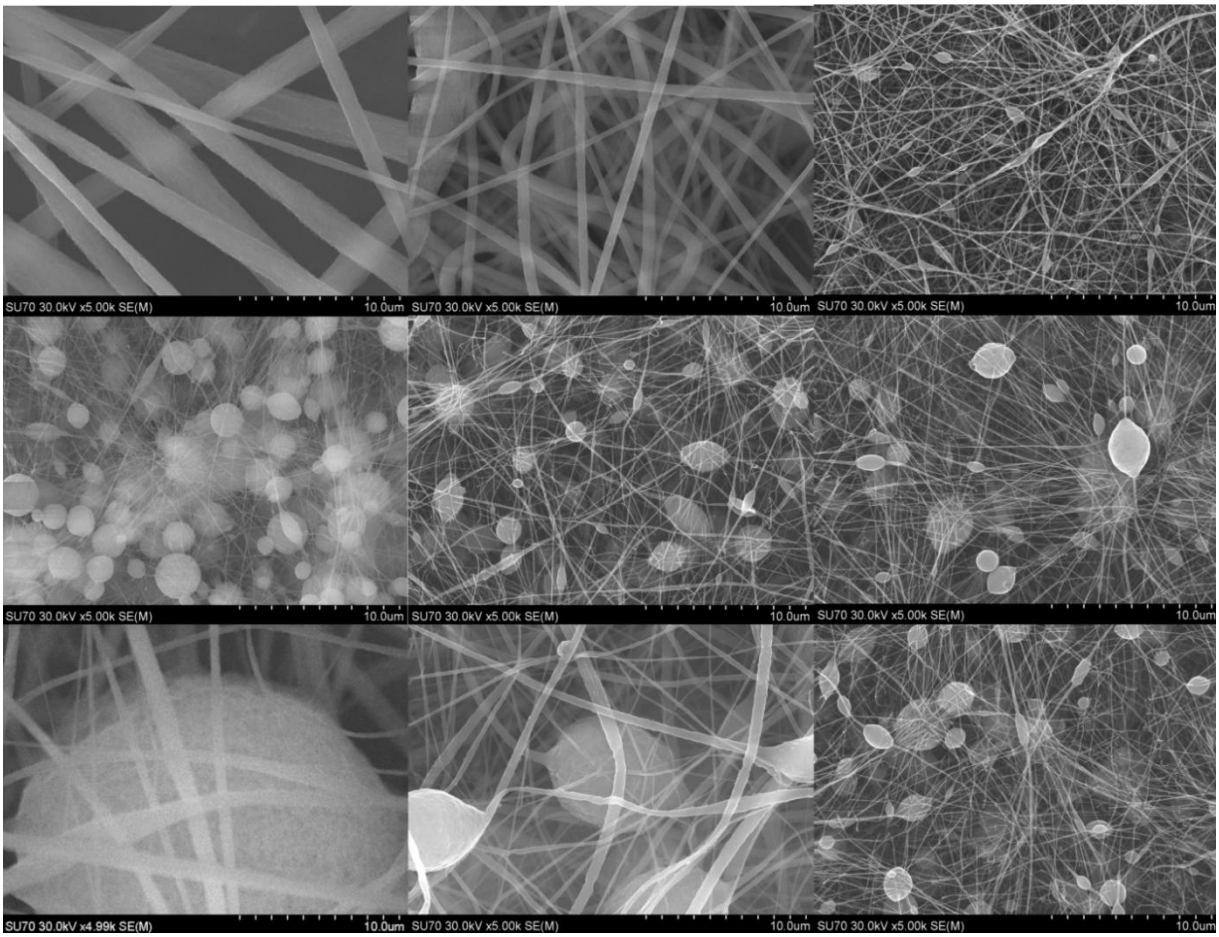

Figure 30. These images were taken at the same magnification and show PVDF fibers with a wide range of fiber diameter, bead nodes per area, and bead diameters.

The ranges measured for each metric are reported in Table 10. The wide ranges in each of the metrics indicated large variations in structure were attainable within the experimental design.

Table 10. Ranges of measured web metrics.

Metric	Range
Average Fiber Diameter	20 nm – 2400 nm
Average Bead Diameter	0.23 µm – 16 µm
Bead Nodes/mm^2	0 – 4.96 x 10^6

The parameter settings for the largest and smallest measured values of each metric are reported in Table 11.

Table 11. Parameter settings for the largest and smallest measured values.

Desired Property	Solution Concentration (wt%)	Solvent Ratio	Conductive Additive (wt%)	Molecular Weight (g/mol)	Voltage (kV)	Depth of Field (cm)	Pumping Rate (5µl/min)	Needle Diameter (mm)
Lowest Fiber Diameter	15	2 to 8	0	180000	10	10	27	0.838
Largest Fiber Diameter	17	1 to 1	0	530000	20	10	50	0.413
Lowest Bead Diameter	15	1 to 1	0	180000	10	10	5	0.413
Largest Bead Diameter	17	1 to 1	0	530000	20	15	5	0.413
No Beading	17	1 to 1	0	530000	20	10	50	0.413
Most Bead Nodes/Area	15	2 to 8	0	180000	10	10	5	0.413

There were many samples with zero bead nodes per area, but only one is reported in Table 1 for brevity. With all the parameters that were changed during the experiment between different samples, it was not possible to know what was causing the change in structure without a regression analysis.

4.4 Regression Models for Different Structures

The next step was to determine which parameters were influencing the web structure. A statistical analysis was conducted in order to investigate the influence of each parameter and interaction on the three fiber metrics: average fiber diameter, average bead diameter, and the number of bead nodes per area. Three regression equations were built based on the statistical analysis. First the important model terms are discussed. Then afterwards, the coefficients of the regression model were discussed.

4.4.1 Regression Model for Fiber Diameter

The regression equation for fiber diameter had an R^2 value of 0.84 and an adjusted R^2 value of 0.82. The regression equation is

$$\begin{aligned}\text{Fiber Diameter (nm)} &= -1400 + 1.08 * 10^{-3}\,(X_1 + 32000) + 48.5\,(X_2 + 15.9) \\ &+ 343\,(X_4 - 0.592) + 3.6\,(X_5 + 25.8) + 3.2 * 10^{-5}\,X_5X_1 \\ &+ 2.67 * 10^{-4}\,X_2X_1 + 4.39\,X_5X_4 + 1.84 * 10^{-3}\,X_4X_1 \\ &+ 35.6\,X_4X_6 - 247\,(X_4)^2 + 1.26 * 10^{-8}\,(X_1)^2\end{aligned} \quad (18)$$

$X_1 = \text{Polymer } M_w - 320000 \text{ g/mol}$
$X_2 = \text{Solution Concentration (wt\%)} - 15.9 \text{ wt\%}$
$X_3 = \text{Conductive Additive (wt\%)} - 1.1 \text{ wt\%}$
$X_4 = \text{Solvent Volume Ratio } (V_{Acetone}\ /V_{DMF}) - 0.592$
$X_5 = \text{Pumping Rate (µl/min)} - 25.8 \text{ µl/min}$
$X_6 = \text{Voltage (kV)} - 17.3 \text{ kV}$
$X_7 = \text{Needle Diameter (mm)} - 0.62 \text{ mm}$
$X_8 = \text{Depth of Field (cm)} - 14.5 \text{ cm}$

Our findings supported previous observations that as molecular weight and solution concentration increased the fiber diameter increased. However, we found that as the relative amount of acetone increased in the solvent mixture the diameter of the fiber increased which was not in agreement with previous reports [64, 71].

The addition of the conductive additive increased the fiber diameter. As an inorganic salt, this additive is expected to reduce the surface tension and increase conductivity. The reduction in surface tension may allow a larger jet to form, and as the solution conductivity increased the electrostatic force on the jet increased and may have caused an increase in the size of the electrospinning jet. As the pumping rate increased the fiber diameter increased. This was attributed to a change in the shape of the droplet at the dispensing tip. It was observed that as the pumping rate increased the size of the droplet increased at the end of the dispensing tip, and as the droplet increased at the tip of the needle a larger jet was formed.

It was visually observed that this parameter tried to achieve a stable equilibrium condition as small solution availability decreased the jet diameter, and more solution increased the size of the jet. This may provide some insight into why many researchers do not find the

pumping rate to be a significant parameter since, for the vast majority of pumping rates, the droplet size tended toward an equilibrium condition that reduced any impact of this parameter.

The findings of this study did not support a significant impact of voltage on fiber diameter. One possible reason for this was reported in the literature [68]. This study said that the voltage was only a significant parameter in the nanofiber regime but not in the microfiber regime [68]. In order to investigate this, a set of parameters that produced a nanofiber sample was identified. Then, all parameters were held constant except the voltage. As shown in Figure 31, the voltage did tend to increase the average fiber diameter for these nanofiber webs.

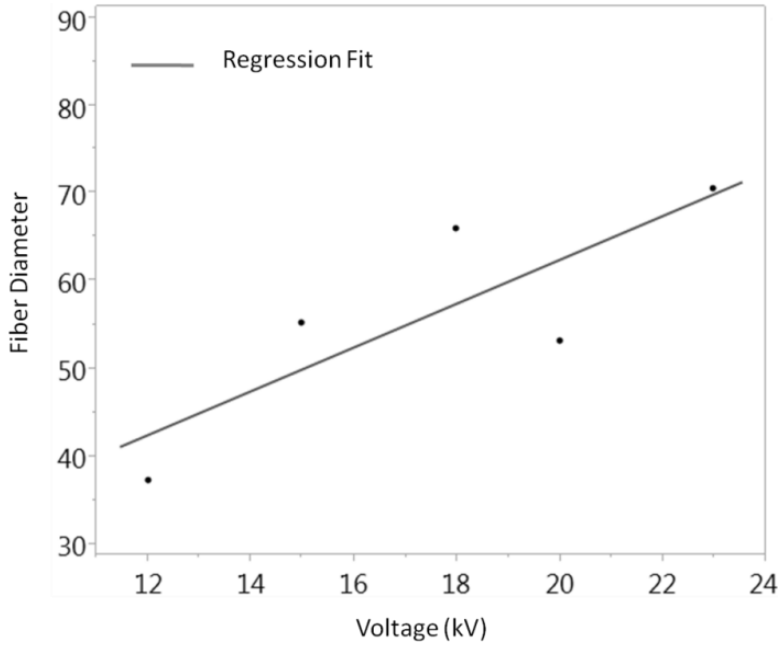

Figure 31. The figure shows the influence of voltage on fiber diameter for a single set of parameters that produced nanofiber webs.

Figure 31 suggests that any future work on modeling the electrospinning system could be improved by exploring the differences in fiber production in the nanoscale regime.

In Figure 32 the fit of the regression equation is observed. The figure is a plot of the predicted average fiber diameter against the measured average fiber diameter. If the regression equation agrees with the model, then the data point will fall directly on the dashed line.

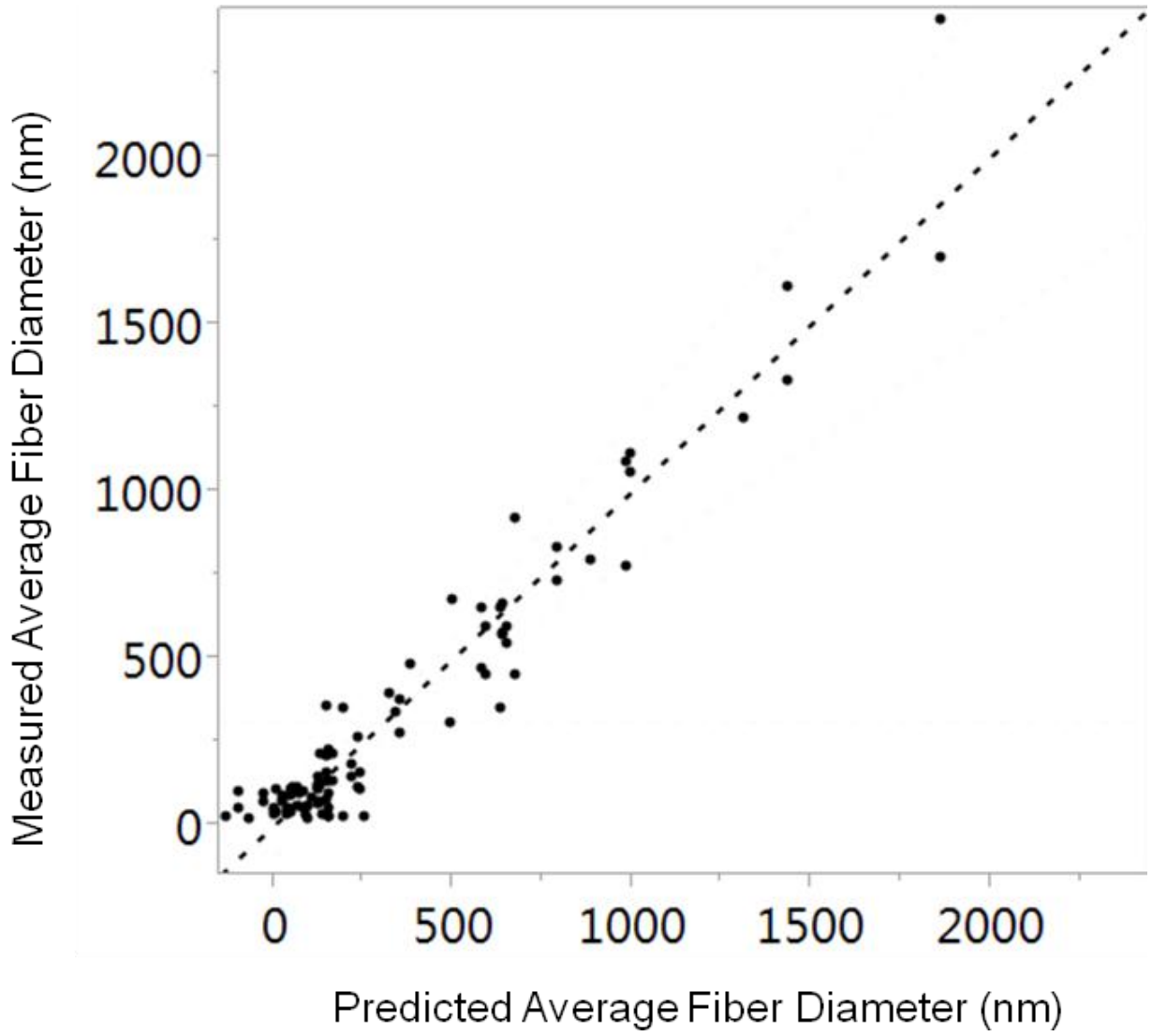

Figure 32. This figure shows the predicted average fiber diameter plotted against the measured average fiber diameter; each data point represents one sample.

The regression equation was able to accurately predict the average fiber diameter within the experimental ranges used in this experiment since the majority of the points fall along the dashed line in Figure 32. Once again, the predicted average fiber diameter was plotted against the measured average fiber diameter, except, this time all the data points that were associated with fiber webs which contained defects were removed. Figure 33 shows that as the samples with defects were removed the regression fit increased; the R^2 increased to 0.96.

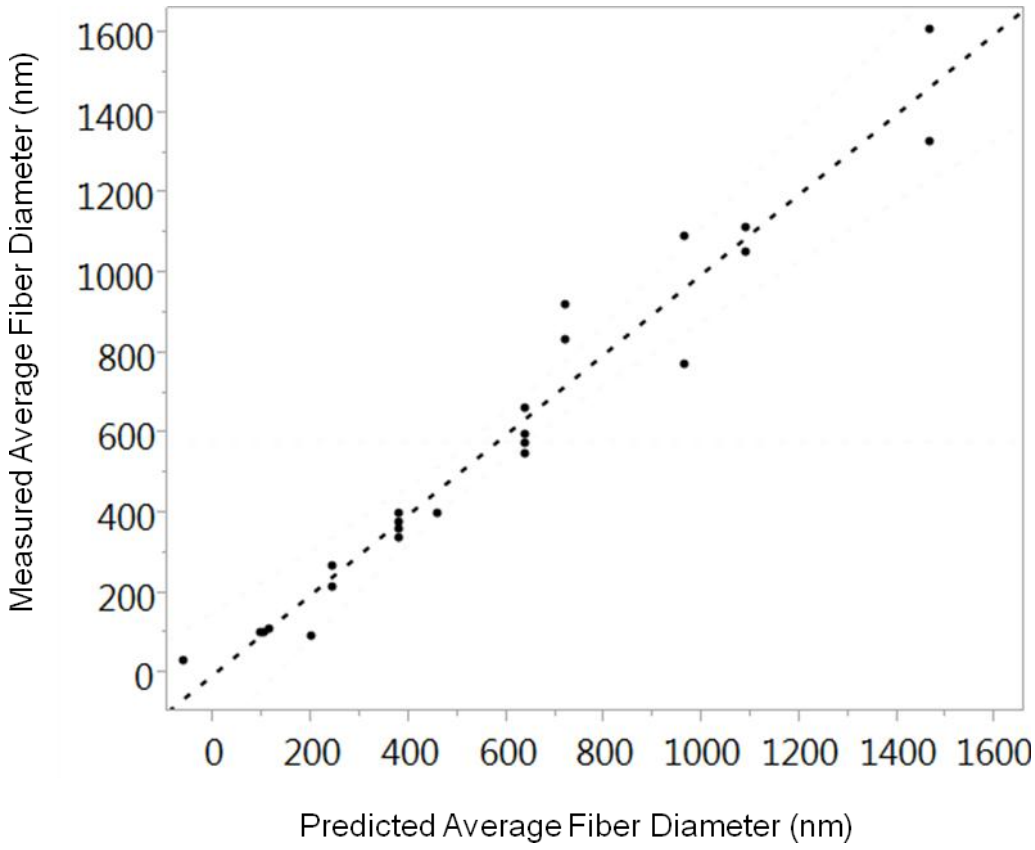

Figure 33. This figure shows the predicted average fiber diameter plotted against the measured average fiber diameter; each data point represents one sample.

Figure 33 suggests that if controlling the fiber diameter is desirable, defects should be avoided when using the regression equation.

Another way to test the validity of the regression equation for predicting average fiber diameter would be to apply the equation to previously reported data and observe whether or not the regression model agrees with what was reported. This method would validate the regression equations use for other electrospinning systems and suggest that it is valid over a wide range of parameters settings. Three studies could be used to test the validity of the regression equation. The studies used to validate the model are summarized in Table 12. In order to use this method, it was assumed that the differences in procedure for solution preparation and web characterization would not significantly affect the measured metric.

Table 12. References used to validate fiber diameter regression equation.

Study Reference	Symbol for Data Point	Assumed Values	Parameters that were Outside of Ranges Intended for the Regression Equation.
Nasir et. al. [20]	+	1	Solution concentration
Akbari et. al. [21]	o	4	Solution concentration
Essalhi et. al. [22]	•	1	Pumping rate and depth of field

Another problem with this approach was that of all the studies found for electrospinning PVDF, none were found that reported all four solution and all four processing parameters. Therefore, missing values were assumed to be a mid-range value. Appendix B shows all the values taken from the literature including the assumed values. Figure 34 shows the predicted average fiber diameter plotted against the measured average fiber diameter.

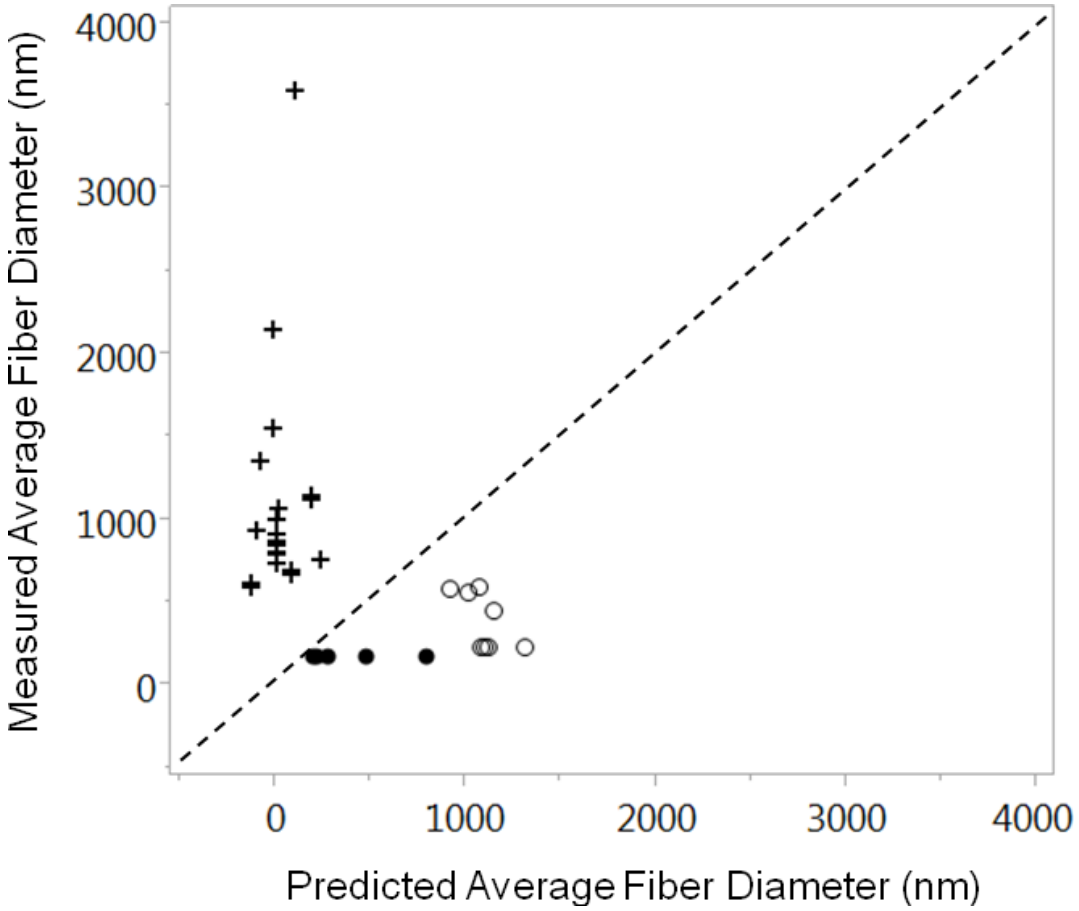

Figure 34. This figure shows the predicted average fiber diameter against the measured average fiber diameter; each data point represents one sample. The regression model used was based on the model developed with the AIC method.

Figure 35 shows that the model developed was not effective at predicting the average fiber diameter outside of this study. One possible reason for this was that as the production range was expanded other terms may have been necessary to predict the average fiber diameter. In order to test this reason, the regression equation using all eight parameters and all parameter interactions was sued. This was done and the results are shown in Figure 35.

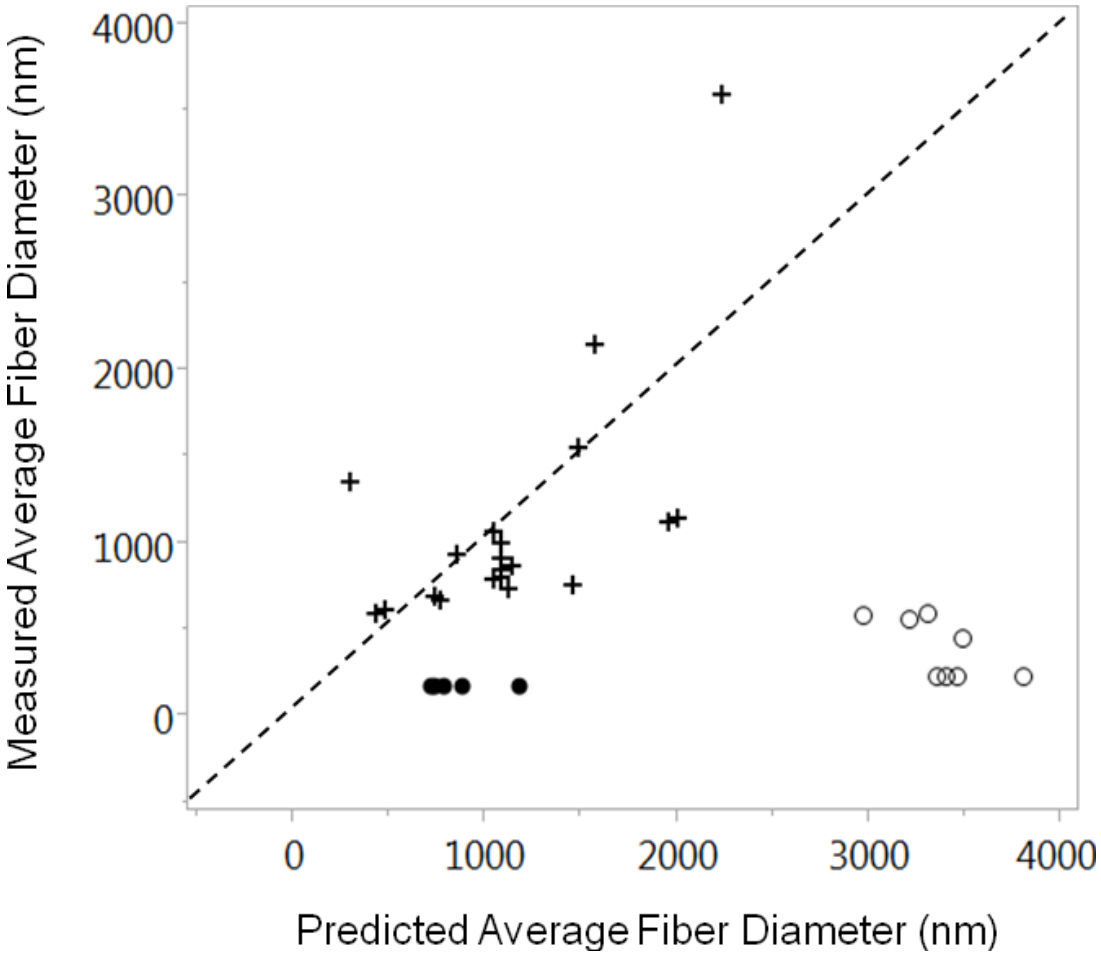

Figure 35. This figure shows the predicted average fiber diameter against the measured average fiber diameter, each data point represents one sample. The regression model used included terms for all the solution and processing parameters and interactions.

The predicted values for one study were off, but in this study four values were assumed. Therefore, it is the least reliable data. By looking at the measured values and the predicted values of the other two studies, in Figure 35, the increase in predictability can be observed. Therefore,

when controlling the fiber diameter outside of the ranges investigated in this study it is beneficial to use the model with all parameters and interactions. The terms of this model t are in Appendix A.5. One or more of the assumptions made could be reducing the power of the regression equations since the model was not as accurate as the previous fit using data from this study. Since the regression model with all the terms was more accurate, other terms, possibly the solution concentration and solution concentration interactions, were important but were not noticeable until the tested range was increased. This does not negate the usefulness of the regression model, but confines the use of the model developed using the AIC method to a certain production space. Just because a parameter was not statistically significant in this study does not mean it is not important. It means there was not enough evidence to reject the null hypothesis, and, therefore, it was not included. The high fit for the previously reported data suggested that many of the parameters were important, and more data collection can be done on these parameters to determine exactly which other parameters and interactions were important.

4.4.2 Regression Model for Bead Diameter

The regression model for bead diameter had an R^2 value of 0.87 and an adjusted R^2 value of 0.85. The regression equation is

$$\begin{aligned}\text{Bead Diameter } (\mu\text{m}) &= -3.71 + 1.46\,(X_4 + 0.592) + 0.0345\,(X_5 \\ &+ 25.8) + 0.178\,(X_6 + 17.3) - 0.0687\,X_2X_5 + 1.48 * (X_1)^2 \\ &+ 2.02 * 10^{-5}\,X_1X_4 + 7.5 * 10^{-2}\,X_6X_8\end{aligned} \tag{19}$$

$X_1 = \text{Polymer } M_w - 320000 \text{ g/mol}$
$X_2 = \text{Solution Concentration (wt\%)} - 15.9 \text{ wt\%}$
$X_3 = \text{Conductive Additive (wt\%)} - 1.1 \text{ wt\%}$
$X_4 = \text{Solvent Volume Ratio } (V_{Acetone}\ /V_{DMF}) - 0.592$
$X_5 = \text{Pumping Rate } (\mu\text{l/min}) - 25.8\ \mu\text{l/min}$
$X_6 = \text{Voltage (kV)} - 17.3 \text{ kV}$
$X_7 = \text{Needle Diameter (mm)} - 0.62 \text{ mm}$
$X_8 = \text{Depth of Field (cm)} - 14.5 \text{ cm}$

Increased acetone to DMF ratio increased bead diameter; this was attributed to higher surface tension of solutions with the higher solvent ratios. This is supported by Table 9 which shows that high solvent ratios had higher surface tensions. The pumping rate impacted the bead diameter; this was attributed to influences on jet diameter and possibly the perturbation frequency. Voltage increased bead diameter, why this parameter influenced the bead structure is not clear. The interaction between the depth of field and voltage was a result of increasing the electric field and the travel time of the jet. As the electric field increased; the charging of the jet increased; and a longer travel time of the jet allowed larger beads to form. Figure 36 plots the predicted average bead diameter against the measured average bead diameter.

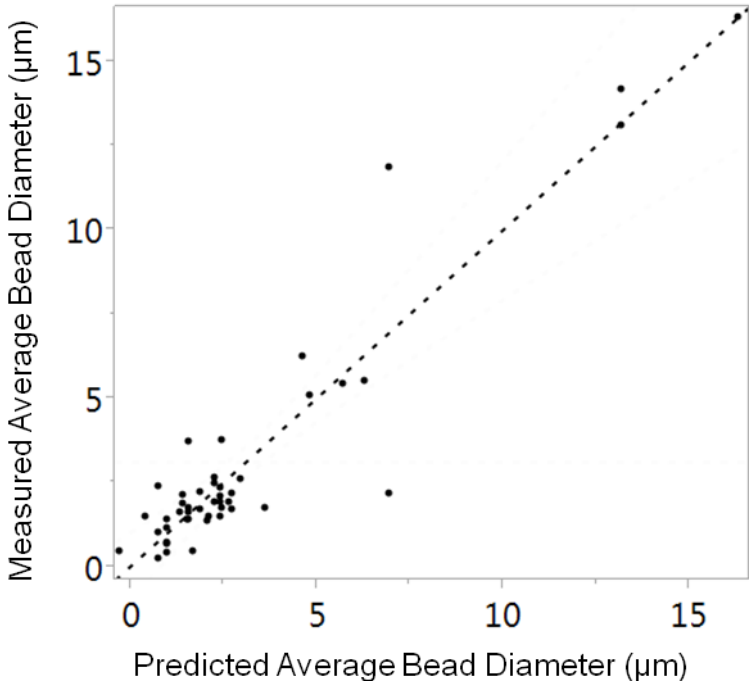

Figure 36. This figure shows the predicted average bead diameter plotted against the measured average bead diameter; each data point represents one sample

Validating the regression equation for average bead diameter with other studies was not possible because no other studies previously reported the average bead diameter for electrospun PVDF fiber webs.

4.4.3 Regression Model for Bead Nodes per Area

The regression model for bead nodes per millimeter squared had an R^2 value of 0.50 and an adjusted R^2 value of 0.46. The low value of the fit suggests that there were other variables that were not accounted for, perhaps electrospinning time. As the electrospinning time increased the number of beads into the web would increase, the influence of the time would be dependent on the penetration depth of the electron beam into the sample. This possibility should be explored further in order to determine a consistent method for measuring the number of bead nodes per area. Nonetheless, the terms of the model were still useful for understanding the influence of the significant parameters on the number of beads in the web.

$$\begin{aligned}\text{Number of Bead Nodes per 12,000 } \mu m^2 \\ = 1597 - 0.0025(X_1 + 32000) - 627(X_4 + 0.592) \\ + 800X_2X_4 + 0.005X_1X_4 + 469X_6X_7 + 0.0009X_1X_2 \\ + 16.8(X_6)^2\end{aligned} \tag{20}$$

$X_1 = \text{Polymer } M_w - 320000 \text{ g/mol}$
$X_2 = \text{Solution Concentration (wt\%)} - 15.9 \text{ wt\%}$
$X_3 = \text{Conductive Additive (wt\%)} - 1.1 \text{ wt\%}$
$X_4 = \text{Solvent Volume Ratio } (V_{Acetone}/V_{DMF}) - 0.592$
$X_5 = \text{Pumping Rate } (\mu l/min) - 25.8 \mu l/min$
$X_6 = \text{Voltage (kV)} - 17.3 \text{ kV}$
$X_7 = \text{Needle Diameter (mm)} - 0.62 \text{ mm}$
$X_8 = \text{Depth of Field (cm)} - 14.5 \text{ cm}$

The reasons for reduced beading due to increased solution concentration and molecular weight were previsouly mentioned in the background and were in agreement with the terms of this regression model. The effect of the needle diameter and the voltage may be a result of the charging phenomena at the tip of the needle. The interaction between the needle diameter and the depth of field was not expected and could be because this term is coupled with an important third level interaction. This interaction is the least signifcant term, and its effect on the number of bead nodes per area was relatively small compared to the other terms of the model. Futher data would

need to be collected in order to understand if this term is influencing the level of fiber beading, or if it is a higher level interaction term. Figure 37 shows the predicted number of bead nodes per area plotted against the measured number of bead nodes per area. The area size chosen, 12,000 μm^2, was based on the most commonly investigated area of the SEM images. This number of bead nodes can be scaled to any area size and is, therefore, arbitrary in most cases.

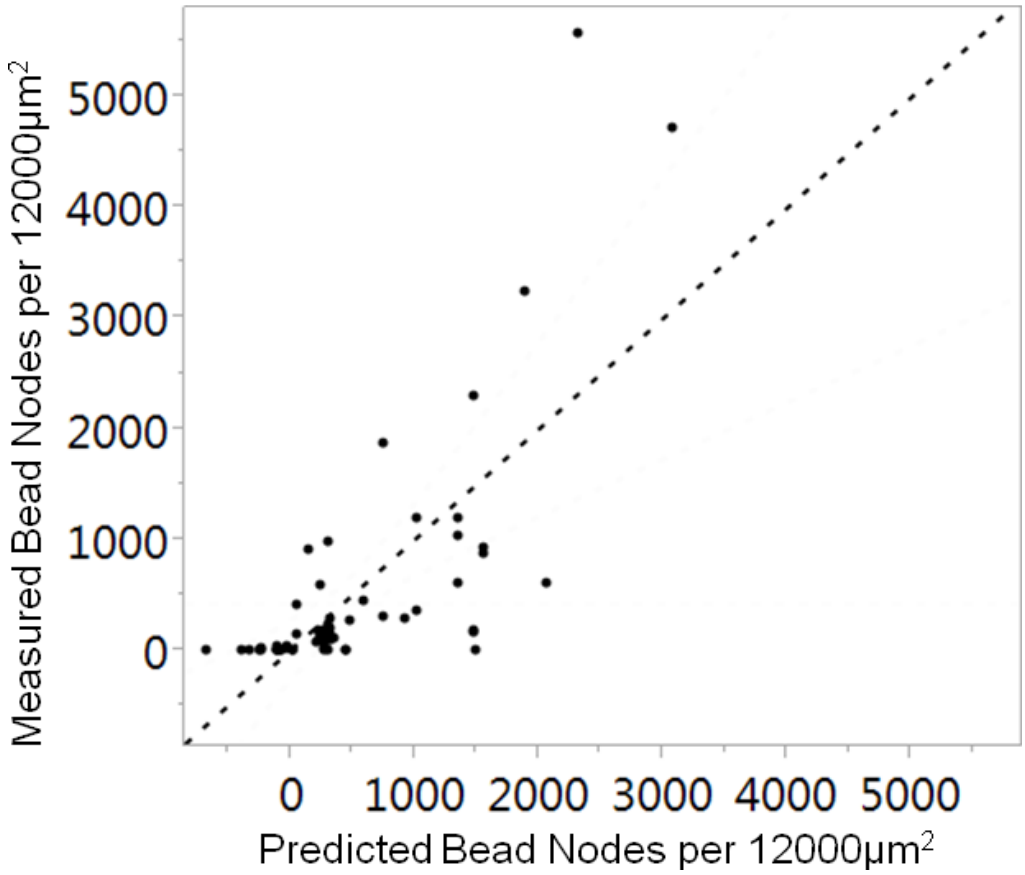

Figure 37. This figure shows the predicted number of bead nodes per area against the measured number of bead nodes; each data point represents one sample.

From Figure 37 it is clear that this regression model was not as powerful as the other models. Nonetheless, the effects of the significant model parameters still provided significant insight into key parameters that can be used to influence the number of bead nodes per area. The lack of fit may be due to the smaller sample size for this metric. Many samples were not sufficiently thick to get a true count and were, therefore, left out of the analysis. Figure 38 shows

two samples. The first SEM image shows a fiber web sample where the number of beads per area could be counted. The second SEM image shows a sample that had beads but did not have a sufficient amount of material to get an accurate count, and, therefore, this data point was missing. The reduction in sample size reduces the ability of the CCD design to be effectively used and, therefore can reduce goodness of fit for the regression model.

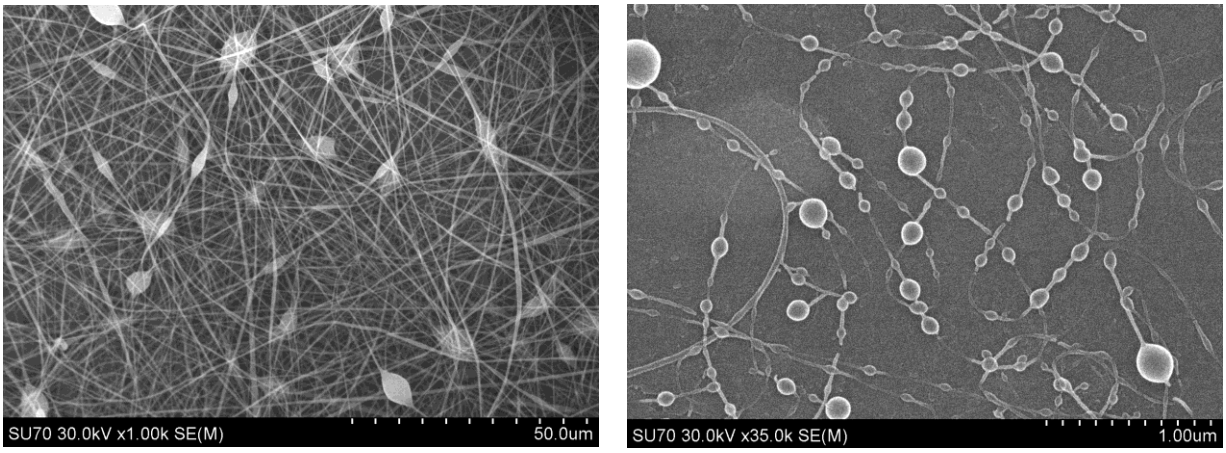

Figure 38. The images show two different PVDF fiber web samples. The sample on the right shows a sample with sufficient fibers to count the number of beads. The sample on the left shows a sample without sufficient material to count the number of beads.

By repeating the experiment with longer electrospinning times, often over many hours, increasing the sample size and discovering new statistically significant parameters may be possible. When all parameters were included in the regression model, regardless of their statistical significance, the model's R^2 value increased. Using all parameters and interactions, the R^2 value was increased to 0.84 and, and an adjusted R^2 value of 0.65. This suggests that there is potential for increasing the goodness of fit but the increase in R^2 value may also be due to over fitting. Validating the regression equation for the number of bead nodes per area with other studies was not possible because no other studies previously reported the number of bead nodes per area for electrospun PVDF fibers.

4.5 System Diagram

Once the regression equations were known, the next step was to understand how each parameter influenced the entire web structure, since it was desirable to control all aspects of the structure during the electrospinning process. The individual regression models only provide information on one metric at a time. Having a web with an average fiber diameter of 20 nm, an average bead diameter of 20 μm, and 100 bead nodes per mm^2 may be desired but this structure may not be possible. A desirability study can be used to determine if this is possible according to the regression equation. This can be done using a computer based method due to the high computational requirements and can be done using the JMP SAS© [106]. Even if theoretically possible, the required parameter settings may not be possible or may be so far outside the investigated range that the model is no longer accurate.

The regression models were useful in understanding what terms are important and the influence of those parameters, but by themselves they do not provide a systematic understanding. In order to have a systematic understanding of the influence of the parameters on the web metrics, a system model diagram was used. The system model diagram was built by using a similar methodology, found in Table 6, for developing the production guidelines for defect free fibers. The significant relationships found from the important terms of the regression equation were used, and the coefficients of each term revealed the type of relationship and the magnitude of the influence. The size of the parameter effect was based on the normalized coefficients of the regression model found in Appendix A. Figure 39 shows the system diagram which is useful to observe the possible tradeoffs of changing parameters. For instance, if the molecular weight is increased, one would expect that the average fiber diameter increases, the average bead diameter increases, and the number of bead nodes per area decreases.

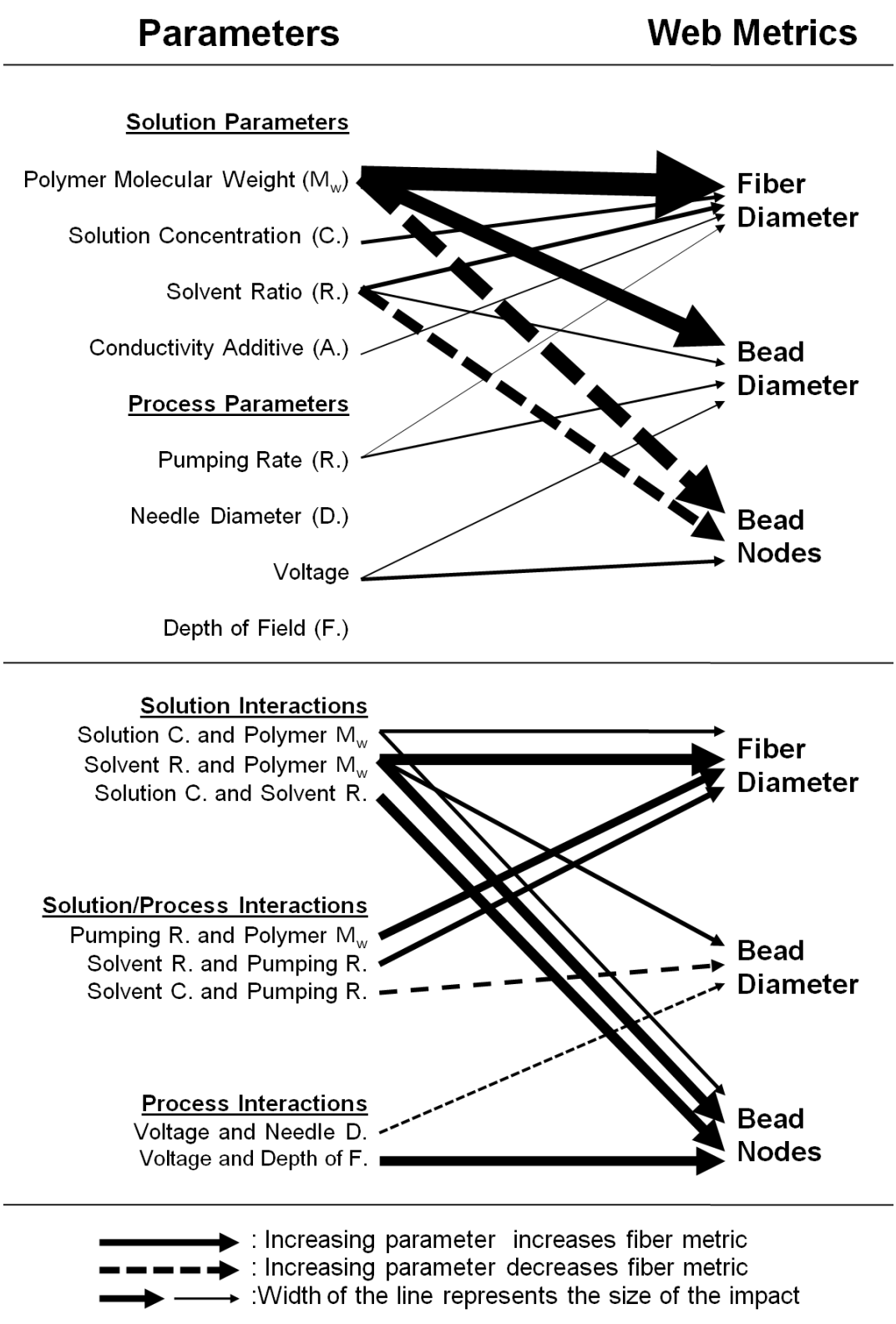

Figure 39. A schematic of the influence of solution and processing parameters on web metrics.

Figure 39 clearly shows that there are complex tradeoffs between controlling different metrics, similar to the tradeoff observed with defects. The dominant parameter is the molecular weight which had the largest influence on all three metrics, and many significant interactions include the molecular weight.

Figure 39 uses the linear relationships of each parameter. For a more complete understanding of the curvature of certain parameter effects, the equations listed in the previous sections should be used, or the values found in Appendix A. So far this analysis was limited to solution parameters and processing parameters, but the system parameters were also investigated.

4.6 System Parameters

The system parameters investigated in this experiment include the Reynolds number, surface tension, electrospinning current, and the electric field. A regression model based on system parameters was desirable for three reasons. First, it could reduce the number of terms used in the predictive model, thereby simplify what needs to be controlled. Second, the system parameters could serve as process monitoring parameters, since many of the parameters can be monitored during the electrospinning process. Third, system parameters may hold the potential for application to a wider range of electrospinning systems and polymer solvent combinations. However, for the most part, the system parameters were not as directly controllable as the solution and processing parameters.

The system parameters were controlled by changing the solution parameters and the processing parameters. However, often they were also dependent on the environmental conditions. The first step was to understand how the controllable solution and processing parameters influenced the system parameters. The influence of each solution and processing

parameters on the electrospinning current and surface tension was established using measured data. The influence of parameters on the electric field was based on the equation for a uniform electric field. The influence of parameters on the Reynolds number was based on measured data for viscosity and the equation of the Reynolds number. Then, the next step was to determine how the system parameters influenced the web metrics.

Using the same method as before, regression equations were developed for each metric. The results of the statistical analysis can be found in Appendix A. Using only system parameters and their interactions, the R^2 values for the models of the fiber diameter, bead diameter, and the number of bead nodes per area was 0.40, 0.24, and 0.72, respectively. Clearly, the large reduction in R^2 values for two out of the three regression equations suggests that using the system parameters was a poor substitute for the regression models that used solution and processing parameters. Although, in the case of the number of bead nodes per area, a large increase in R^2 value suggested that this was a better pathway for controlling the number of beads in the web. Because of the low R^2 values, the equations were not included in this discussion but can be built using the terms documented in Appendix A.

Even though the regression equations did not have a high R^2 value, the significance of the parameters and the coefficients of the model were still useful since, previously, there was not a systematic understanding of how the solution and processing parameters related to the system parameters and how the system parameters influenced the structure of PVDF fiber webs. Figure 40 shows the system diagram of solution parameters, processing parameters, system parameters, interactions, and metrics. As previously noted, the size and sign of the influence of the effect was based on the normalized coefficient of the regression model. This figure can be used to determine different pathways for influencing system parameters and metrics.

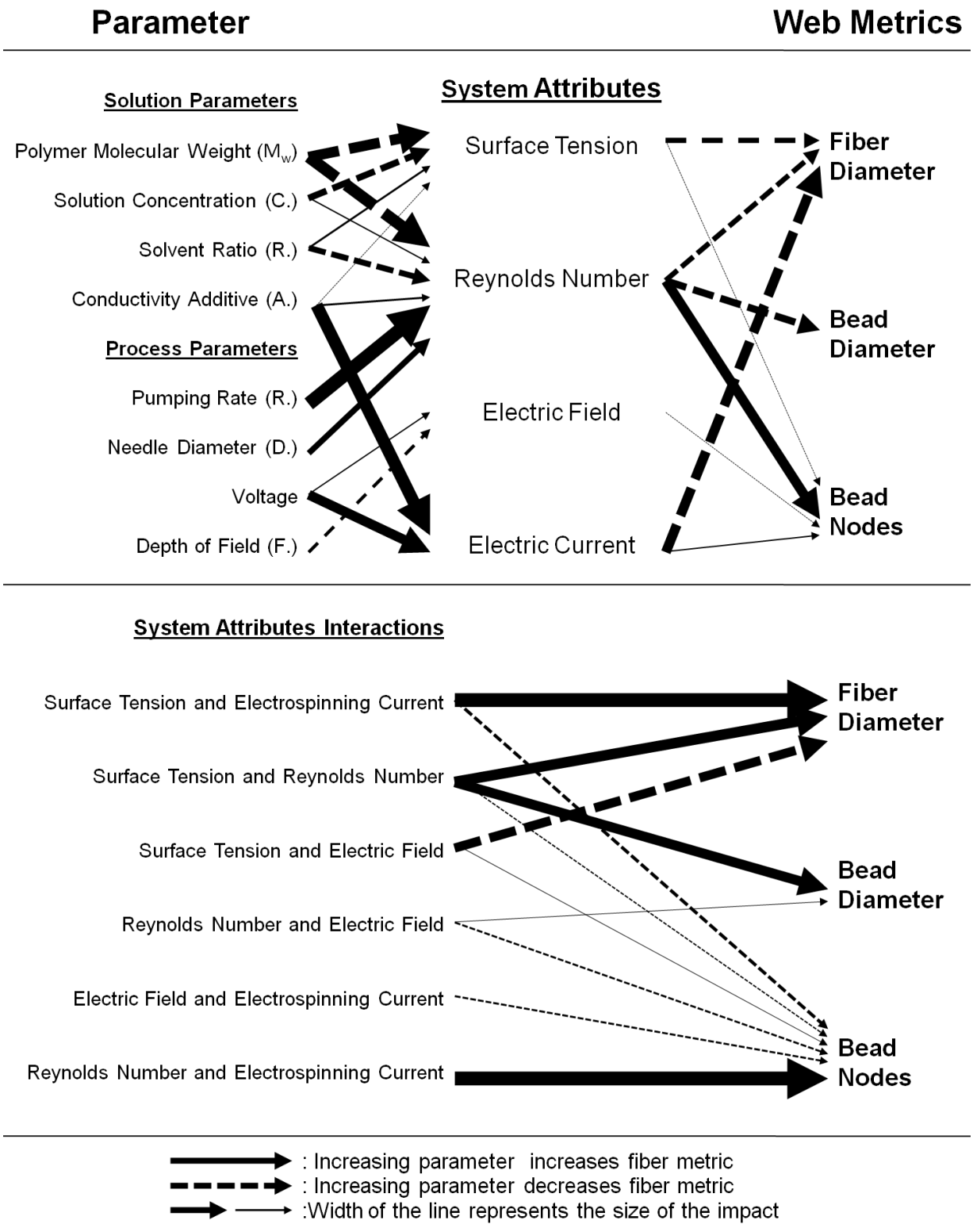

Figure 40. A schematic of the influence of solution and processing parameters on system parameters and the influence of system parameters on web metrics.

One of the most significant findings of this analysis was the statistical significance of the Reynolds number. While many researchers discussed the significance of the Reynolds number, it was in reference to the Reynolds number of the jet after it exited the syringe and was being pulled toward the collector [61, 62]. However, this analysis showed the influence of the Reynolds number as calculated from the pipe flow characteristics that occurred in the needle. In addition to finding the significance of the Reynolds number, the influence of surface tension, the electrospinning current, and the electric field on the bead metrics is a substantial contribution to the fundamental understanding of the electrospinning process.

Two methods were used so far – one using only solution parameters, processing parameters, and the interactions; and one using only system parameters and the interaction of system parameters. However, it was also possible to use a hybrid regression equation that utilized terms from all of the parameters. The difficulty in doing this from a statistical standpoint was that the sample size was small for an eleven parameter model with interactions. Using additional parameters always increased the model fit, which does not tell us much since this is expected. But by using the AIC method, the Reynolds number in combination with solution parameters and processing parameters in the regression model for the average fiber diameter increased the model fit significantly. In this case, the model R^2 value increased to 0.92. Therefore, it was possible to further increase the fit of the model by knowing the viscosity of the solution, which is used to find the Reynolds number, in addition to all of the processing and solution parameters. This was the only case where the addition of a system parameter increased the goodness of fit in a statistically significant way.

Chapter 5: Influence of Web Structure on Porosity

5.1 Introduction to the Influence of Web Structure on Porosity

The literature was clear that one way to control the functional properties of fiber webs was by controlling the porosity [39, 41, 107-110]. For example, the performance of desalination filtration membranes was impacted by PVDF fiber web thickness, interfiber spacing, and by the porosity. For desalination, it was reported that webs with high porosity and high interfiber spacing was desired [38]. Another study reported that the porosity influenced the mechanical properties and biological properties of fiber webs [108]. Lower porosities had higher tensile strengths, but higher porosities had increased cell proliferation and infiltration. A similar report stated that decreased porosity contributed to more interconnected fibers increasing the mechanical strength of the web [110]. The applications of porous PVDF fiber webs included antibacterial membranes [15], protein absorbers [16], bone growth stimulators [17], tissue scaffolds [18], and ultra-filtration membranes [26, 27]. Therefore, by controlling the porosity, the properties of the web could be controlled and used for a wide variety of applications.

Attempts to control web porosity focused on the effects of fiber diameter. Theoretical calculations performed by Eichorn and Sampson [39] noted an almost linear relationship between increasing fiber diameter and increased pore space [39]. As the mean pore size increased, the porosity increased [39]. Eichorn and Sampson were able to model electrospun fibers as solid straight rods and concluded that the width, length, linear density, and cross sectional area were important parameters for controlling pore size [39]. The pore space within electrospun fiber webs were typically complex, but treating the web as a two dimensional

network of pores was helpful. This two dimensional approach was used before and treated pores as the polygons created by intersecting fibers [111]. Figure 41 shows a layer of PVDF fibers that created multiple polygons of different pore sizes.

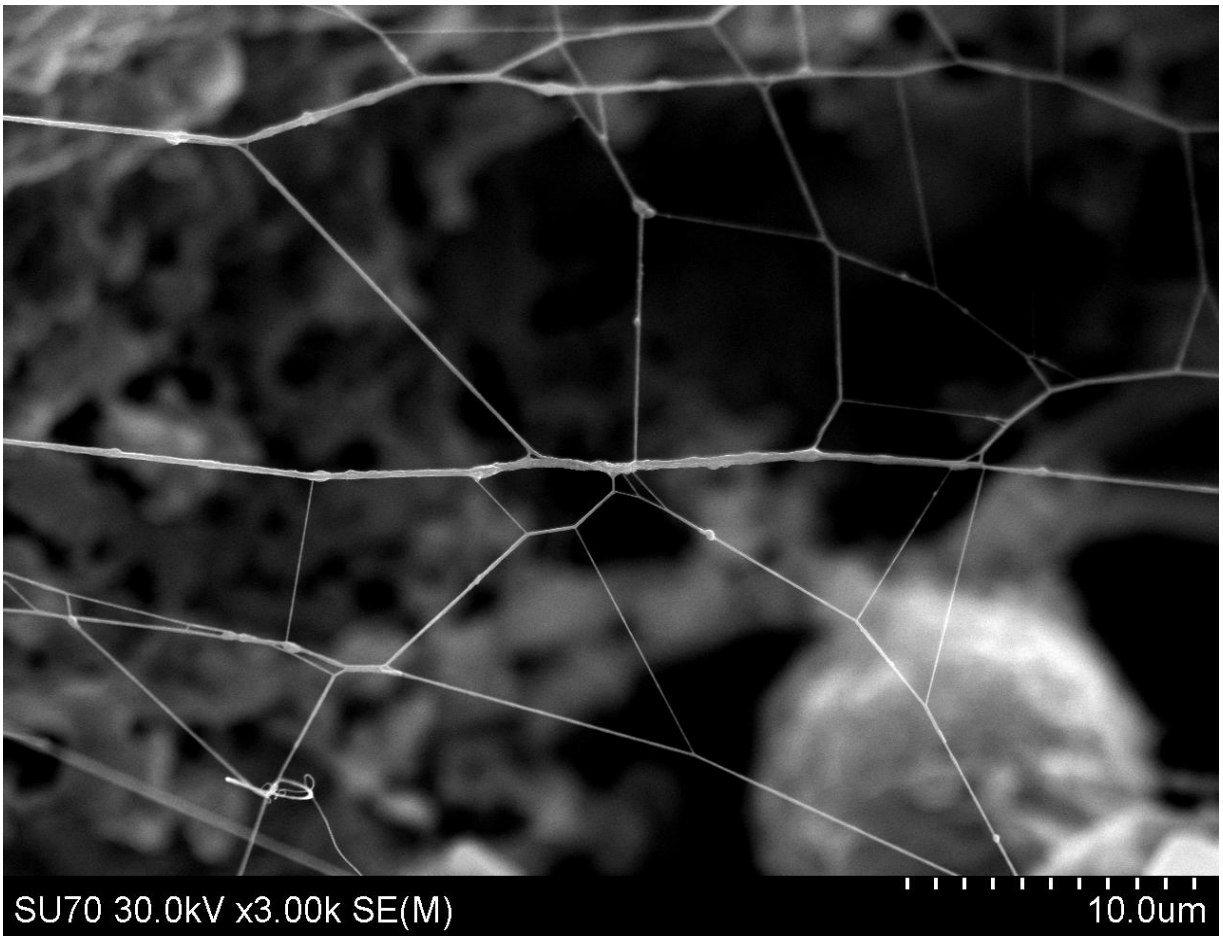

Figure 41. An example of the pores formed by PVDF fibers that validates the use of the polygon model approach.

The work presented by Eichorn and Sampson [39] was critical in establishing a fundamental understanding of how the porous structure of electrospun fiber webs affected cell culture and mechanical strength. In this study, the web structure was reported to influence the porosity. The theoretical model, developed by Eichorn and Sampson, was for defect free fibers. As shown earlier there were many defects that can occur within fiber webs, and, yet, there was little known about how these structures influence the porosity of webs. Therefore, understanding

the influence of defects on web porosity was important. If defects did influence the web structure, this would provide a new technique for controlling the porosity of electrospun webs. The web structure is influence by the average fiber diameter, average bead diameter, number of beads per area, and the occurrence of incomplete evaporation. Therefore, the influence of each of these structures on web porosity needed to be investigated.

5.1.1 Electrospinning Setup and Materials

The experimental setup, materials, solution preparation, sample characterization, and statistical analysis were the same as outlined in previous sections. The sample size was much smaller in this study because many samples were too thin to accurately measure the porosity. A total of 21 samples were thick enough to get accurate porosity measurements.

5.1.2 Pore Size and Pore Area

The pore size, or interfiber spacing, was a difficult property to measure due to the often subjective nature of where a pore starts and stops. In a few samples, it was clear, and this was done by measuring the distance from one side of the polygon to the other side of the pore created between fibers. But in general, this was a difficult parameter to measure because the electrospun fibers were not packed together in an organized way but were interconnected and often twisted in a complex way around one another. In this research, a digital image processing method was used for measuring the total area of pore space. This was different than an average pore size. The main difference was that the fraction of the pore space was related to how the fibers were packed together.

The analysis of the pore space at different levels of the web was previously done by utilizing different thresholds of a grayscale image [112]. As the depth of the impending electrons increased, the number of electrons that left the web was reduced, consequently reducing the

signal. The effect of different threshold values was already documented and related to the characterization thickness of the web [112]. The image analysis for this research was done using Image J software. First, the image grayscale threshold was adjusted to exclude anything above three quarters of the mean grayscale value. Then the image was converted into a black and white image. Next the area fraction of the black space was calculated; the information bar at the bottom of the image was not included in the measurement. A sample of the original images and the processed images are shown in Figure 42.

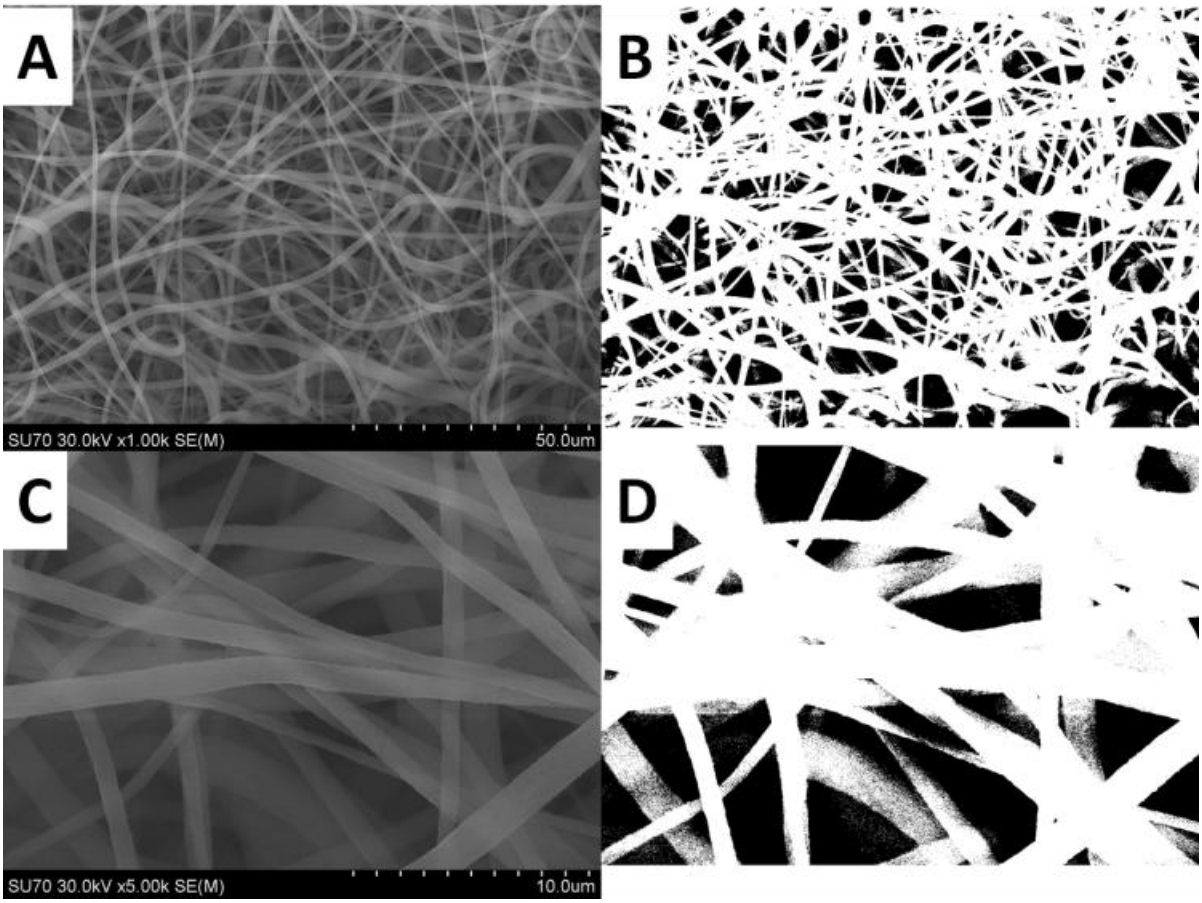

Figure 42. SEM images at different magnifications converted to black and white images.

Figure 42 shows the digital image processing of the SEM image of the same sample under two different magnifications. Sample A is at a magnification of 1000x, and the digitally processed image is sample B. Image C was taken at a magnification of 5000x, and the digitally processed

image shown is sample D. The percent area fraction calculated for images B and D was 27.8 and 27.7, respectively. Therefore, the area fraction of pore space calculation was repeatable even under different magnifications.

The advantage of using this method was that it provided a measurable parameter that was related to the packing of fibers in the web. Replicated samples were produced, and the measurements showed high repeatability for different samples made under the same electrospinning parameters. In addition, this method showed high repeatability for the same sample at different magnifications and between images of the same magnification. However, if the image magnification was set very high (around 100,000x) or set very low (around 100x) the repeatability of the measurement decreased.

To ensure that the data was valid, multiple images of the same sample were analyzed to ensure a consistent measurement and to establish an average value. There were only a couple of studies in the literature that used this technique; therefore, it was important to test the relationship between interfiber spacing and the percent area of pore space for webs. This relationship would need to be based on images under similar magnification in order to be valid. This was done for four different defect free fibers with similar fiber diameters near one micrometer, under the same magnification. Figure 43 shows an almost linear relationship between the percent area of pore space and the interfiber spacing and it validates this approach when the scale of the picture is taken into consideration. The use of the area fraction of pore space to estimate pore size may have applications for quality control in industrial scale production of electrospun fibers if this property can be continuously monitored during production.

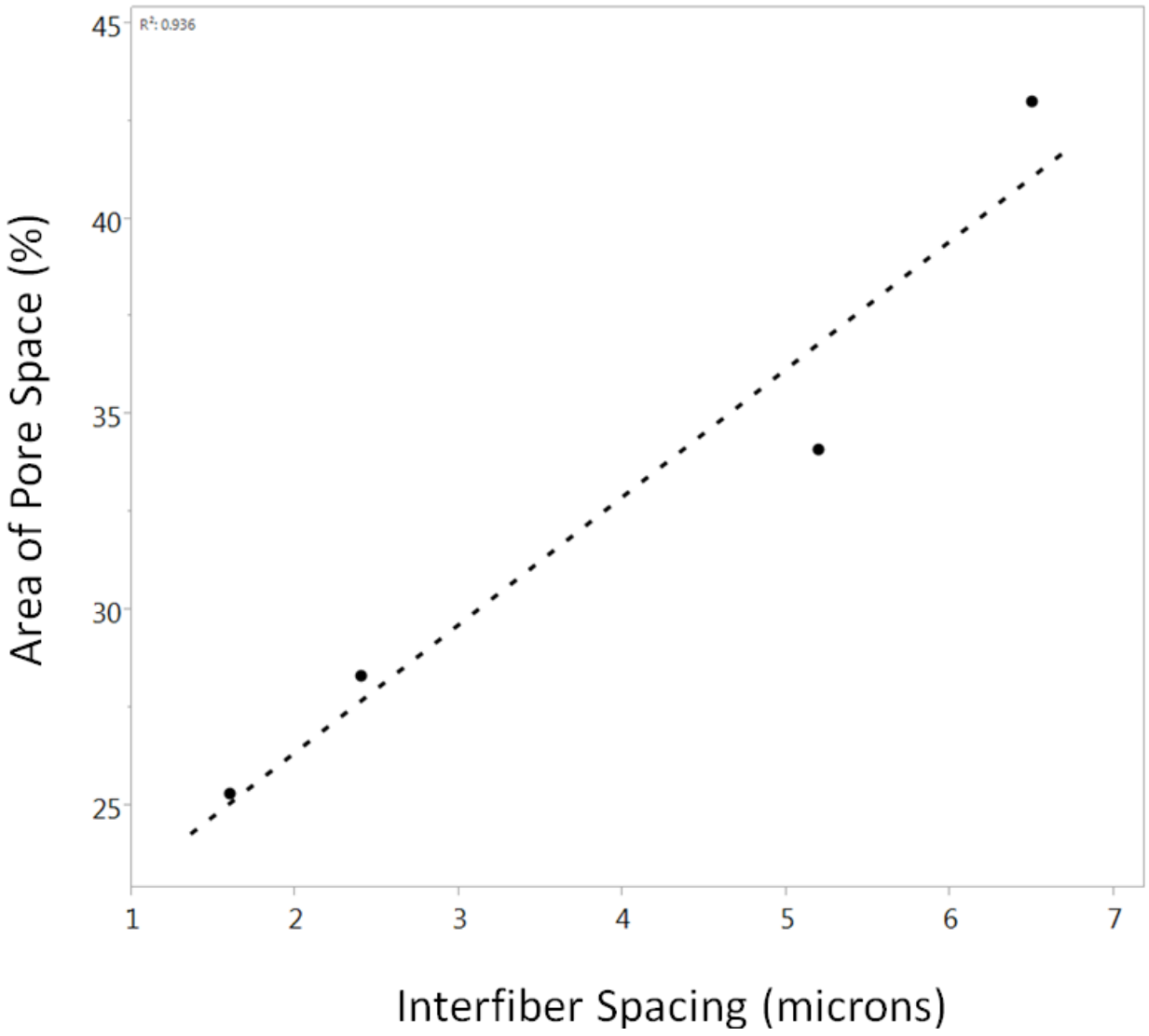

Figure 43. Interfiber spacing plotted against area of pore space for defect free fiber webs; the area of pore space was calculated from SEM images of similar scale.

5.1.3 Fiber Web Porosity

The web porosity was calculated using a gravimetric approach. The porosity of the web can be expressed as

$$\text{Web Porosity} = 1 - \frac{\rho_{\text{appearent}}}{\rho_{\text{bulk}}} \qquad \text{Equation 21}$$

This method was well established for measuring porosity and was used for measuring the

porosity of electrospun fibers before [113, 114]. One study also noted that a mercury porosimeter was not effective at measuring porosity because the high pressure altered the size of the pores [112]. The bulk density was a property of the material, and the apparent density was measured using a micrometer, digital calipers, and a microgram scale. The main limitation to this method was that a sufficiently thick membrane was needed in order to get an accurate measurement. This study looked at the web porosity and not the porosity of the fibers themselves. There were studies that reported porous fibers [115], but that was not in the scope of this study.

5.2 Results

As mentioned earlier, 21 unique samples were produced, each with a different web structure. The web metrics and ranges are listed in Table 10.

Table 13. Measured metrics and ranges for porous webs measured in this study.

Metric	Approximate Range
Average Fiber Diameter	45 nm to 2400 nm
Average Bead Diameter	230 nm to 17,000 nm
Bead Nodes/12,000μm^2	0 – 3,000

The porosities ranged from 0.61 to 0.99, with the majority of porosities falling between 0.7 and 0.95. Therefore, the different web structures did result in a wide range of possible web porosities. Figure 44 shows three SEM images of PVDF fibers that illustrate the three types of common structures possible. By looking at the data collected and SEM images there was a clear relationship between the different types of structures and the measured web porosities. In Figure 44, image A shows a microfiber PVDF web without defects; image B shows PVDF microfibers with incomplete solvent evaporation; image C shows PVDF nanofibers with beads. The following sections will discuss the effects of each different web category separately.

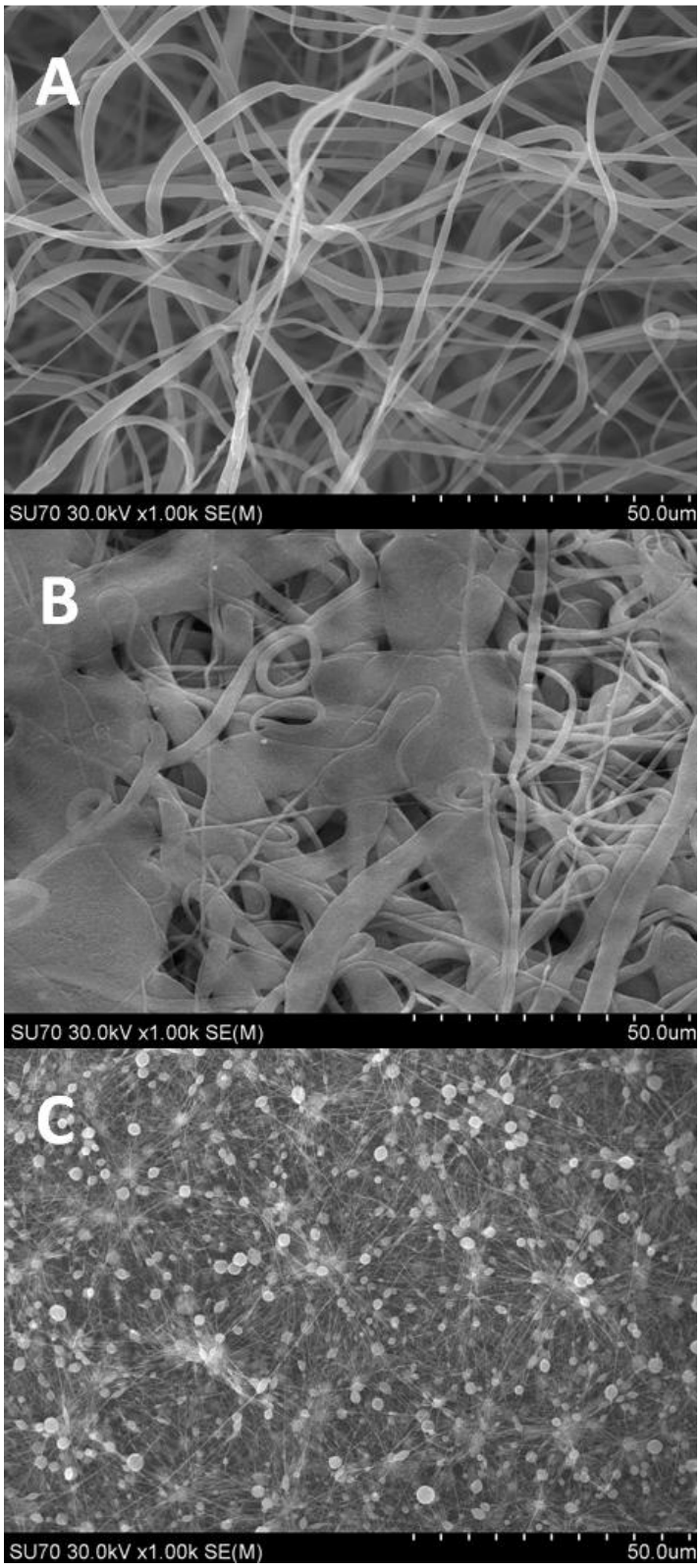

Figure 44. Fiber webs with different morphologies that were investigated to explore the influence of structure on porosity.

5.2.1 Porosity of Fiber Webs without Defects

This study looked at four samples without any defects in order to verify what was previously stated with regards to the influence of fiber diameter and pore space on the porosity. In general, increasing the area of pore space was expected to increase the porosity; this was observed, and the relationship is shown in Figure 45.

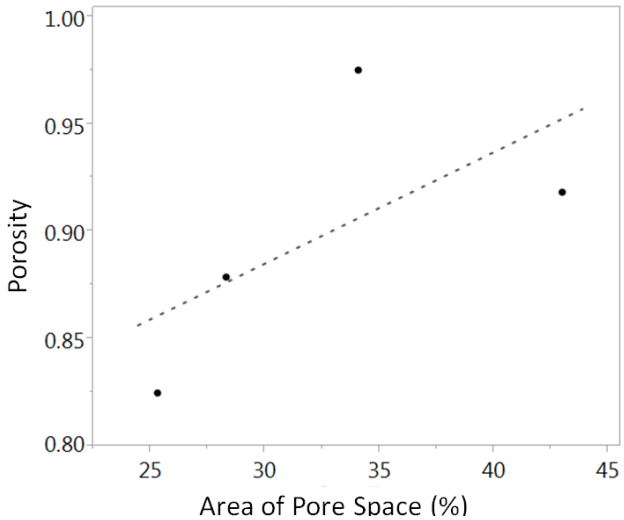

Figure 45. Area of pore space plotted with porosity.

The influence of the fiber diameter on the web porosity was also observed and is shown in Figure 46. As expected, increasing the fiber diameter increased the porosity.

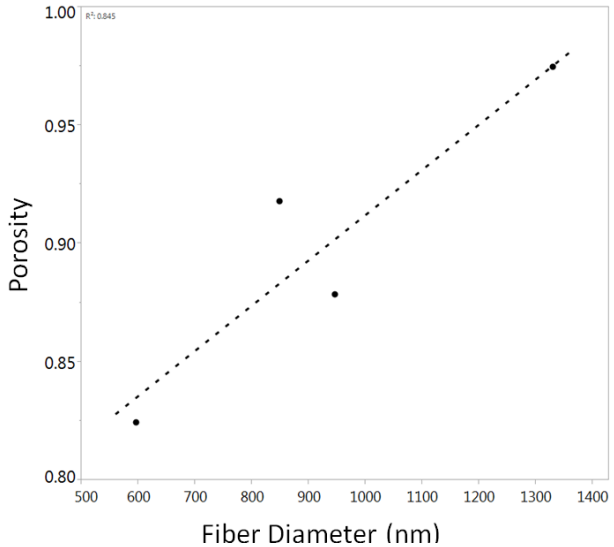

Figure 46. Fiber diameter plotted with porosity.

In both Figure 45 and Figure 46 the trend was not completely linear. Figure 47 shows the regression fit using both the fiber diameter and the percent area of pore space. Figure 47 clearly shows that the fit was accurate and that the area of pore space and the average fiber diameter influence the porosity in fiber webs without defects, as expected from the previously mentioned literature.

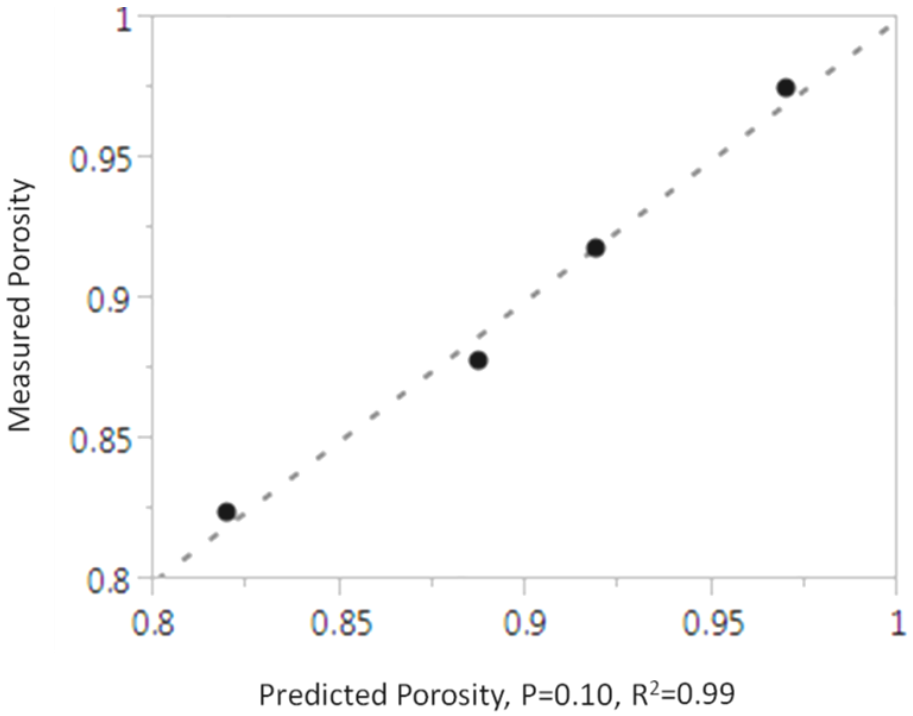

Figure 47. Predicted and measured porosity of defect free fibers.

The R^2 value of the regression model was found to be 0.99. The limited sample size limits this analysis and may be a reason for the high R^2 value, but this was only done to confirm what was already established, in the literature and the research agrees with what was previously reported. When only the fiber diameter was used in the regression equation, the fit was still high with an R^2 value of 0.84. This suggested that the fiber diameter was the more important route for controlling the porosity and that knowing the pore size can enhance the accuracy of the model. This analysis was limited to fiber webs without defects.

5.2.2 Porosity of Webs with Incomplete Solvent Evaporation

There were eight samples measured that had incomplete evaporation. Figure 48 shows the deformed fiber geometry that fibers have when not all of the solvent evaporates from the jet as it travels from the dispenser to the collector, during the electrospinning process.

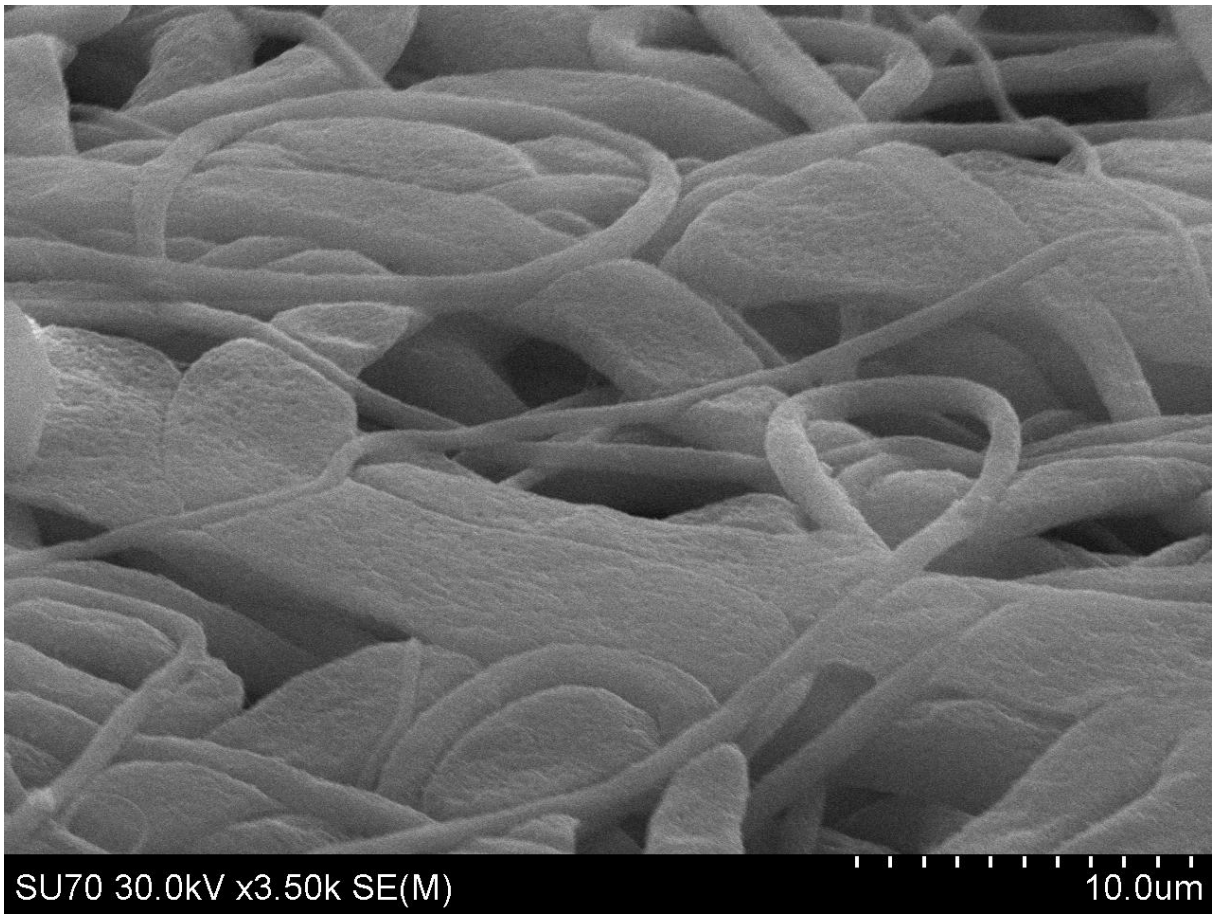

Figure 48. Fiber web with incomplete evaporation that shows the fibers fill in the pore space.

The same relationships concerning the fiber diameter and the percent area of pore space were expected for fiber webs with incomplete evaporation. The main difference observed was that as the fiber diameter increased, the degree of flattening of the fiber increased. In addition, as shown in Figure 48, larger fibers often absorbed smaller fibers that were deposited on top. This allowed the fibers to be packed into a smaller volume. The fiber webs with incomplete evaporation

accounted for the lowest measured porosities with the lowest measured porosity being approximately 0.6. A plot of the average fiber diameter did not show any apparent trends; nor did the area of pore space as shown in Figure 49 and Figure 50.

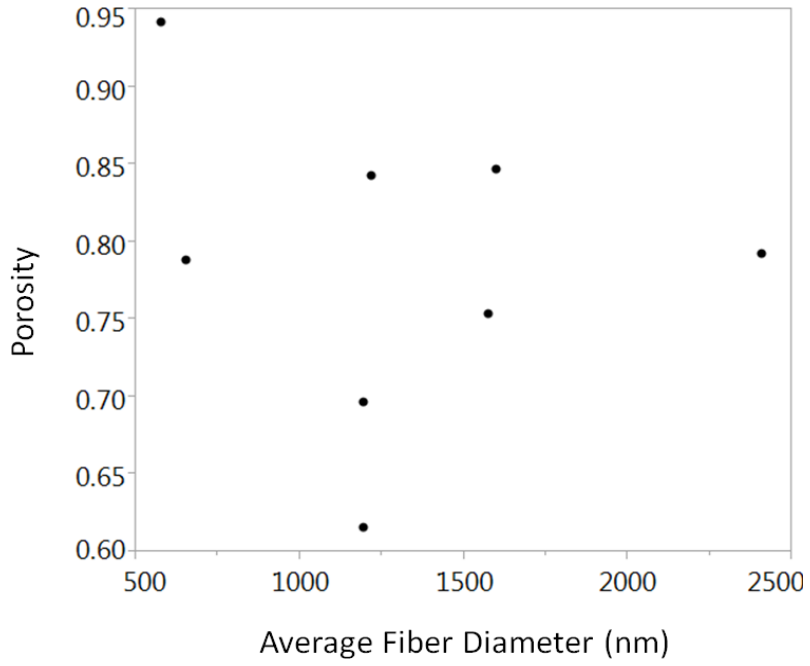

Figure 49. Average fiber diameter and porosity.

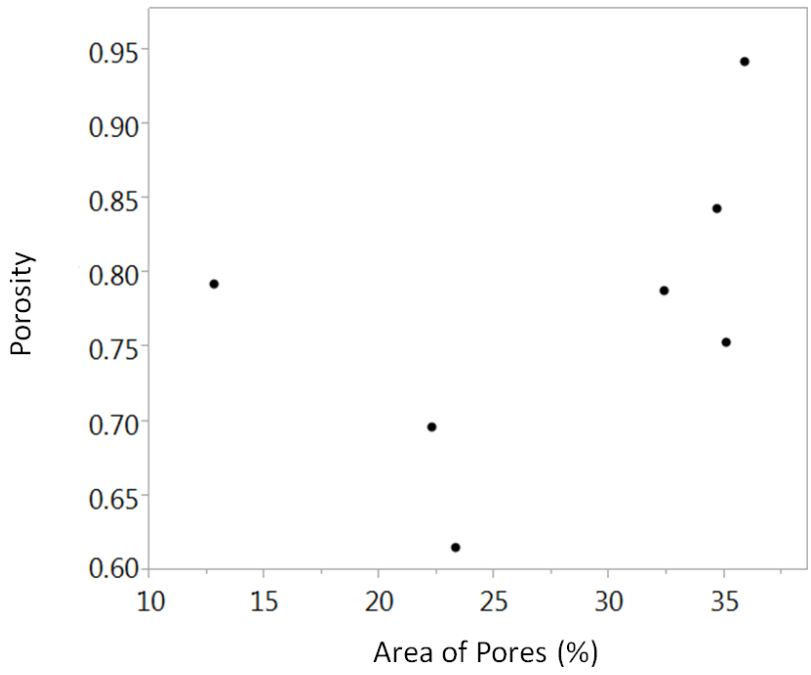

Figure 50. Area of pores and porosity.

The regression analysis showed that when both the area of pore space and the fiber diameter were taken into account, there was a correlation. The predicted values plotted against the measured values are shown in Figure 51.

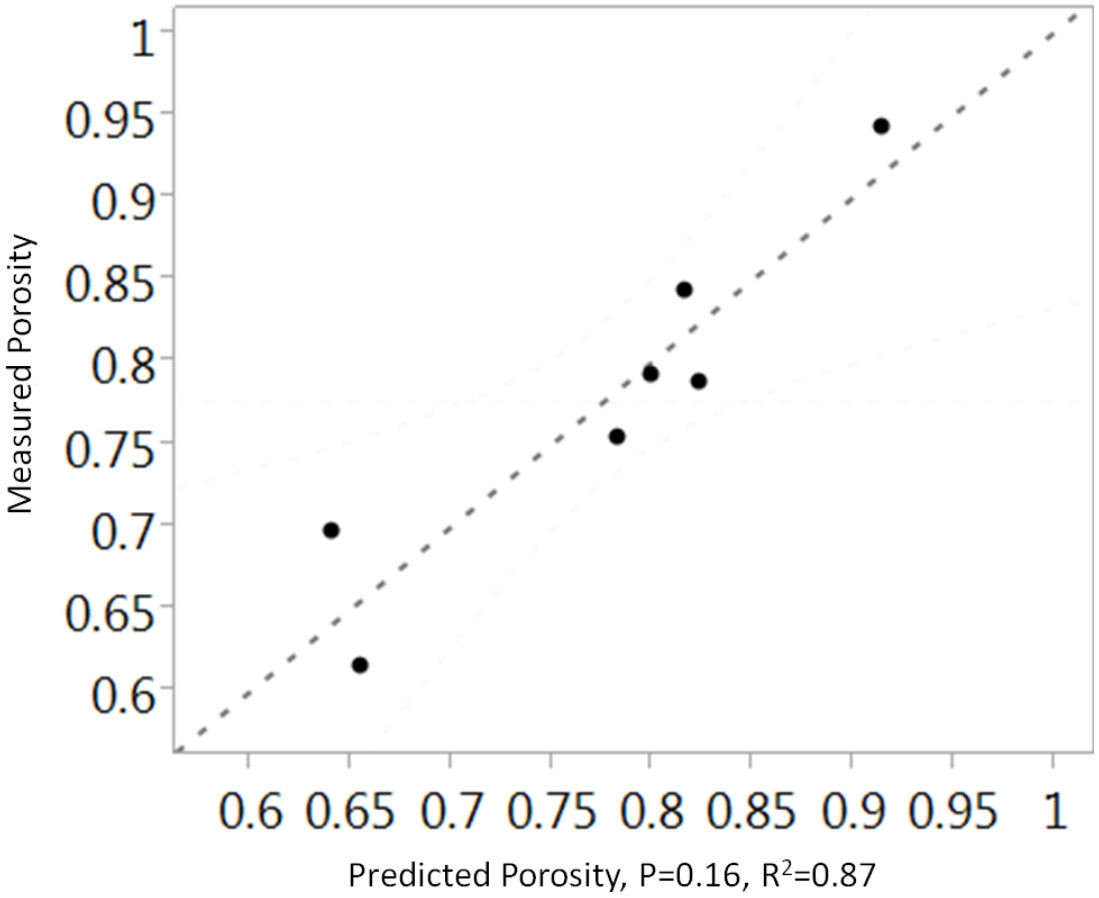

Figure 51. Regression fit for fiber webs with incomplete solvent evaporation.

A perfect fit would have all of the data points along the dotted line. Data points above the dotted line suggest the predicted porosity values are underestimating the value, and data points below the line suggest the predicted values are overestimating the value of the porosity. The good fit of the regression equation showed that when the average fiber diameter and the area fraction of pore space are taken into account, a trend was observable. The coeficients of the model terms for the area fraction of pore space and the average fiber diameter are called estimates and the statistical results of the analysis are listed in Table 14.

Table 14. ANOVA for porosity with incomplete solvent evaporation.

Term	Estimate	Std Error	t Ratio	Prob>|t|
Intercept	0.347	0.0864	4.02	0.0159
Area Fraction of Pore Space	0.0134	0.00274	4.89	0.0081
Area of Fraction Pore Space x Fiber Diameter	-0.000016	3.56e-6	-4.49	0.0109

Table 14 showed that, as before, increased area of pore space increased porosity. But, instead of just looking at the fiber diameter, the fiber diameter and the pore space interaction was significant. This was because the interaction was a more significant term than just the fiber diameter alone. The interaction was significant because it captured what was going on with the filled pore space. As the fiber diameter increased and the area of pore space increased, this reduced porosity. This term may be accounting for the absorption of smaller fibers into larger fibers shown in Figure 48. Using the area of pore space and the interaction, the R^2 value of the regression fit of the observed data was 0.87.

5.2.3 Porosity of Webs with Beading

Figure 52 shows an image of fibers and beads on an aluminum substrate. The image shows how fibers and beads stack on top of one another.

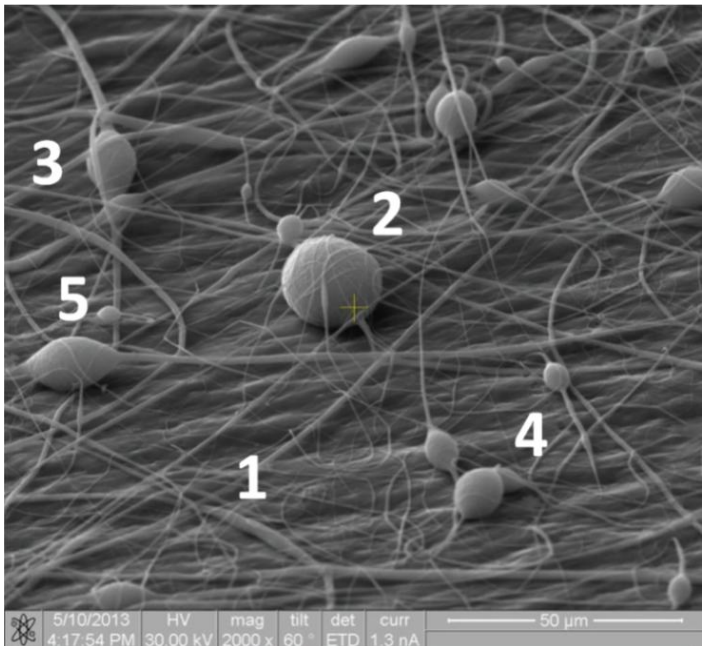

Figure 52. Image of PVDF fibers with beads.

Figure 52 pictures at least five different scenarios illustrating the complexity of how fibers and beads can impact the web structure. Number 1 shows fibers stacking on fibers. Number 2 shows fibers stacking on a single bead. Number 3 shows an example of a fiber forming a bridge over two beads. Number 4 shows a bead stacked on another bead. Lastly, Number 5 shows that large variance is possible between bead diameters.

In comparison to webs with just fibers, the number of fibers per volume was decreased due to beading. The magnitude of the decrease was dependent on the frequency with which the five previously listed scenarios occurred. The frequency depends on the amount of beads per volume. The amount of beads per volume was related to the observed number of beads per area.

This study investigated a way to predict the porosity in terms of the fiber and bead structure and the number of beads. The developed conceptual framework suggested that the fiber diameter, area fraction of pore space, bead diameter, and number of bead nodes are important parameters. The complexity of how beads and fibers interacted with themselves and each other suggested that the interactions of these parameters could be of interest as well. The model framework so far ignored the effects of variance in mean values. But the variance, or standard deviation, of the mean values may affect the degree of packing possible for the fibers and beads. Therefore, the standard deviation of the average fiber diameter and average bead diameter was included in the analysis. This study produced a total of ten samples with beaded fibers.

The regression analysis revealed which parameters were significant and the influence of each parameter. The summary of the statistical analysis is shown in Table 15. Table 15 shows that increasing the fiber diameter increased the porosity.

Table 15. Analysis of variance for beaded fiber webs.

Term	Estimate	Std Error	t Ratio	Prob>|t|
Intercept	2.66	0.496	5.37	0.0126
Average Fiber Diameter	0.000577	0.000429	1.35	0.2711
Number of Bead Nodes / Area	0.000761	0.000293	2.60	0.0802
Average Bead Diameter (um)	0.606	0.190	3.19	0.0498
Standard Deviation of the Bead Diameter	-1.04	0.290	-3.60	0.0369
Area Fraction of Pore Space	-0.0603	0.0170	-3.55	0.0382
(Number Bead Nodes / Area) • (Average Bead Diameter)	0.000533	0.000178	3.00	0.0577

One possible explanation for this is that as the fiber diameter increased, the stiffness of the fibers increased. This explanation is reinforced by the appearance of small fibers in comparison to large fibers behave in Figure 53. The larger fibers appeared to stay straighter than the smaller fibers which appear less stiff.

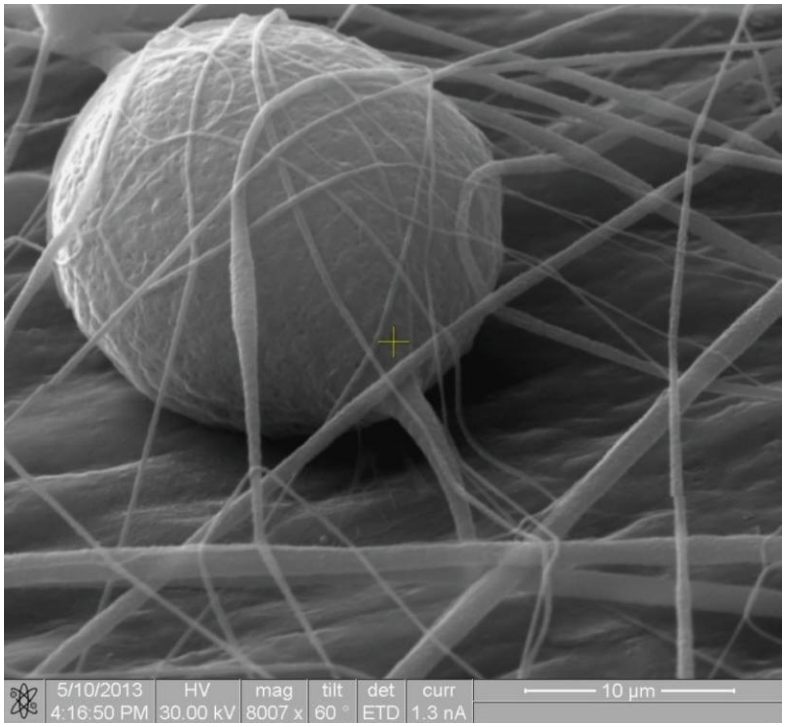

Figure 53. PVDF fibers with different diameters on a bead.

This would be an important property if the beads are acting like the nodes of a scaffold. Therefore, as the thicker fibers provided stiffer connecting fibers for the nodes and created a web structure with high amounts of void pace, it would have increased the porosity. The influence of the fraction of pore space was different than previously observed for webs without defect. For

beaded fiber webs, increasing the area fraction of pore space decreased the porosity. The area fraction in this case was no longer dependant solely on interfiber spacing but was now also dependant on the bead diameter and the number of beads per area. The influence of this parameter on the porosity is counterintuitive. The decrease in pore space may indicate a high level of beading, and increased amounts of bead stacking and scaffolding phenomenon would increase the porosity. An image showing this scaffolding is shown in Figure 54.

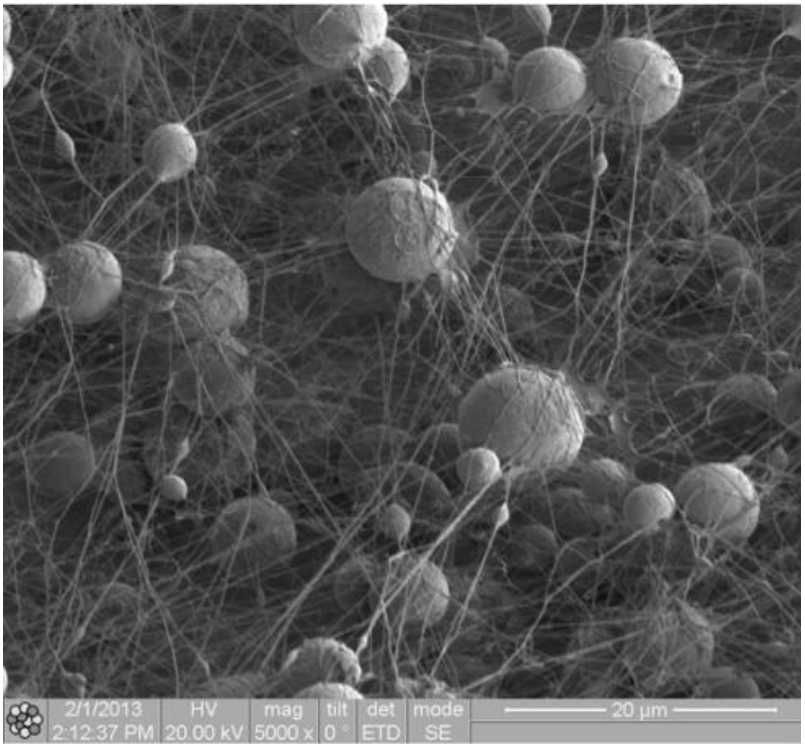

Figure 54. Image showing scaffolding phenomena of fibers and beads.

This idea was reinforced by finding that an increased number of beads per area increased the porosity. Using the conceptual framework developed in this study suggests a limit at which the influence of beading on porosity would reach a maximum value and eventually cause the porosity to decrease as the number of beads increases. Increased standard deviation decreased porosity; as the standard deviation increased the possibility of packing additional material into the pores was possible. The number of beads per area and the average bead diameter is the one

important interaction identified as significant. This term suggests the importance of fiber diameter in relationship to the number of bead nodes. If, for instance, both of these values are increased, this term increased. This term could be accounting for a variety of relationships identified in Figure 4. A plot of the predicted and measured porosity values is shown in Figure 55.

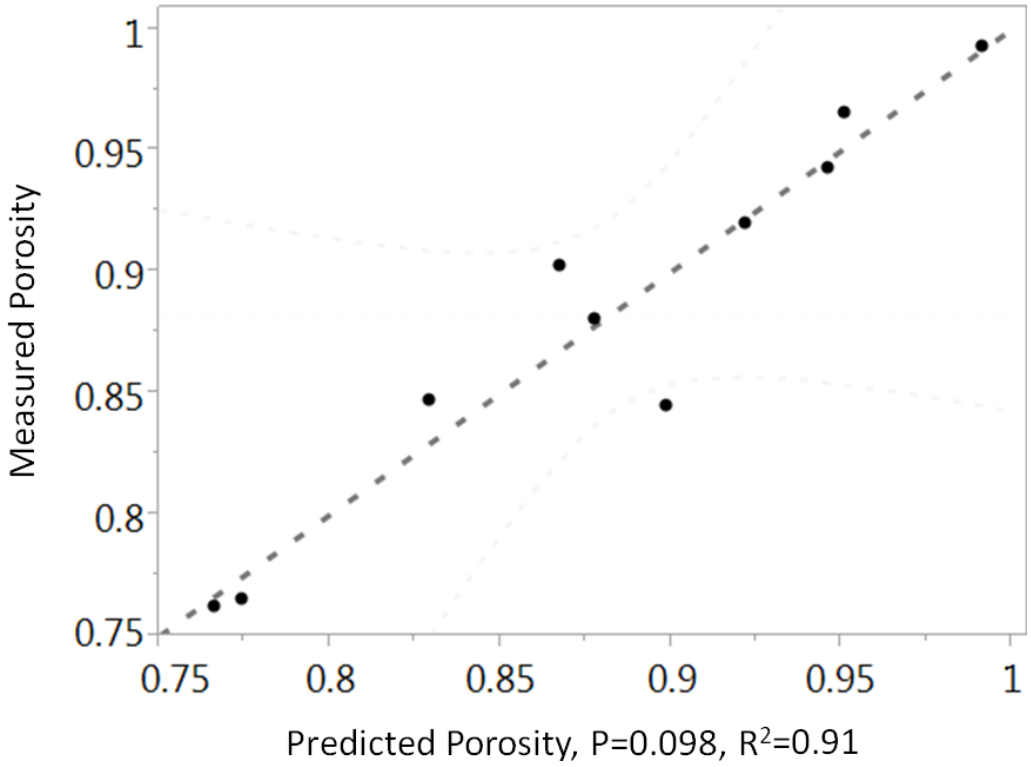

Figure 55. Predicted and measured porosity of fiber webs with beads.

Table 15 shows the statistical analysis of beaded fibers and the coefficient of each term in the regression model, found in the estimate column. The linear regression model had an R^2 value of 0.91. Therefore, this model shows that are many terms needed to predict the porosity in fiber webs with beading. There were three samples that were not included in the analysis since these samples had beads with incomplete evaporation. The morphologies are shown in Figure 56 and do not fall into one of the three distinct categories in this study.

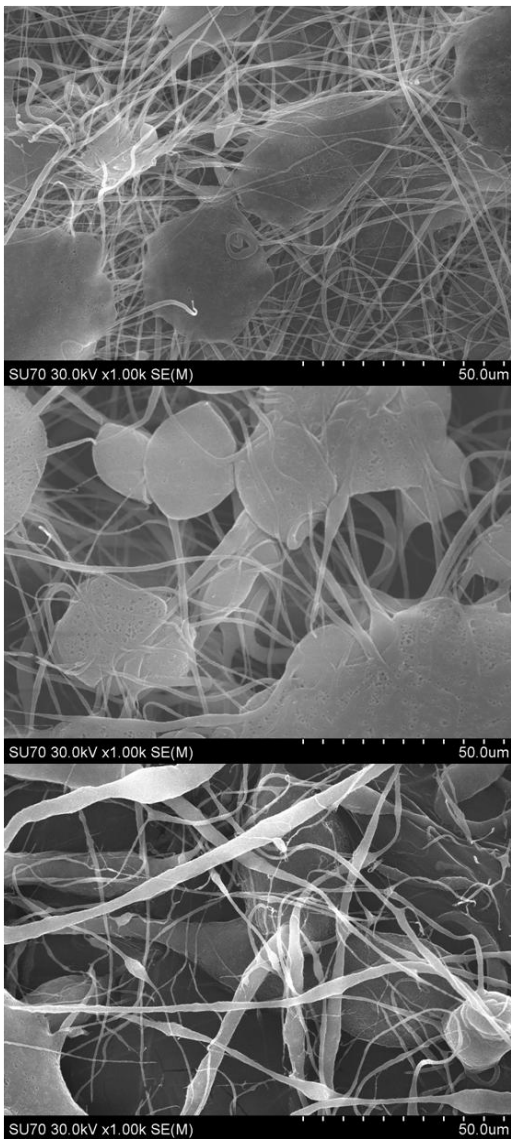

Figure 56. Images of outliers.

The regression equations suggest that the porosity of fiber webs can be tailored by controlling the average fiber diameter, area of pore space, average bead diameter, number of beads per area, standard deviation of bead diameter, and occurrence of incomplete evaporation. Different web structures required different regression models, but in general the trends of each parameter on the porosity were similar. The high R^2 value for the regression equations indicated that the terms identified and the effects quantified for modeling porosity of fiber webs were accurate.

Increasing the fiber diameter increased porosity except when incomplete evaporation was present in the web. Therefore, if producing a web with large fiber diameters and low porosities is desired settings that result in incomplete evaporation may be necessary. Also, if nanofiber webs are desired with high porosities, utilizing beading in order to increase the web porosity may be necessary. Therefore, defects can be used to influence the web porosity and in many cases may be beneficial depending on the desired fiber diameter and porosity. This research showed that by controlling the defects of fiber webs, one can also control the porosity. This was a new approach to controlling porosity of fiber webs.

Chapter 6: Piezoelectric Response of PVDF Webs

In the literature, the fiber diameter and fiber alignment were reported to influence the piezoelectric response [13, 17, 24, 33, 47, 54]. One study suggested that the optimized web processing conditions occurred at 30 kV with a pumping rate of 1ml/hr, needle diameter of 200 um, depth of field of 6 cm, and a rotating collector with 16 m/s face velocity [55]. The average porosity of these webs was approximately 65%, with an average fiber diameter of 260 nm, and average thickness from 10-40 um, and a piezoelectric response ranging from 0.41 to 0.79 mV/Pa [55].

While the influence of fiber diameter and fiber alignment was reported, influence of defects and bead structure was unknown. This study attempted to investigate the influence of defects and bead structure on the piezoelectric performance of fiber webs. In order to answer this question a reliable way to measure the piezoelectric performance of fiber webs was needed. One method found in the literature [36, 55, 116] that was used to estimate piezoelectric performance was by measuring and comparing the size of the diffraction peaks of XRD data of different PVDF samples to determine the degree of beta phase crystallinity.

6.1 Method for Characterizing Crystallinity

XRD was used to quantify the degree of alignment and crystallinity for PVDF fiber webs. Figure 57 shows XRD data from thin films purchased from PiezoTech© and XRD data of PVDF fibers created in the lab for this study. The piezoelectric beta phase peak occurs at 20° [24, 59, 117]. In this research, an Xpert Pro Diffractometer (Philips) was used to characterize the

crystalline phase. The voltage and current, of the diffractometer, were set at 45 kV and 40 mA, respectively. In most cases the samples were scanned over a 2-theta range of 10 - 35°.

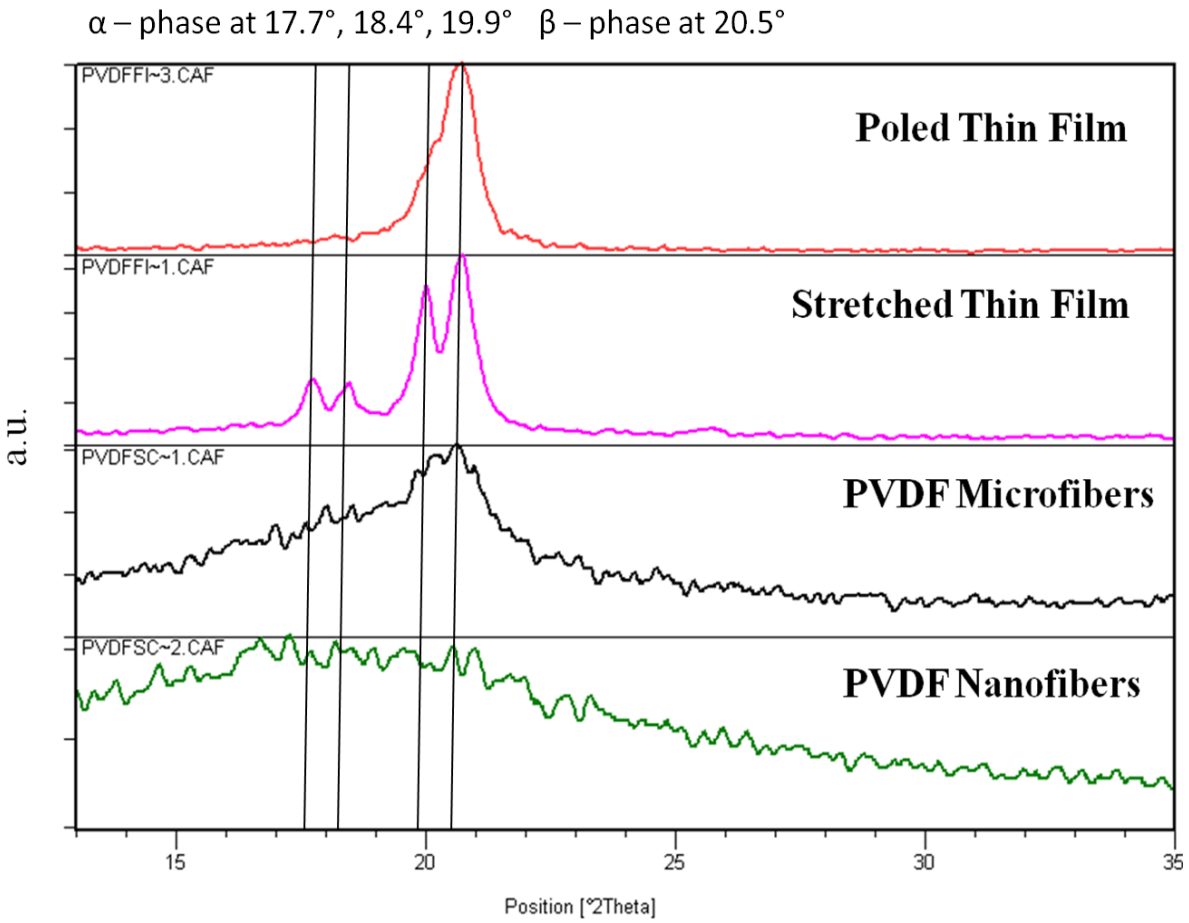

Figure 57. XRD data for purchased thin films and produced fiber webs.

The poled film was expected to have a peak around 20.5 degrees due to the high beta phase content which has the strongest piezoelectric response. It was noted that in some cases, for electrospun fiber web, the peaks shifted to the left [116] and could cause difficulty in distinguishing the alpha and beta phase peaks. Therefore, this technique was not used to compare different web performances but was used to verify whether or not the beta phase crystallinity was present in the webs with micro fiber and nanofiber. The stretched film showed alpha phase and beta phase peaks. The major alpha peak is around 19.9° in addition to the beta peak; the beta peak was present because this film was stretched. Stretched films were reported to contain both

alpha and beta phase crystallinity [118]. The PVDF microfiber web had a broader peak with some evidence of the beta phase at 20.5° degrees, while the XRD output for the nanofiber web showed a broad and ill-defined peak at approximately 17°.

The reasons for peak broadening were unknown, but when comparing XRD peaks in Figure 57 the XRD peak of fiber webs are not as well defined as those of thin film samples and suggest that the fiber orientation, porosity, or surface roughness of webs may be causing the XRD results to differ from thin film results. In order for XRD to be a viable route for comparing different PVDF webs, these results needed to be connected to an observed piezoelectric response. Therefore, in addition to measuring the crystallinity, it was important to compare the voltage response of different fiber webs.

6.2 Method for Testing Piezoelectric Performance

In the literature, PVDF fiber web performance was measured by comparing the voltage response of webs under a given pressure and/or displacement [21]. When the voltage was measured across the piezoelectric webs, understanding the effects of contact placement was important [10, 14, 119]. This study looked at measuring and comparing the piezoelectric response through the thickness of the web because it was possible to replicate the same device. The device was fabricated using two copper plates with conductive silver adhesive that were used to create contacts for the fiber webs. Then, wires were bonded to the copper plates in order to measure the voltage. A schematic of the structure of the device and a measured voltage response is shown in Figure 58. In addition to the device shown in Figure 58, an interdigitated electrode setup was used to measure the response through the length of fiber web, but the fabrication of the device was difficult to replicate. A voltage response was observed in both types of device.

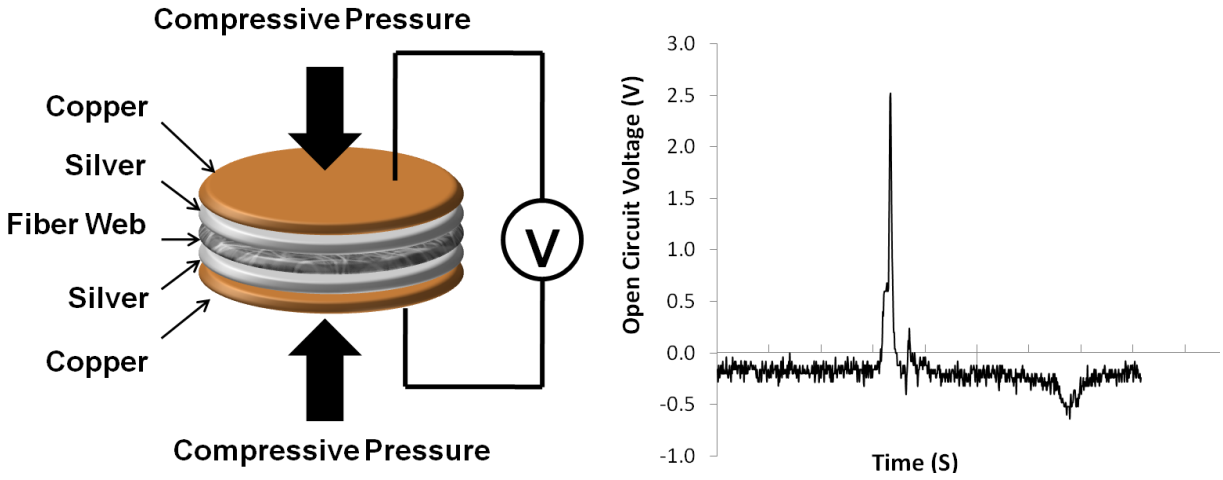

Figure 58. PVDF device and voltage response during one compression cycle.

The same device shown in Figure 58 was fabricated using a commercially purchased poled PVDF thin film and non-poled PVDF thin film from PiezoTech©. The poled thin film showed a high voltage response, while the non-poled film showed no voltage response. The non-poled film did have the piezoelectric beta phase but showed voltage response; this was most likely due to the low level of alignment of the beta phase. In order to compare different samples, the same procedure was used to fabricate multiple devices. Seventeen total devices were made, but only three samples showed a measureable response that was above the noise level of approximately 50 mV.

All the samples that did not work showed voltage measurements with levels of noise that were characteristic of a short circuit. This observation suggested that the current was moving through the web. Many of the webs were thin and porous making it possible for the silver adhesive to penetrate into the web, causing the short. The fiber webs for the devices that showed a significant response were thicker than the other fiber webs which did not show any response. The smallest PVDF fiber web sample that showed a voltage response was 150 microns thick. Therefore, it may be necessary for thin webs to find a way to fill the pores in the web. One

option was to fill the pores of the fiber webs with PDMS. A PVDF fiber web filled with PDMS is shown in Figure 59 suggesting this may be a viable approach.

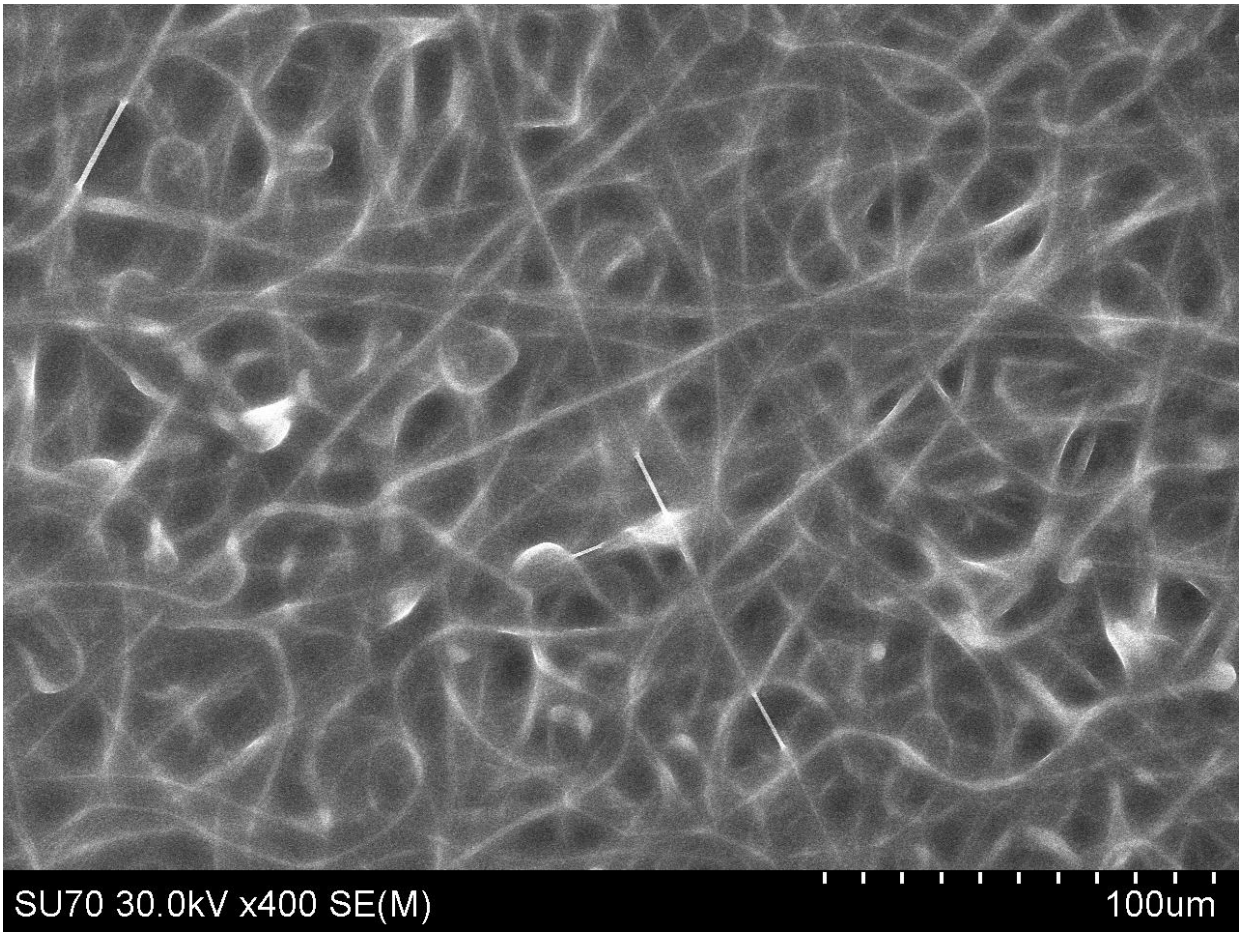

Figure 59. PDMS filled fiber web.

However, in order to be able to get an accurate comparison between devices, reducing the complexity of the device was important. The effect of filling the pores of the web may differ from sample to sample since there are extra processing steps, which included heating the composite. The additional heat treatment needed to cure the PDMS web matrix may influence the piezoelectric properties. Also, the reduction in surface area and change in electrical properties of the composite may influence the measured piezoelectric response. Therefore, this

approach was not used for comparison but is included to show that this would be a viable option in certain cases where fiber webs were thin.

In order, to test the samples that showed a piezoelectric response, a method was needed for applying a repeatable force. A pendulum was used to apply an impact force to the devices. An impact force was desired because it resulted in a high voltage response. The pendulum was brought to a height of 30° and released. This was done at least ten times in order to get an average for the voltage response. The voltage was measured with an oscilloscope. Table 16 shows the average piezoelectric response for each working device and includes the web structure of the sample.

Table 16. Voltage response.

PVDF Structure	Average Fiber Diameter	Bead Nodes Per 12,000μm^2	Average Bead Diameter(μm)	Porosity	V/mm	V/g
Thin Film Non Poled				0	0	0
Thin Film Poled				0	10.53	0.52
Fiber Web with Incomplete Evaporation	1194	0	0	0.62	0.20	0.025
Nanofiber Web	148	81	6.2	0.88	0.28	0.12
Nanofiber Web	147	9	11.9	0.83	1.34	0.38

Table 16 shows, as expected, that the non-poled film showed no piezoelectric response. Also, the poled thin film device outperformed each of the fiber web devices. When compared on a mass basis one of the fiber webs does approach the performance of the poled thin film. When comparing the fiber web devices, the smaller average fiber diameter webs performed better then the larger average fiber diameter webs, but this may be due to the incomplete evaporation defect. This was in contrast to what was expected by the XRD results shown in Figure 57 and supports earlier statements that further work was needed to understand the exact relationship between the XRD data and piezoelectric performance of PVDF fiber webs. The sample with high levels of

beads showed worse performance than the sample with a lower number of beds. These observations provided evidence that, in addition to controlling the fiber diameter, there were additional ways to influence the piezoelectric performance of the web. Additional measurements were needed to confirm these observations and elaborate on the effect of each structure.

Another reported method for measuring piezoelectric functionality of PVDF thin films was measuring the remnant polarization of the material [120]. This was accomplished by measuring the polarization hysteresis with a Sawyer–Tower circuit [25]. Hysteresis measurements of remnant polarization were not performed on PVDF fiber webs, but this method was used to evaluate the electrical properties of ferroelectric thin films [120, 121]. This method was attempted in the lab, but films were too porous, and there was dielectric breakdown; or films were too thick, and the voltage supply could not provide a sufficient electric field to perform the test.

Even though PVDF thin films showed a higher piezoelectric response than fiber webs in this study, there are reasons why fiber webs are desired over thin film. First, production of piezoelectric fibers does not require the additional poling step; this saves on processing time and equipment. If the poling process was added it may be possible to enhance the piezoelectric response of fiber webs. Second, fiber webs are porous and can allow material to pass through the fiber membrane which may be needed for filtration applications. In addition, the porous nature of webs could be used to provide the support structure of another functional material. If there is a material that can be activated using electric charge, PVDF webs would be an ideal choice. Third, fiber webs were more compliant than thin films.

This research showed that the structure of PVDF fiber webs influenced the piezoelectric performance. This research showed that the peaks of the XRD results do not necessarily predict

the piezoelectric performance in fiber webs. Future work should explore more reliable testing methods for piezoelectric performance. Perhaps one of the best options would be using piezoforce microscopy to directly measure the piezoelectric force at the atomic level [36]. This tool would be beneficial to future research in this field. Future work should also include a comparison between different contact setups for PVDF webs. Also, the influence of PDMS in the fiber web requires additional investigation before these samples can be tested and compared to the piezoelectric performance of other fiber webs.

Chapter 7: Discussion of Systems Approach

The systems approach was multifaceted and, therefore, provided a comprehensive understanding for the production of electrospun PVDF fibers. The systems approach for understanding the electrospinning system was comprised of multiple subsystems, including the solution system, processing system, web structure, including defects, system, and the functional system properties. Figure 7 shows that many relationships within the entire electrospinning system were still unknown and debated; also, many of the relationships reported in Figure 7 were for electrospinning other polymers, and it was unknown whether these relationship were the same for electrospinning PVDF.

By using the systems approach, many new relationships were established. In Figure 60 and Figure 61, the arrows in green represent findings from this research that were not reported in the literature, were not observed for electrospinning PVDF, or were confirming a relationship of a debated parameter. The black arrows show parameters that were reported in the literature and verified by this research. The high number of green arrows validated the need for research based on a systems understanding. Since many relationships in Figure 60 and Figure 61 would not be observed without testing the entire system of parameters.

The interconnected nature of the relationships between each system emphasized the importance of this approach. The most successful model used to predict the average fiber diameter of the web used all eight parameters and all interactions. This validated the expected complexity of the electrospinning process and suggested that, in most cases, the system was

accurately described by using the eight parameters and second level interactions identified in this study.

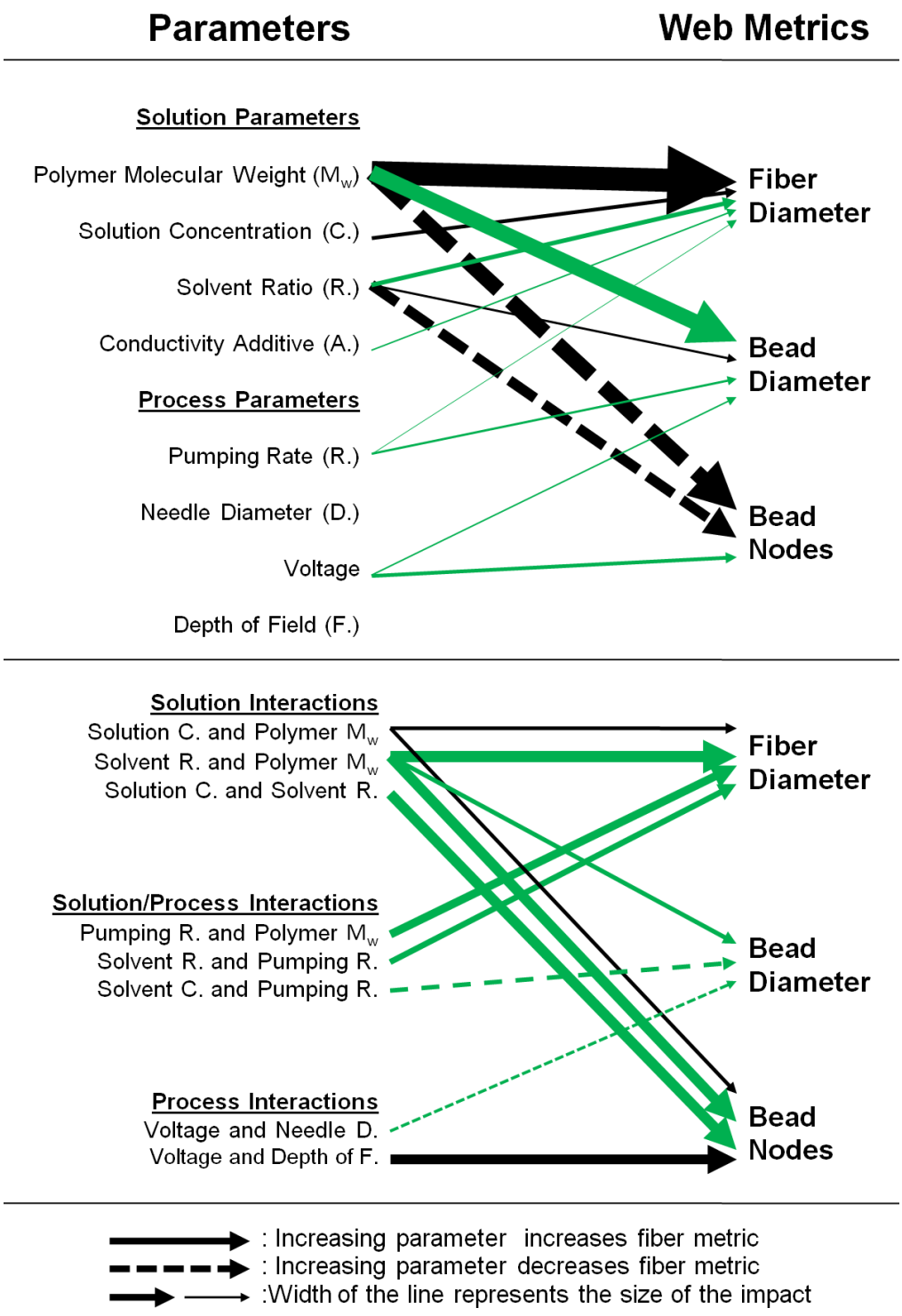

Figure 60. System diagram with solution and processing parameters with contributions of this work highlighted in green.

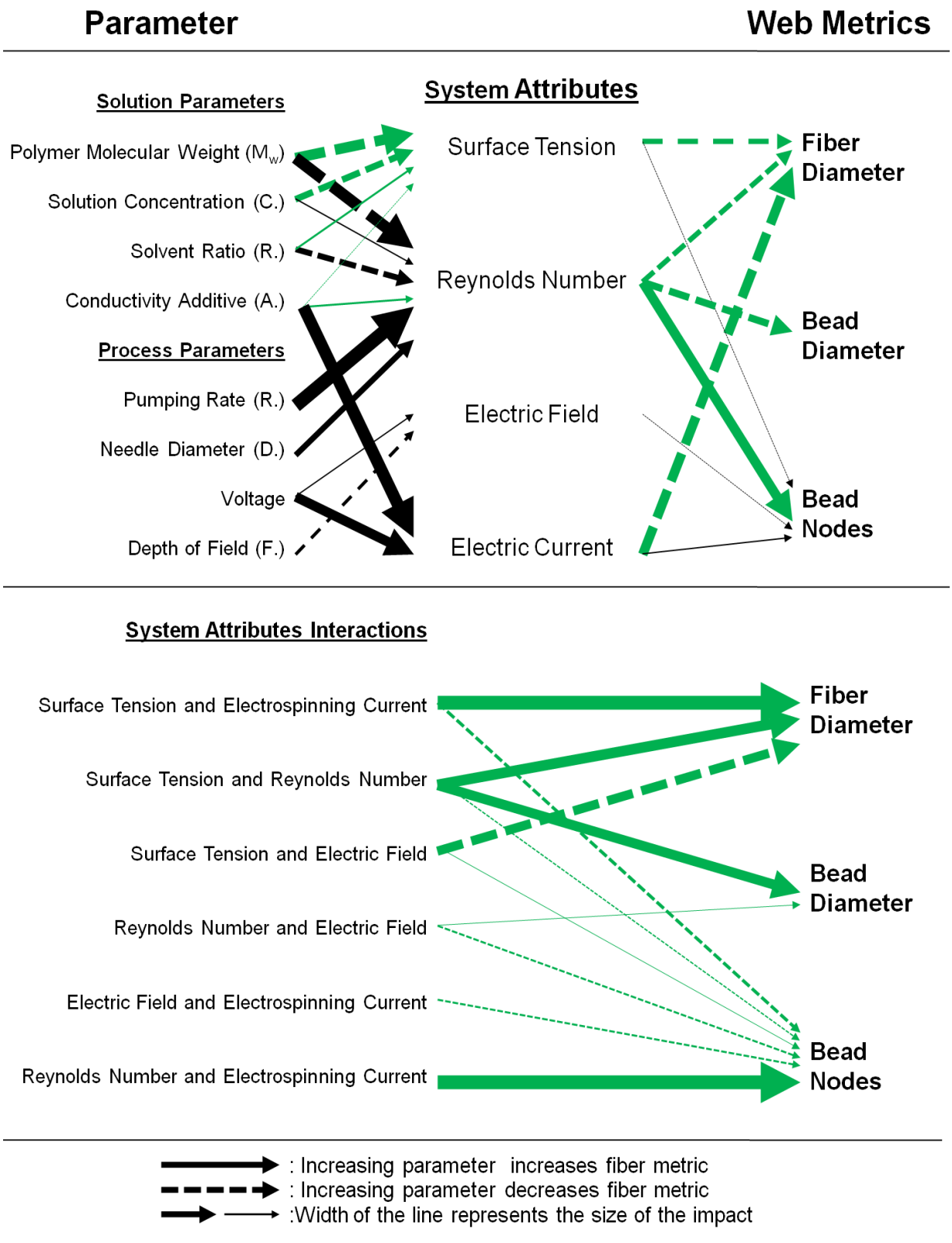

Figure 61. System diagram using system parameters with contributions of this work highlighted in green.

Also, the systems understanding was necessary in order to tailor the performance of the web. As outlined earlier, the first step of this systems approach was to develop regression equations that could be used to predict the occurrence of defects for a specific set of parameters. Therefore, it was possible, using the production guidelines in Table 7, to provide a streamlined approach for manufacturers to reduce defect occurrence and anticipate the effect of changing electrospinning parameters. In addition, the logistic regression equations can be used to explore new defect free production space with a controlled web structure. Next, the regression equations for controlling the web structure were developed. Finally, the influence of the defect occurrence and web structure on the performance was explored.

Once structure-processing-function relationships were understood, influencing the desired porosity and piezoelectric response was possible. Now, when certain functionality is desired, the web structure can be identified. Therefore, if obtaining a fiber web with an average fiber diameter of 100 nm without any defects is desirable conducting a desirability study in order to obtain a set of parameters or multiple sets of parameters would be possible for producing the desired web. Once the webs were produced and characterized, then the production guidelines and system diagram could be used to make modifications to the structure and performance of the web as needed. Due to the nature of many of the applications suggested for PVDF fiber webs, knowing how both the porosity and the piezoelectric response of the webs changed with structure was important, further emphasizing the need for a systems understanding.

Lastly, the systems understanding was useful because it provided multiple pathways for monitoring the occurrence of defects and the web structure using the system parameters. Different ranges of the Reynolds number, surface tension, and the electrospinning current were associated with different defects. Therefore, the values of the system parameters could be

monitored during production in order to anticipate defect occurrence and, in some cases, web structure.

Chapter 8: Conclusions

In its entirety, this research demonstrated that a comprehensive systems analysis was an effective method for understanding the relationships between electrospinning parameters and web structure, which can be used to tailor the web performance. The regression equations showed that many parameters influenced multiple defects and web structures. Therefore, due to the completive nature of electrospinning parameters, a systems approach was needed to understand the influence of parameters on defect occurrence and the web structure.

Production guidelines and system diagrams presented the competition between different metrics due to the interrelationships of electrospinning parameters and, in some cases, system parameters. Now that this methodology was validated for PVDF, extending the model for electrospinning other polymers may be possible. The relationships developed for the guidelines and processing system diagrams may be applicable to other polymers. Another possibility would be to find new regression coefficients, specific to the desired polymer and solvent, for the regression equations using the parameters identified in this work as a framework.

The high occurrence of defects at the nanoscale highlighted the challenges of nanomanufacturing for the electrospinning technique. Electrospraying and beading occurred as the fiber diameter was driven smaller into the nanoscale, while incomplete solvent evaporation and fiber bridging tended to occur as the fiber diameter was driven higher into the microscale. The molecular weight tended to have the most influence on the occurrence of different defects in this study. The Reynolds number, surface tension, and electrospinning current were identified as possible parameters to monitor during the electrospinning process in order to anticipate defects.

Future work could look at expanding the production space for defect free PVDF fibers using the regression equations developed for defect occurrence.

Next, this research showed that regression models based on system parameters were not as effective as the eight parameter regression models based on more controllable electrospinning parameters. This was due to the high significance of parameter interactions which were not captured by the regression models that used system parameters. Also, this showed that the initial electrospinning conditions were important. Once again, in this study, the polymer molecular weight was identified as the most significant parameter. The Reynolds number was identified as the most significant system parameter when controlling the structure of fibers and beads. The research showed the importance of many interaction terms for defect occurrence and web structure that were not previously considered for electrospinning.

In conclusion, functional webs were achieved by controlling the structure of the fiber webs. This study showed that, in general, incomplete evaporation reduced the porosity of fiber webs, and beading increased the porosity of fiber webs. Therefore, the ability to control the occurrence of defects also led to a new method for tailoring porosity. Also, by controlling the bead structure modifying the porosity. A large range of web porosities are possible by controlling the occurrence of defects, fiber diameter, bead diameter, and the number of beads per area. In addition to measuring and controlling porosity, the piezoelectric response of fiber webs was documented. Only certain fiber webs were capable of producing a piezoelectric response due to the limitations of using a porous web. There is an opportunity for future work that explores the influence of defect structure on piezoelectric properties but first a standardized method to test the piezoelectric response of porous webs is needed.

References

[1] Kelly, K. L., Coronado, E., Zhao, L. L., and Schatz, G. C., 2002, "The Optical Properties of Metal Nanoparticles: The Influence of Size, Shape, and Dielectric Environment," The Journal of Physical Chemistry B, 107(3), pp. 668-677.
[2] Reibold, M., Paufler, P., Levin, A. A., Kochmann, W., Patzke, N., and Meyer, D. C., 2006, "Materials: Carbon nanotubes in an ancient Damascus sabre," Nature, 444(7117), pp. 286-286.
[3] BCC Research, 2013, "Global Markets and Technologies for Nanofibers," No. NAN043C. http://www.bccresearch.com/market-research/nanotechnology/nanofibers-market-nan043c.html
[4] Future Markets, 2012, "Global Market for Nanofibers (Alumina, Polymer, Carbon and Cellulose) to 2017," No. 2303361. http://www.researchandmarkets.com/reports/2303361/global_market_for_nanofibers_alumina_polymer
[5] McKinsey Global Institute., 2012, "Manufacturing the future: The next era of global growth and innovation," NIST.
[6] Nalwa, H. S., 1995, Ferroelectric Polymers: Chemistry: Physics, and Applications, Taylor & Francis.
[7] Dargaville, T., Celina, M., Elliott, J., Chaplya, P., Jones, G., Mowery, D., Assink, R., Clough, R., and Martin, J., 2005, "Characterization, Performance and Optimization of PVDF as a Piezoelectric Film for Advanced Space Mirror Concepts," Sandia National Laboratories.
[8] Jiang, Y., Ye, Y., Yu, J., Wu, Z., Li, W., Xu, J., and Xie, G., 2007, "Study of thermally poled and corona charged poly(vinylidene fluoride) films," Polymer Engineering & Science, 47(9), pp. 1344-1350.
[9] Chen, Q., Natale, D., Neese, B., Ren, K., Lin, M., Zhang, Q. M., Pattom, M., Wang, K. W., Fang, H., and Im, E., 2007, "Piezoelectric polymers actuators for precise shape control of large scale space antennas," Jet Propulsion Laboratory, National Aeronautics and Space Administration.
[10] Rathod, V. T., Mahapatra, D. R., Jain, A., and Gayathri, A., 2010, "Characterization of a large-area PVDF thin film for electro-mechanical and ultrasonic sensing applications," Sensors and Actuators A: Physical, 163(1), pp. 164-171.
[11] Li, S., Yuan, J., and Lipson, H., 2011, "Ambient wind energy harvesting using cross-flow fluttering," Journal of Applied Physics, 109(2).
[12] Tamjidi, N., Sato, K., Sakurai, J., and Hata, S., 2013, "PVDF actuator for high-frequency fatigue test of thin-film metals," IEEJ Transactions on Electrical and Electronic Engineering, 8(2), pp. 199-205.
[13] Sharma, T., Aroom, K., Naik, S., Gill, B., and Zhang, J. J., 2013, "Flexible Thin-Film PVDF-TrFE Based Pressure Sensor for Smart Catheter Applications," Annals of Biomedical Engineering, 41(4), pp. 744-751.
[14] Measurement Specialties, 1999, "Piezo Film Sensor Technical Manual," Sensor Products Division, Norristown.

[15] Yao, C., Li, X., Neoh, K. G., Shi, Z., and Kang, E. T., 2009, "Antibacterial activities of surface modified electrospun poly(vinylidene fluoride-co-hexafluoropropylene) (PVDF-HFP) fibrous membranes," Applied Surface Science, 255(6), pp. 3854-3858.
[16] Liu, Y., Yang, D., Yu, T., and Jiang, X., 2009, "Incorporation of electrospun nanofibrous PVDF membranes into a microfluidic chip assembled by PDMS and scotch tape for immunoassays," Electrophoresis, 30(18), pp. 3269-3275.
[17] Damaraju, S. M., Wu, S., Jaffe, M., and Arinzeh, T. L., 2013, "Structural changes in PVDF fibers due to electrospinning and its effect on biological function," Biomedical Materials, 8(4), p. 045007.
[18] Guo, H.F., Li, Z.S., Dong, S.W., Chen, W.J., Deng, L., Wang, Y.F., and Ying, D.J., 2012, "Piezoelectric PU/PVDF electrospun scaffolds for wound healing applications," Colloids and Surfaces B: Biointerfaces, 96(0), pp. 29-36.
[19] Pua J., X. Yana, Y. Jiangb, C. Changa, and Lina, L., 2010, "Piezoelectric actuation of direct-write electrospun fibers," Sensors Actuators, 164(1-2), p. 131.
[20] Manesh, K. M., Santhosh, P., Gopalan, A., and Lee, K.-P., 2007, "Electrospun poly(vinylidene fluoride)/poly(aminophenylboronic acid) composite nanofibrous membrane as a novel glucose sensor," Analytical Biochemistry, 360(2), pp. 189-195.
[21] Chang, C., Tran, V. H., Wang, J., Fuh, Y.-K., and Lin, L., 2010, "Direct-Write Piezoelectric Polymeric Nanogenerator with High Energy Conversion Efficiency," Nano Letters, 10(2), pp. 726-731.
[22] Mandal, D., Yoon, S., and Kim, K. J., 2011, "Origin of Piezoelectricity in an Electrospun Poly(vinylidene fluoride-trifluoroethylene) Nanofiber Web-Based Nanogenerator and Nano-Pressure Sensor," Macromolecular Rapid Communications, 32(11), pp. 831-837.
[23] Li, F., Liu, W., Stefanini, C., Fu, X., and Dario, P., 2010, "A Novel Bioinspired PVDF Micro/Nano Hair Receptor for a Robot Sensing System," Sensors, 10(1), pp. 994-1011.
[24] Wang, Y. R., Zheng, J. M., Ren, G. Y., Zhang, P. H., and Xu, C., 2011, "A flexible piezoelectric force sensor based on PVDF fabrics," Smart Materials and Structures, 20(4), p. 045009.
[25] Li, Q., Xi, S., and Zhang, X., "Conservation of paper relics by electrospun PVDF fiber membranes," Journal of Cultural Heritage.
[26] Zhou, W., Bahi, A., Li, Y., Yang, H., and Ko, F., 2013, "Ultra-filtration membranes based on electrospun poly(vinylidene fluoride) (PVDF) fibrous composite membrane scaffolds," RSC Advances, 3(29), pp. 11614-11620.
[27] Gopal, R., Kaur, S., Ma, Z., Chan, C., Ramakrishna, S., and Matsuura, T., 2006, "Electrospun nanofibrous filtration membrane," Journal of Membrane Science, 281(1–2), pp. 581-586.
[28] Pelipenko, J., Kristl, J., Janković, B., Baumgartner, S., and Kocbek, P., 2013, "The impact of relative humidity during electrospinning on the morphology and mechanical properties of nanofibers," International Journal of Pharmaceutics, 456(1), pp. 125-134.
[29] Wang, X., and Shi, J., 2012, "Piezoelectric Nanogenerators for Self-powered Nanodevices," Piezoelectric Nanomaterials for Biomedical Applications, pp. 135-172.
[30] Andrew, J. S., and Clarke, D. R., 2008, "Effect of Electrospinning on the Ferroelectric Phase Content of Polyvinylidene Difluoride Fibers," Langmuir, 24(3), pp. 670-672.
[31] Ribeiro C., S. Moreira, V. Correia, V. Sencadas, J.G. Rocha, F. M. Gama, Ribelles, J. L. G., and Lanceros-Méndez, S., 2012, "Enhanced proliferation of pre-osteoblastic cells by dynamic piezoelectric stimulation," RSC Advances, 2(30), p. 11504.

[32] Zheng, J., He, A., Li, J., and Han, C. C., 2007, "Polymorphism Control of Poly(vinylidene fluoride) through Electrospinning," Macromolecular Rapid Communications, 28(22), pp. 2159-2162.
[33] Pu, J., Yan, X., Jiang, Y., Chang, C., and Lin, L., 2010, "Piezoelectric actuation of direct-write electrospun fibers," Sensors and Actuators A: Physical, 164(1–2), pp. 131-136.
[34] Li, D., and Xia, Y., 2004, "Electrospinning of nanofibers: reinventing the wheel?," Advanced materials, 16(14), pp. 1151-1170.
[35] Reneker, D. H., and Yarin, A. L., 2008, "Electrospinning jets and polymer nanofibers," Polymer, 49(10), pp. 2387-2425.
[36] Baji, A., Mai, Y.-W., Li, Q., and Liu, Y., 2011, "Electrospinning induced ferroelectricity in poly(vinylidene fluoride) fibers," Nanoscale, 3(8), pp. 3068-3071.
[37] Bune, A. V., Fridkin, V. M., Ducharme, S., Blinov, L. M., Palto, S. P., Sorokin, A. V., Yudin, S. G., and Zlatkin, A., 1998, "Two-dimensional ferroelectric films," Nature, 391(6670), pp. 874-877.
[38] Essalhi, M., and Khayet, M., 2013, "Self-sustained webs of polyvinylidene fluoride electrospun nanofibers at different electrospinning times: 1. Desalination by direct contact membrane distillation," Journal of Membrane Science, 433(0), pp. 167-179.
[39] Eichhorn, S., and Sampson, W., 2005, "Statistical geometry of pores and statistics of porous nanofibrous assemblies," Journal of the Royal Society Interface, 2(4), pp. 309-318.
[40] Pham, Q. P., Sharma, U., and Mikos, A. G., 2006, "Electrospinning of Polymeric Nanofibers for Tissue Engineering Applications: A Review," Tissue Engineering, 12(5), pp. 1197-1211.
[41] Wang, S., Yang, Y., Zhang, Y., Fei, X., Zhou, C., Zhang, Y., Li, Y., Yang, Q., and Song, Y., 2014, "Fabrication of large-scale superhydrophobic composite films with enhanced tensile properties by multinozzle conveyor belt electrospinning," Journal of Applied Polymer Science, 131(1).
[42] Huang, Z. M., Zhang, Y. Z., Kotaki, M., and Ramakrishna, S., 2003, "A review on polymer nanofibers by electrospinning and their applications in nanocomposites," Composites Science and Technology, 63(15), pp. 2223-2253.
[43] Anton, F., 1934, "Process and apparatus for preparing artificial threads".
[44] Nasir, M., Matsumoto, H., Danno, T., Minagawa, M., Irisawa, T., Shioya, M., and Tanioka, A., 2006, "Control of diameter, morphology, and structure of PVDF nanofiber fabricated by electrospray deposition," Journal of Polymer Science Part B: Polymer Physics, 44(5), pp. 779-786.
[45] Cozza, E. S., Monticelli, O., Marsano, E., and Cebe, P., 2013, "On the electrospinning of PVDF: influence of the experimental conditions on the nanofiber properties," Polymer International, 62(1), pp. 41-48.
[46] Elmarco, "Nanospider Technology Parameters," http://www.elmarco.com/upload/soubory/obsah/63-1-nanospidertm-technology-parameters.pdf.
[47] Chang, J., Dommer, M., Chang, C., and Lin, L., 2012, "Piezoelectric nanofibers for energy scavenging applications," Nano Energy, 1(3), pp. 356-371.
[48] Sedo, P., 2009, ELMARCO. http://www.czechtechnologydays.org/sites/default/files/3_%C5%A0edo_Elmarco.pdf
[49] Wang, X., Hu, X., Qiu, X., Huang, X., Wu, D., and Sun, D., 2013, "An improved tip-less electrospinning with strip-distributed solution delivery for massive production of uniform polymer nanofibers," Materials Letters, 99(0), pp. 21-23.

[50] Chanunpanich, N., Lee, B., and Byun, H., 2008, "A study of electrospun PVDF on PET sheet," Macromolecular Research, 16(3), pp. 212-217.
[51] Lee, J., Lee, S. Y., Jang, J., Jeong, Y. H., and Cho, D.-W., 2012, "Fabrication of Patterned Nanofibrous Mats Using Direct-Write Electrospinning," Langmuir, 28(18), pp. 7267-7275.
[52] Leung, L. H., Fan, S., and Naguib, H. E., 2012, "Fabrication of 3D electrospun structures from poly(lactide-co-glycolide acid)–nano-hydroxyapatite composites," Journal of Polymer Science Part B: Polymer Physics, 50(4), pp. 242-249.
[53] Bisht, G. S., Canton, G., Mirsepassi, A., Kulinsky, L., Oh, S., Dunn-Rankin, D., and Madou, M. J., 2011, "Controlled Continuous Patterning of Polymeric Nanofibers on Three-Dimensional Substrates Using Low-Voltage Near-Field Electrospinning," Nano Letters, 11(4), pp. 1831-1837.
[54] Liu, Z. H., Pan, C. T., Lin, L. W., and Lai, H. W., 2013, "Piezoelectric properties of PVDF/MWCNT nanofiber using near-field electrospinning," Sensors and Actuators A: Physical, 193(0), pp. 13-24.
[55] Persano, L., Dagdeviren, C., Su, Y., Zhang, Y., Girardo, S., Pisignano, D., Huang, Y., and Rogers, J. A., 2013, "High performance piezoelectric devices based on aligned arrays of nanofibers of poly(vinylidenefluoride-co-trifluoroethylene)," Natue Communications, 4, p. 1633.
[56] Teo, W., and Ramakrishna, S., 2006, "A review on electrospinning design and nanofibre assemblies," Nanotechnology, 17(14), p. R89.
[57] Teo, W.-E., Inai, R., and Ramakrishna, S., 2011, "Technological advances in electrospinning of nanofibers," Science and Technology of Advanced Materials, 12(1), p. 013002.
[58] Ali, U., Zhou, Y., Wang, X., and Lin, T., 2011, "Electrospinning of Continuous Nanofiber Bundles and Twisted Nanofiber Yarns, Nanofibers - Production, Properties and Functional Applications," http://www.intechopen.com/books/nanofibers-production-properties-and-functional-applications/electrospinning-of-continuous-nanofiber-bundles-and-twisted-nanofiber-yarns.
[59] Gasparini, T. M., Suman Bretas, R. E., da Silva, A. B., and Gregorio, R., 2012, "Processing and characterization of oriented electrospun poly(vinylidene fluoride) mats," Journal of Polymer Science Part B: Polymer Physics, 50(18), pp. 1304-1311.
[60] Yee, W. A., Nguyen, A. C., Lee, P. S., Kotaki, M., Liu, Y., Tan, B. T., Mhaisalkar, S., and Lu, X., 2008, "Stress-induced structural changes in electrospun polyvinylidene difluoride nanofibers collected using a modified rotating disk," Polymer, 49(19), pp. 4196-4203.
[61] Hohman, M. M., Shin, M., Rutledge, G., and Brenner, M. P., 2001, "Electrospinning and electrically forced jets. I. Stability theory," Physics of Fluids (1994-present), 13(8), pp. 2201-2220.
[62] Yarin, A. L., Koombhongse, S., and Reneker, D. H., 2001, "Bending instability in electrospinning of nanofibers," Journal of Applied Physics, 89(5), pp. 3018-3026.
[63] Yarin, A. L., Koombhongse, S., and Reneker, D. H., 2001, "Taylor cone and jetting from liquid droplets in electrospinning of nanofibers," Journal of Applied Physics, 90(9), pp. 4836-4846.
[64] Cui, W., Li, X., Zhou, S., and Weng, J., 2007, "Investigation on process parameters of electrospinning system through orthogonal experimental design," Journal of Applied Polymer Science, 103(5), pp. 3105-3112.
[65] Thompson, C. J., Chase, G. G., Yarin, A. L., and Reneker, D. H., 2007, "Effects of parameters on nanofiber diameter determined from electrospinning model," Polymer, 48(23), pp. 6913-6922.

[66] Shenoy, S. L., Bates, W. D., Frisch, H. L., and Wnek, G. E., 2005, "Role of chain entanglements on fiber formation during electrospinning of polymer solutions: good solvent, non-specific polymer–polymer interaction limit," Polymer, 46(10), pp. 3372-3384.
[67] Beachley, V., and Wen, X., 2009, "Effect of electrospinning parameters on the nanofiber diameter and length," Materials Science and Engineering: C, 29(3), pp. 663-668.
[68] Yördem, O. S., Papila, M., and Menceloğlu, Y. Z., 2008, "Effects of electrospinning parameters on polyacrylonitrile nanofiber diameter: An investigation by response surface methodology," Materials & Design, 29(1), pp. 34-44.
[69] Li, Z., and Wang, C., 2013, "One-Dimensional Nanostructures: Effects of Working Parameters on Electrospinning."
[70] Jarusuwannapoom, T., Hongrojjanawiwat, W., Jitjaicham, S., Wannatong, L., Nithitanakul, M., Pattamaprom, C., Koombhongse, P., Rangkupan, R., and Supaphol, P., 2005, "Effect of solvents on electro-spinnability of polystyrene solutions and morphological appearance of resulting electrospun polystyrene fibers," European Polymer Journal, 41(3), pp. 409-421.
[71] L. Costa, R.Bretas, R. Gregorio, 2010, "Effect of Solution Concentration on the Electrospray/Electrospinning Transition and on the Crystalline Phase of PVDF," Materials Sciences and Applications, 1(4).
[72] Zong, X., Kim, K., Fang, D., Ran, S., Hsiao, B. S., and Chu, B., 2002, "Structure and process relationship of electrospun bioabsorbable nanofiber membranes," Polymer, 43(16), pp. 4403-4412.
[73] Cramariuc, B., Cramariuc, R., Scarlet, R., Manea, L. R., Lupu, I. G., and Cramariuc, O., 2013, "Fiber diameter in electrospinning process," Journal of Electrostatics, 71(3), pp. 189-198.
[74] Heikkilä, P., and Harlin, A., 2008, "Parameter study of electrospinning of polyamide-6," European Polymer Journal, 44(10), pp. 3067-3079.
[75] Katti, D. S., Robinson, K. W., Ko, F. K., and Laurencin, C. T., 2004, "Bioresorbable nanofiber-based systems for wound healing and drug delivery: Optimization of fabrication parameters," Journal of Biomedical Materials Research Part B: Applied Biomaterials, 70B(2), pp. 286-296.
[76] Yee, W. A., Kotaki, M., Liu, Y., and Lu, X., 2007, "Morphology, polymorphism behavior and molecular orientation of electrospun poly(vinylidene fluoride) fibers," Polymer, 48(2), pp. 512-521.
[77] Cozza, E., Monticeli, O., Marsano, E., Cebe, P., 2013, "On the electrospinning of PVDF: influence of the experimental conditions on the nanofiber properties," Polymer International, 62(1), p. 41.
[78] Nezarati, R. M., Eifert, M. B., and Cosgriff-Hernandez, E., 2013, "Effects of Humidity and Solution Viscosity on Electrospun Fiber Morphology," Tissue Engineering Part C: Methods, 19(10).
[79] Hohman, M. M., Shin, M., Rutledge, G., and Brenner, M. P., 2001, "Electrospinning and electrically forced jets. II. Applications," Physics of Fluids, 13(8), pp. 2221-2236.
[80] Gupta, P., Elkins, C., Long, T. E., and Wilkes, G. L., 2005, "Electrospinning of linear homopolymers of poly(methyl methacrylate): exploring relationships between fiber formation, viscosity, molecular weight and concentration in a good solvent," Polymer, 46(13), pp. 4799-4810.
[81] Fridrikh, S. V., Yu, J. H., Brenner, M. P., and Rutledge, G. C., 2003, "Controlling the Fiber Diameter during Electrospinning," Physical Review Letters, 90(14), p. 144502.

[82] Fong, H., Chun, I., and Reneker, D. H., 1999, "Beaded nanofibers formed during electrospinning," Polymer, 40(16), pp. 4585-4592.
[83] Liu, Y., He, J.-H., Yu, J.-y., and Zeng, H.-m., 2008, "Controlling numbers and sizes of beads in electrospun nanofibers," Polymer International, 57(4), pp. 632-636.
[84] Fong, H., and Reneker, D. H., 1999, "Elastomeric nanofibers of styrene–butadiene–styrene triblock copolymer," Journal of Polymer Science Part B: Polymer Physics, 37(24), pp. 3488-3493.
[85] Arrhenius, S., 1917, "The Viscosity of Solutions," Biochemical Journal, 11(2), pp. 112-133.
[86] Darby, R., 2001, Chemical Engineering Fluid Mechanics, Revised and Expanded, Taylor & Francis.
[87] Morgret, L. D., and Pawlowski, K. J., 2005, "Electrospinning of Polyvinylidene Fluoride and Polyetherimide From Mixed Solvents," NASA Langley Research Center.
[88] Zhao, Z., Li, J., Yuan, X., Li, X., Zhang, Y., and Sheng, J., 2005, "Preparation and properties of electrospun poly(vinylidene fluoride) membranes," Journal of Applied Polymer Science, 97(2), pp. 466-474.
[89] Jing, H., Du, X., and Jiang, Y., 2009, "Control of diameter and morphology of poly(vinylidene fluoride) nanofibers fabricated by electrospinning," pp. 750814-750814.
[90] de Gennes, P. G., 1980, "Conformations of Polymers Attached to an Interface," Macromolecules, 13(5), pp. 1069-1075.
[91] Reynolds, O., 1883, An experimental investigation of the circumstances which determine whether the motion of water shall be direct or sinuous : and of the law of resistance in parallel channels, Royal Society of London, London.
[92] He, J.H., and Wan, Y.Q., 2004, "Allometric Scaling and Instability in Electrospinning," International Journal of Nonlinear Sciences and Numerical Simulation, p. 243.
[93] Nima Technology, 2003, "Surface Tensiometers: Operating Manual." http://www.brownwaite.com/download/i/mark_dl/u/4012060545/4597460485/Tensiometer.PDF
[94] Lee, K. H., Kim, H. Y., Bang, H. J., Jung, Y. H., and Lee, S. G., 2003, "The change of bead morphology formed on electrospun polystyrene fibers," Polymer, 44(14), pp. 4029-4034.
[95] R. Gregorio, R. B. a. L. C., 2010, "Effect of Solution Concentration on the Electrospray/Electrospinning Transition and on the Crystalline Phase of PVDF," Materials Sciences and Applications, 1(4), pp. 247-252.
[96] Sarlak, N., Nejad, M. A. F., Shakhesi, S., and Shabani, K., 2012, "Effects of electrospinning parameters on titanium dioxide nanofibers diameter and morphology: An investigation by Box–Wilson central composite design (CCD)," Chemical Engineering Journal, 210(0), pp. 410-416.
[97] Coles, S. R., Jacobs, D. K., Meredith, J. O., Barker, G., Clark, A. J., Kirwan, K., Stanger, J., and Tucker, N., 2010, "A design of experiments (DoE) approach to material properties optimization of electrospun nanofibers," Journal of Applied Polymer Science, 117(4), pp. 2251-2257.
[98] Akaike, H., 1974, "A new look at the statistical model identification," Automatic Control, IEEE Transactions on, 19(6), pp. 716-723.
[99] Burnham, K. P., and Anderson, D. R., 2004, "Multimodel Inference: Understanding AIC and BIC in Model Selection," Sociological Methods & Research, 33(2), pp. 261-304.
[100] Yang, Y., 2005, "Can the strengths of AIC and BIC be shared? A conflict between model indentification and regression estimation," Biometrika, 92(4), pp. 937-950.
[101] Tomczak, N., Van Hulst, N. F., and Vancso, G. J., 2005, "Beaded Electrospun Fibers for Photonic Applications," Macromolecules, 38(18), pp. 7863-7866.

[102] Patra, S. N., Easteal, A. J., and Bhattacharyya, D., 2009, "Parametric study of manufacturing poly(lactic) acid nanofibrous mat by electrospinning," Journal of Materials Science, 44(2), pp. 647-654.
[103] Theron, S. A., Zussman, E., and Yarin, A. L., 2004, "Experimental investigation of the governing parameters in the electrospinning of polymer solutions," Polymer, 45(6), pp. 2017-2030.
[104] Deitzel, J. M., Kleinmeyer, J., Harris, D., and Beck Tan, N. C., 2001, "The effect of processing variables on the morphology of electrospun nanofibers and textiles," Polymer, 42(1), pp. 261-272.
[105] Chen, Y., Wang, L., Xue, Y., Jiang, L., and Zheng, Y., 2013, "Bioinspired tilt-angle fabricated structure gradient fibers: micro-drops fast transport in a long-distance," Scientific Reports, 3.
[106] SAS Institute., "Desirability Profiling and Optimization," http://www.jmp.com/support/help/Desirability_Profiling_and_Optimization.shtml.
[107] Simonet, M., Stingelin, N., Wismans, J. G. F., Oomens, C. W. J., Driessen-Mol, A., and Baaijens, F. P. T., 2014, "Tailoring the void space and mechanical properties in electrospun scaffolds towards physiological ranges," Journal of Materials Chemistry B, 2(3), pp. 305-313.
[108] Soliman, S., Sant, S., Nichol, J. W., Khabiry, M., Traversa, E., and Khademhosseini, A., 2011, "Controlling the porosity of fibrous scaffolds by modulating the fiber diameter and packing density," Journal of Biomedical Materials Research Part A, 96A(3), pp. 566-574.
[109] Dotti, F., Varesano, A., Montarsolo, A., Aluigi, A., Tonin, C., and Mazzuchetti, G., 2007, "Electrospun Porous Mats for High Efficiency Filtration," Journal of Industrial Textiles, 37(2), pp. 151-162.
[110] Millert, V., Simona, B., Neuenchwander, P., and Hall, H., 2011, "Tuning electrospinning parameters for production of 3D-fiber-fleeces with increased porosity for soft tissue engineering applications," European Cells and Materials, 21, pp. 286-303.
[111] Miles, R. E., 1964, "Random Polygons Determined by Random Lines in a Plane," Proceedings of the National Academy of Sciences of the United States of America, 52(4), pp. 901-907.
[112] Ghasemi-Mobarakeh, L., Semnani, D., and Morshed, M., 2007, "A novel method for porosity measurement of various surface layers of nanofibers mat using image analysis for tissue engineering applications," Journal of Applied Polymer Science, 106(4), pp. 2536-2542.
[113] Mannarino, M. M., and Rutledge, G. C., 2012, "Mechanical and tribological properties of electrospun PA 6(3)T fiber mats," Polymer, 53(14), pp. 3017-3025.
[114] Ma, Z., Kotaki, M., Yong, T., He, W., and Ramakrishna, S., 2005, "Surface engineering of electrospun polyethylene terephthalate (PET) nanofibers towards development of a new material for blood vessel engineering," Biomaterials, 26(15), pp. 2527-2536.
[115] Dayal, P., Liu, J., Kumar, S., and Kyu, T., 2007, "Experimental and Theoretical Investigations of Porous Structure Formation in Electrospun Fibers," Macromolecules, 40(21), pp. 7689-7694.
[116] Weber, N., Lee, Y., Shanmugasundaram, S. Jaffe, M. Arinzeh, T. 2010, "Characterization and in vitro cytocompatibility of piezoelectric electrospun scaffolds," Acta Biomaterialia, 6(9), p. 3550.
[117] Sencadas, V., Lanceros-Mendez, S., Mano, J. 2004, "Characterization of poled and non-poled β-PVDF films using thermal analysis techniques," Thermochimica Acta, 424(1-2), p. 201.

[118] Sencadas, V., Gregorio, R., and Lanceros-Méndez, S., 2009, "α to β Phase Transformation and Microestructural Changes of PVDF Films Induced by Uniaxial Stretch," Journal of Macromolecular Science, Part B, 48(3), pp. 514-525.
[119] Falconi, C., Mantini, G., D'Amico, A., and Wang, Z. L., 2009, "Studying piezoelectric nanowires and nanowalls for energy harvesting," Sensors and Actuators B: Chemical, 139(2), pp. 511-519.
[120] Pecherskaya, E. A., 2007, "The use of the Sawyer-Tower method and its modifications to measure the electrical parameters of ferroelectric materials," Measurement Techniques, 50(10), pp. 1101-1107.
[121] Dickens, B., Balizer, E., DeReggi, A. S., and Roth, S. C., 1992, "Hysteresis measurements of remanent polarization and coercive field in polymers," Journal of Applied Physics, 72(9), pp. 4258-4264.
[122] Akbari, A., Lehi, A. Y., and Bojaran, M., 2012, "Formation of Poly(vinylidenefluoride) Nanofibers: Part I: Optimization by Using of Central Composite Design," Journal of Nanostructres, pp. 69-77.

Appendix A. Statistical Analysis Results

It should be noted that terms that were not included for some of the interactions, these correction terms were only important when using the equation for prediction, they do not change the effects and therefore were not included in the table values. These correction terms were shown for the equations. In addition, the intercept term for the model was also left out, except in cases where a regression equation was not provided, since this was only useful for the equation as well.

Appendix A.1 Fiber Beading Statistical Analysis

Table A1. Fiber beading statistical analysis results with solution and processing parameters

Term	Estimate	Std Error	Chi^2	L-R Chi^2	Prob>Chi^2	Normalized Estimate
Solution Concentration	-24.1	3496	-	13	0.0002	-0.323
Solvent Ratio	50.0	6407	-	29	<.0001	0.669
Conductive Additive	-53.4	7528	-	28	<.0001	-0.716
Polymer M_w	74.5	8911	-	60	<.0001	1
Voltage	-15.6	2299	-	8.2	0.0042	-0.21
Voltage · Needle Diameter	-15.7	2281	-	7.7	0.0053	-0.210

Table A2. Fiber beading statistical analysis results with system parameters

Term	Estimate	Std Error	Chi^2	L-R Chi^2	Prob> Chi^2
Surface Tension	-0.457	0.19	5.39	7.1	0.0074
Reynolds Number	-4609	2346	3.86	20.3	<.0001
Electric Field	-0.902	0.573	2.48	2.88	0.0895

Appendix A.2 Electrospraying Statistical Analysis

Table A3. Electrospraying statistical analysis results with solution and processing parameters

Term	Estimate	Std Error	Chi^2	L-R Chi^2	Prob>Chi^2	Normalized Estimate
Solvent Ratio	1.6	0.50	7.06	11.1	0.0009	-0.48
Conductive Additive	-4.8	1.82	8.73	7.2	0.0075	-0.69
Pumping Ratio	-6.8	2.59	5.85	7.0	0.0083	0.39
Solution C. · Conductive A.	3.8	3.13	6.02	9.9	0.0017	0.32
Solution C. · Polymer M_w	3.1	1.23	5.07	5.9	0.015	1
(Polymer Mw)^2	9.8	1.56	4.93	6.2	0.0127	0.31
Pumping R. · Pumping R.	3	1.32	8.16	5.6	0.0177	-0.48

Table A4. Electrospraying statistical analysis results with system parameters

Term	Estimate	Std Error	Chi^2	L-R Chi^2	Prob>Chi^2
Surface Tension	16.32	4.75	11.81	14.7	0.0001
Reynolds Number	-0.42	0.13	10.96	25.2	<.0001
Electric Field	-281.25	84.63	11.04	4.00	0.0455

Appendix A.3 Complete Solvent Evaporation Statistical Analysis

Table A5. Complete solvent evaporation statistical analysis results with solution and processing parameters

Term	Estimate	Std Error	Chi^2	L-R Chi^2	Prob>Chi^2	Normalized Estimate
Polymer M_w	2.73	0.90	9.2	12.44	0.0004	0.95
Depth of Field	-1.69	0.62	7.5	9.78	0.0018	-0.58
Needle Diameter	1.50	0.58	6.58	8.59	0.0034	0.52
Solution C. · Voltage	1.22	0.47	6.75	9.15	0.0025	0.42
Solvent R. · Voltage	-1.00	0.50	3.96	4.55	0.0329	-0.35
Solution C. · Depth of Field	-2.88	1.08	7.18	14.22	0.0002	-1.00
Polymer M_w · Depth of Field	-1.87	0.63	8.85	8.64	0.0033	-0.65

Table A6. Complete solvent evaporation statistical analysis results with system parameters

Term	Estimate	Std Error	Chi^2	L-R Chi^2	Prob>Chi^2
Surface Tension	9.41	7.03	1.79	2.24	0.134
Reynolds Number Formula	-0.28	0.20	2.01	9.92	0.0016
Electric Field	-3067.93	1855.53	2.73	0.035	0.851
Electrospinning Current	0.12	0.62	0.04	0.066	0.796

Appendix A.4 Bridging from the Dispenser to the Collector Statistical Analysis

Table A7. Bridging from the dispenser to the collector statistical analysis results with solution and processing parameters

Term	Estimate	Std Error	Chi^2	L-R Chi^2	Prob>Chi^2	Normalized Estimate
Solution Concentration	-1.41	1.01	1.96	2.1	0.148	-0.44
Conductive Additive	2.62	0.77	11.62	24.8	<.0001	0.82
Polymer M_w	3.21	1.02	9.96	22.4	<.0001	1.00
Depth of Field	-0.91	0.61	2.24	2.6	0.1	-0.28
Solution C. · Polymer M_w	2.89	0.27	5.180	8.3	0.0	0.90
Solution C. · Voltage	-1.00	0.62	2.590	2.8	0.1	-0.31

Table A8. Bridging from the dispenser to the collector statistical analysis results with system parameters

Term	Estimate	Std Error	Chi^2	L-R Chi^2	Prob> Chi^2
Surface Tension	0.98	0.38	6.66	15.1	<.0001
Reynolds Number Formula	167	138	1.47	1.28	0.256
Electric Field	-1.25	0.86	2.1	2.28	0.130
Electrospinning Current*	-	-	-	-	-

*The electrospinning current was measured during electrospinning but was erratic and did not settle on an average value therefore this parameter was not included

Appendix A.5 Fiber Diameter Statistical Analysis

Table A9. Fiber diameter statistical analysis results with solution and processing parameters

Term	Orthogonal Estimate	Std Error	P-Value	Normalized Estimate
Polymer M_w	189	21.0	<.0001	0.48
(Polymer M_w)^2	393	41.2	<.0001	1.00
Solvent R.	312	15.8	<.0001	0.79
Solvent R. · Polymer M_w	293	17.0	<.0001	0.74
Polymer Mw. · Pumping Rate	201	14.4	<.0001	0.51
Pumping Rate	129	14.9	<.0001	0.33
Solution C. · Polymer M_w	104	18.8	0.003	0.26
Solvent R. · Pumping R.	149	15.5	0.005	0.38
(Solvent R.)^2	-190	90.3	0.0375	-0.48
Solution Concentration wt%	99.9	31.7	0.0021	0.25

Table A10. Fiber diameter statistical analysis results with system parameters

Term	Estimate	Std Error	P-Value	Normalized Estimate
Surface Tension · Electrospinning Current	615	344	0.0806	1
Surface Tension · Reynolds Number	461	217	0.0393	0.749
Electric Field	214	46.9	<.0001	0.348
Surface Tension	108	60.2	0.0784	0.176
Reynolds Number	-238	97.7	0.019	-0.387
Surface Tension · Electric Field	-242	92.3	0.012	-0.393
Electrospinning Current	-412	113	0.0007	-0.670

Table A11. Fiber diameter statistical analysis results with all solution and processing parameters

Term	Estimate	Std Error	P-Value
Intercept	-952	382	0.0145
Pumping Rate	3.3	0.90	0.0004
Needle Diameter	-134	90	0.14

Table A11. (Continued)

Solution Concentration	26.4	23	0.254
Polymer M_w	0.00129	0.00022	<.0001
Conductive Additive	-39.6	26	0.128
Solvent Ratio	358.3	50	<.0001
Depth of Field	0.510	3.75	0.892
Voltage	-3.5	6.39	0.590
(Needle Diameter)^2	1487.8	3.86	0.363
Needle Diameter · Pumping Rate	-1.9	0.06	0.618
(Pumping Rate)^2	0.0108	6.39	0.853
Needle Diameter · Solution Concentration	-75.9	100	0.450
Pumping Rate · Solution Concentration	0.94	0.93	0.317
(Solution Concentration)^2	29.2	28	0.308
Needle Diameter · Polymer M_w	-0.000873	0.000546	0.113
Pumping Rate · Polymer M_w	0.0000301	0.00000509	<.0001
Solution Concentration · Polymer M_w	0.000187	0.000137	0.175
(Polymer M_w)^2	0.0000000064	0.0000000027	0.018
Needle Diameter · Conductive Additive	10.2	69	0.883
Pumping Rate · Conductive Additive	-1.7	0.66	0.013
Solution Concentration · Conductive Additive	-19.0	17	0.266
Polymer M_w · Conductive Additive	-0.000228	0.000102	0.029
Conductive Additive^2	24.0	19	0.205
Needle Diameter · Solvent Ratio	-11.7	249	0.963
Pumping Rate · Solvent Ratio	3.9	2	0.087
Solution Concentration · Solvent Ratio	46.1	57	0.422
Polymer M_w · Solvent Ratio	0.00202	0.000305	<.0001
Conductive Additive · Solvent Ratio	-7.4	40	0.853
(Solvent Ratio)^2	-262.2	113	0.023
Needle Diameter · Depth of Field	19.2	17	0.252
Pumping Rate · Depth of Field	0.095	0.182	0.604
Solution Concentration · Depth of Field	-1.8	4.1	0.664
Polymer M_w · Depth of Field	-0.00000060	0.0000212	0.978
Conductive Additive · Depth of Field	1.8	2.7	0.501
Solvent Ratio · Depth of Field	-6.0	10	0.533
(Depth of Field)^2	0.345	1.10	0.754
Needle Diameter · Voltage	-19.5	34	0.565
Pumping Rate · Voltage	0.13	0.355	0.726
Solution Concentration · Voltage	-3.9	9.3	0.674
Polymer M_w · Voltage	-0.000048	0.000039	0.226
Conductive Additive · Voltage	-5.4	6.01	0.37
Solvent Ratio · Voltage	40.5	19	0.04
Depth of Field · Voltage	-1.0	1.53	0.525
(Voltage)^2	2.8	1.84	0.129

Appendix A.6 Bead Diameter Statistical Analysis

Table A12. Bead diameter statistical analysis results with solution and processing parameters

Term	Orthogonal Estimate	Std Error	P-Value	Normalized Estimate
(Polymer M_w)^2	4.91	0.661	<.0001	1
Solution Concentration · Pumping Rate	-1.54	0.306	<.0001	-0.314
Voltage · Depth of Field	0.899	0.283	0.0031	0.182
Pumping Rate	0.830	0.274	0.0046	0.168
Solvent Ratio · Polymer M_w	1.395	0.481	0.0065	0.283
Voltage	0.431	0.234	0.0744	0.087
Solvent Ratio	0.586	0.332	0.0864	0.119

Table A13. Bead diameter statistical analysis results with system parameters

Term	Estimate	Std Error	P-Value	Normalized Estimate
Surface Tension	-0.42	1.58	0.789	-0.032
Reynolds Number	-9.87	4.21	0.026	-0.748
(Surface Tension)^2	1.23	2.70	0.650	0.093
Surface Tension · Reynolds Number	13.1	6.47	0.050	1
(Reynolds Number)^2	10.3	5.78	0.085	0.78
Electric Field	-0.59	1.11	0.598	-0.045
Reynolds Number · Electric Field	1.17	4.45	0.794	0.088

Appendix A.7 Number of Bead Nodes per Area Statistical Analysis

Table A14. Number of bead nodes per area statistical analysis results with solution and processing parameters

Term	Orthogonal Estimate	Std Error	P-Value	Normalized Estimate
Polymer M_w	-448	86.1	<.0001	-1
Solvent Ratio · Polymer M_w	307	85.6	0.0006	0.686
Voltage · Needle D.	-276	85.2	0.0019	-0.616
Solvent Ratio · Solution Concentration	305	102	0.0039	0.680
Solvent Ratio	-211	87.2	0.0181	-0.47
(Voltage)^2	105	55.9	0.0637	0.235
Solution Concentration · Polymer M_w	150	89.7	0.0991	0.334

Table A15. Number of bead nodes per area statistical analysis results with system parameters

Term	Estimate	Std Error	P-Value	Normalized Estimate
Reynolds Number · Electrospinning Current	52031	9590	<.0001	1
Reynolds Number	17250	2569	<.0001	0.331

Table A15. (Continued)

Electrospinning Current	6068	1296	0.0001	0.116
Surface Tension · Electric Field	1591	518	0.006	0.030
Electric Field	-2438	410	<.0001	-0.046
Surface Tension	-4382	721	<.0001	-0.084
Surface Tension · Reynolds Number	-8215	1527	<.0001	-0.157
Electric Field · Electrospinning Current	-8892	1940	0.0002	-0.170
Reynolds Number · Electric Field	-9003	1496	<.0001	-0.173
Surface Tension · Electrospinning Current	-15460	2999	<.0001	-0.297

Appendix B. Previously Reported Data

Table B1. Parameters from previous studies

Ref.	Polymer M_w	Solvent Ratio ($V_{Acetone}/V_{DMF}$)	Solution Concentration (wt%)	Needle Diameter (mm)	Pumping Rate (µl/min)	Voltage (kV)	Depth of Field (cm)	TBAC wt%
[122]	275000	0	22.5	0.6	1.66	15	15	0
	275000	0	23.99	0.6	9.63	12	12	0
	275000	0	22.5	0.6	6.44	15	10	0
	275000	0	22.5	0.6	6.44	15	15	0
	275000	0	21.01	0.6	9.63	18	18	0
	275000	0	20	0.6	6.44	15	15	0
	275000	0	22.5	0.6	6.44	20	15	0
	275000	0	23.99	0.6	3.652	18	18	0
	275000	0	22.5	0.6	6.44	15	15	0
	275000	0	22.5	0.6	6.44	15	20	0
	275000	0	21.01	0.6	3.652	12	18	0
	275000	0	23.99	0.6	9.63	12	18	0
	275000	0	22.5	0.6	6.44	10	15	0
	275000	0	22.5	0.6	6.44	15	15	0
	275000	0	25	0.6	6.44	15	15	0
	275000	0	22.5	0.6	11.62	15	15	0
	275000	0	22.5	0.6	6.44	15	15	0
	275000	0	21.01	0.6	9.63	18	12	0
	275000	0	22.5	0.6	6.44	15	15	0
	275000	0	21.01	0.6	3.652	12	12	0
	275000	0	23.99	0.6	3.652	18	12	0
[44]	427000	0	26	1	6	7.5	15	0
	427000	0	26	1	6	10	15	0
	427000	0	26	1	6	12.5	15	0
	427000	0	26	1	6	15	15	0
	427000	0	26	1	1	11	15	0
	427000	0	26	1	4	11	15	0
	427000	0	26	1	8	11	15	0
	427000	0	26	1	12	11	15	0
[17]	275000	1	20	0.413	8.3	12	20	0
	275000	1	20	0.413	8.3	15	20	0
	275000	1	20	0.413	8.3	20	20	0
	275000	1	20	0.413	8.3	25	20	0
	275000	1	20	0.413	8.3	30	20	0

Red text indicates that the parameter was not available and an estimate was used based on the electrospinning setup in the literature or taken as a middle value to reduce its effect. For the solvent ratio this can also mean that DMAC was used instead of DMF.